A Study on the Self-Assembly of Block Copolymer Thin Films and Their Nanocomposites

Siti Aisyah Binti Shamsudin

2013

Contents

CHAPTER 1. Introduction

CHAPTER 2. Influence of Temperature and Type of Solvents on the Microdomain Orientation of PS-b-P2VP Ultrathin Films by Solvent Annealing

CHAPTER 3. Controlling Ordered Structures of PS-b-P2VP Block Copolymer Thin Film by Tuning Solvent's Annealing Time

CHAPTER 5. Aligning CdS Quantum Dots in Apo-ferritin Protein and PS-b-P2VP Organic Templates

CHAPTER 6. Introducing the Safe Capsule for CdS Quantum Dots as Bio-labelling Device

1
Introduction

1.1 Research Background

1.1.1 Relationship between Nanotechnology and Self-assembly

The underlining issue in nanotechnology is developing simple construction techniques for fabricating nanoscale structures.[1] Nanotechnology is the manipulation of matter on an atomic and molecular scale. With a variety of potential applications, nanotechnology is the key technology for the future.[2] Nanotechnology is very diverse, ranging from extension of conventional device physics to completely new approaches based on molecular-assembly.[2] The method of producing materials in nano-range scale can be achieved through top-down and bottom-up approaches. The top-down approach is a conventional technique which is wasteful and energy intensive as this procedure usually breaks-down the entire specification of the system, such as film, until it has been reduced to the base elements.[1,3] Therefore, in order to decrease the size of the structure by using this approach, the construction of expensive facilities are required. For this reason, a natural alternative for the top-down construction called the bottom-up, which is another approach that builds nanoscale structures from their atomic and molecular components via self-assembly, is necessary to be used.[1] Thus, the goal in tailoring nanostructured devices by supramolecular interfacial forces and interactions can be achieved.[4] On the other hand, this approach also relies on the exploitation of specific intermolecular interactions which is one of the key building principles of all living organisms. Hence, biological structures can be used as templates for directing self-assembly.[1]

Self-assembly is an important tool for generating integrated nanoscale devices. Self-assembly commonly occurs in nature for the creation of multi-dimensional, complex biological structures such as cells.[5] Robust structures with exceptional mechanical stabilities are formed through self-assembly either by favourable free-energy changes or kinetics. In self-assembly, specific non-covalent interactions are fundamental in organizing atomic, molecular and other nanoentities, leading to spontaneously formed hierarchical and complex architectures. Thus, self-assembly is very important in the effort of improving the present technology. Interesting analogies to nature's art of putting things together are the main aspirations for nanotechnologists. In this context, exploitation of the spontaneous and directed assembly of nanoobjects with supramolecular structures,[6] polymers,[7] dendrimers,[8] biological molecules[9] or inorganic nanoparticles[10, 11, 12] are well investigated. By altering the substituents of nanoparticle-assembly building blocks, the possibility of exploiting either the spatial or temporal attributes of nanoparticles which have been tailored to desirable assembly formations, is endless. Moreover, desirable properties and structural effects in the assembled materials can be accomplished using suitable templates. Therefore, self-assembly is achievable by introducing simple methods such as the evaporation-based assembly that spontaneously produces ordered multi-dimensional structures.[13-17] It can also be done via more advanced methods such as patterned self-assembly using lithography [18] and micro-contact printing.[19] By applying these advanced methods, the area of eligible chemical functionalities has patterns that can create organized nanoparticle networks on the selected substrates.

Self-assembly has been widely used in nanotechnology, notably in interface and colloid science to develop carbon nanotube and fullerenes of nanoparticles or nanorods. These materials can be used as nanoionics and nanoelectronic devices due to fast ion transportation.

DNA and other nucleic acid can also be assembled with nanoparticles that have been fabricated for use as bionano sensors in nanomedicine. Other than that, silicons in nanoscale are used to develop solar cells because of its greater efficiency compared to bulk materials. Semiconductor nanoparticles, which are also called quantum dots, have received huge attention because they have excellent properties that can be developed into various applications such as lighting, solar cell, biological imaging, etc.[2]

1.1.2 Nanoparticles

Nanoparticles are also receiving a great deal of attention due to their astonishing properties and numerous possibilities for applications in nanotechnology. Assembled nanoparticles have generated new nanostructures due to their unexpected collective and internal physical properties. These properties can be exploited for various applications such as in nanoelectronics, spintronics, sensors, etc. Quantum size effects (QSE)[20] stem from the quantization of the electronic states of nanoparticles, which are also the driving forces behind the current intense study towards synthesizing and the applications of nanoparticles. The physicochemical properties of nanoparticles are size and shape dependent.[21-25] The size-dependent properties are usually associated with magnetic, photonic, chemical, and electrical behaviour, which are different from the properties in their bulk materials.[4] These properties are drastically changed in the nanometer range, thus making nanoparticles as the ideal candidates for applications in single-electron devices,[26] nanoelectronics,[27] sensing,[28] biodiagnostics,[29] catalysis,[30] etc. The most important and challenging part is their organization at the nanoscale. The multi-dimensional assembly of nanoparticles with controlled morphology in highly ordered arrays is important for realizing their novel applications.[31-33] Thus, these properties can be controlled through immobilization and the assembly of nanoparticles on an appropriate substrate or in a suitable medium.[4] The self-

assembled nanostructures show remarkable collective properties,[34-37] that are useful for engineering nanoarchitectures.

Numerous research have been carried out to find ways to assemble metal nanoparticles in various modes, for example, via template-directed methods by using surfactants[38] or polymers.[39] The important factor in determining a stable integration between the nanoparticles within a block-copolymer (BCP) matrix mainly lies in the compatibility of the nanoparticles with the block-copolymer's microstructures. This integration can be controlled by considering the symmetry of both the composition and the block-copolymer host matrix. Thus, surface modifications of the nanoparticles (NPs) are necessary to stabilize them against aggregation within the BCP-matrix, in which the NPs normally tend to attract to one domain of block-copolymer that drive by the other block of the block-copolymer. The resulting materials can assemble the nanoparticles into one microphase of the BCP that tended the pattern formed by the respective microphase.[4] If metal nanoparticles can be incorporated or arranged only into one domain of a microphase-separated block copolymer, it is possible to transfer the microphase separation of the BCP into ordered arrays of NPs' structures with a unique spatial distribution in the matrix polymers.[40]

Cadmium sulphide (CdS) has shown strong confinement effects near its Bohr radius (5.8nm),[41] whose main application is in light detection. CdS has gained a lot of attention as a quantum dot because of its diverse applications such as in lasers, light emitting diodes, and biological imaging. Most of CdS QDs have fluorescence peak at the wavelength of 500 nm, as shown in Figure 1, as a green peak. The debates regarding the key to making successful applications for nanoparticle-based devices is in creating well-defined and defect free ordered nanostructures. Therefore, numerous researches committed towards creating periodic

assembled nanostructures through different, novel and innovative procedures have attracted much attention lately.[40]

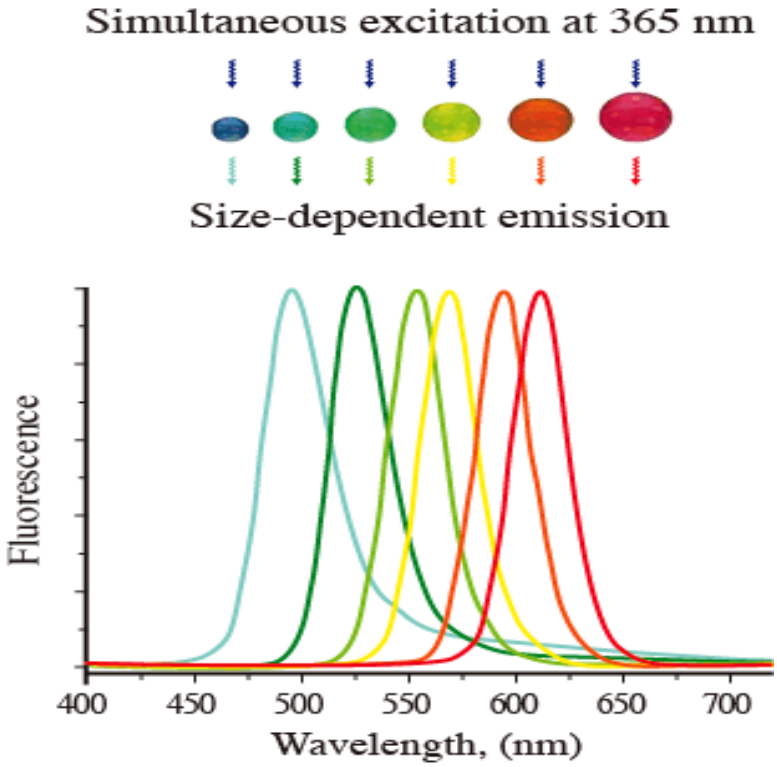

Figure 1: Size-dependent emission of Quantum Dots.

(from: Hideki Ooba; On-site Sensing and Diagnosis Research Laboratory)

One of the important properties of QDs is their ability to change the colour that depends on their particles' sizes when placed under UV lamp. The colour of QDs can change from indigo to red, depending on the size of their particles. Figure 2 shows that the quantum dots can change their colour when UV lamp is switched on. It has also been determined that the sizes of quantum dots are in the range between the size of water molecules and white blood cells.

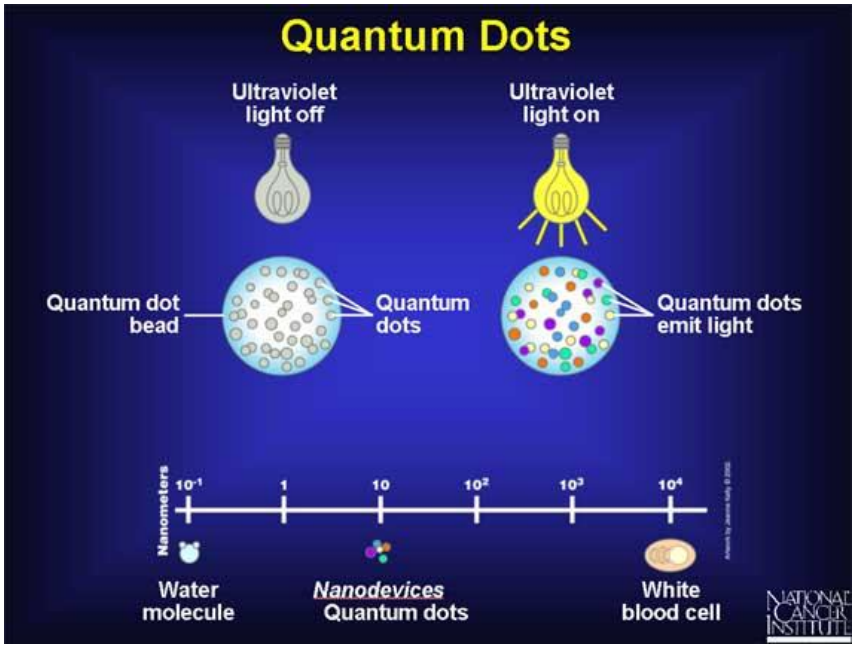

Figure 2: Quantum Dots molecules under visible light and ultraviolet light.

(Web Format by: Web Books Publishing with permission if use for educational purposes)

1.1.3 Bio-template

Biological structures are attractive to be used as templates for the formation of nanoscale architectures because of their size, geometry and ability to interact with inorganic materials.[42] Biotemplated and biomediated control of crystallization is a relatively recent area of investigation, which already has far-reaching implications for generating complex forms in inorganic systems.[43] As an alternative to top-down lithography approaches, which are reaching theoretical and practical limits,[44,45] biotemplating provides the means of assembling nanoparticles into conductive nanowires and nanowire arrays that serve as the building blocks for logic and memory devices as well as interconnects and interconnect arrays.[44,46–48] For these reasons, a number of biological filaments including histidine-rich peptides,[49] peptide nanotubes,[50] DNA,[46,51,52] M13 bacterial phage,[53–56] tobacco mosaic virus (TMV),[57,58] flagella,[59] and amyloid fiber from yeast[60] have been explored as

templates for nanowires. The electrical properties of these structures have just recently been reported.[51,56,60]

Protein cage supramolecules such as ferritin and viral capsids have been attracting attention as building blocks for novel fabrications of functional nanostructures because they can lodge a variety of nanometer sized inorganic materials within their interior spaces.[61] The native apo-ferritin molecule is composed of 24 subunits that form a spherical cage-shaped protein shell, the inner and outer diameters of which are 7 and 12 nm, respectively, as shown in Figure 3. The assembled structure of apo-ferritin is remarkably stable and robust, as well as able to withstand extreme biological environments; high temperatures (up to 70°C) and wide pH variations (pH 2.0–10.0).[62]

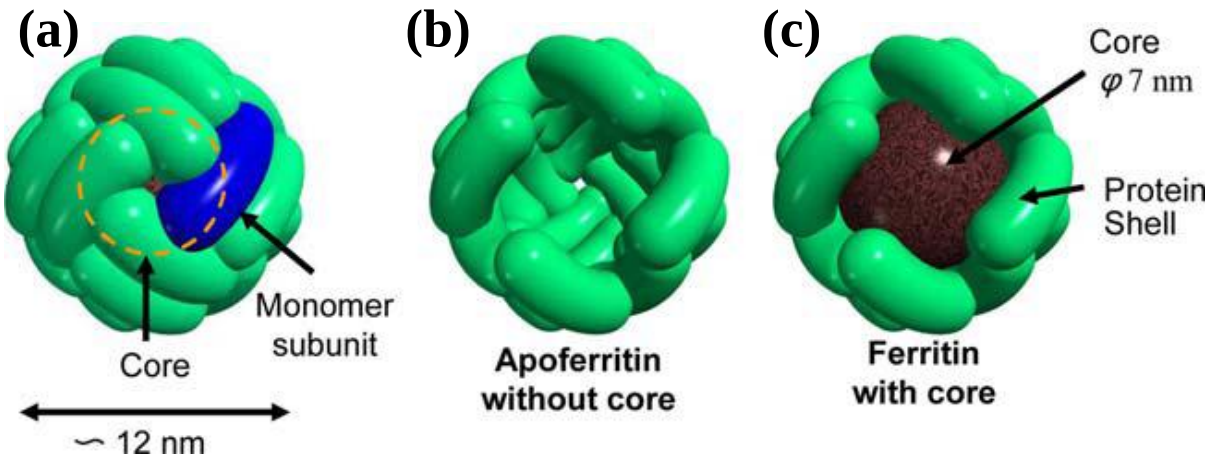

Figure 3: Schematic drawing of the cage-shaped proteins (b) apo-ferritin without core and (c) ferritin with core. Copyright 2013 with permission from Springer.

Apo-ferritin stores iron as a hydrated iron oxide core in the interior space, which is called ferritin (Figure 3 (c)). The inner cavity of apo-ferritin has been used as a bio-template to synthesize size-confined nanoparticles.[63–70] The two or three dimensional assemblies of these protein cage architectures such as ferritin on substrates, have also been used in various ways to obtain functional structures which may be applied in biosensor, bioelectronic, and

nanoelectron devices. The physicochemical process and modulation of electrostatic interactions between the apo-ferritin and the surface of the precursor film can effectively control the adsorption type, density and morphology of apo-ferritin on a substrate. Studies on the techniques of immobilizing protein supramolecules (apo-ferritin), may lead to the possibility of forming more complex functional inorganic nanostructures by using hollow cavities as templates for constraining materials used during synthesizing and producing nanoparticles. The self-assembly can be done via electrostatic adsorption of ferritin and nanoparticle conjugate onto the surface of polyelectrolyte multilayers.[71]

1.1.4 Block Copolymer

Block copolymers (BCPs) are an attractive alternative to advanced lithographic techniques due to their ability to form a variety of well-defined morphologies with length scales ranging from 10 nm to 100 nm. Not only due to such achievable length scales that have made BCPs relevant in many nanotechnology applications, but also their chemical structure may be tailored for desired functionality.[72] BCPs self-assembly is one of the bottom-up approaches in nanoscience and nanotechnology that has been used for the preparation of functional nanomaterials.[73] BCPs consist of two or more chemically different polymers, frequently immiscible and are connected covalently. There are various ways in which blocks can be attached to one another.[74] Due to thermodynamic in compatibility and chain connectivity, the phase separation between two (or more) blocks occurs only in the size of tens of nanometer range.[75–86]

The incompatibility between the A and B blocks drives a collection of A–B diblock molecules to self-organize via microphase separation in which the contact between similar and dissimilar blocks are maximized and minimized, respectively. Macrophase separation is

prevented by entropic forces because of the covalent bonds that are holding the A and B blocks together. The segregation of blocks in block copolymer can be obtained from spherical structure to lamellar structure with different relative composition fraction of A block and B block, as shown in Figure 4. The system, then, must reach a compromise between mixing and separating. The temperature-dependent Flory–Huggins interaction parameter, χ_{AB}, describes the free energy cost of contact between dissimilar monomers that governs this process.[87]

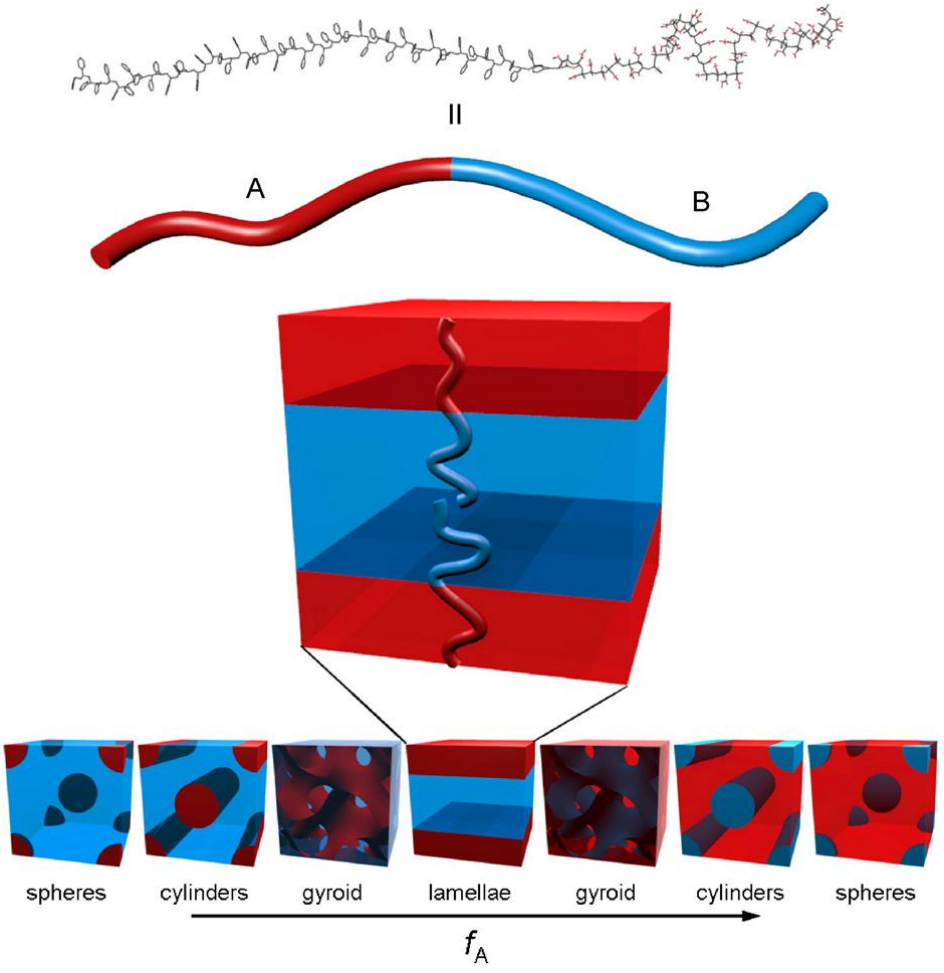

Figure 4: Schematics drawing of thermodynamically stable diblock copolymer phases. The segregation of blocks in block copolymer can be obtained from spherical structure to lamellar structure with different relative composition fraction of A block and B block, with the structure determined primarily by the relative lengths of the two polymer blocks (f_A). Copyright 2013 with permission from Elsevier.

Two additional parameters that determine the ultimate morphology of the microphase system are the degree of polymerization, N, and the relative composition fractions, f_A and f_B, where $f_A = N_A/N$ and $f_A+f_B = 1$.[88] The complex structure of BCP materials leads to a variety of useful properties for industrial applications. Thus, self-assembled block copolymers have found uses in micro-electronics,[89] storage devices,[90] solar cells,[91] molecular sieves,[92-93] low-k dielectrics,[94] and organic semiconductor applications.[95, 96]

Additionally, block copolymers can also be formed as *amphiphilic* block copolymer (AmBC) macromolecules if they are composed of two chemically different homopolymer blocks, in which one is hydrophilic (water soluble) and the other is hydrophobic (water insoluble).[97] *Amphiphilic* block copolymers can self-assemble into nanosized aggregates of various morphologies in aqueous solution, such as micelles, cylinders, or vesicles.[98–103] These supramolecular assemblies have great potentials for applications in drug delivery, diagnostic biosensors and tissue engineering.[104–108] Therefore, this discussion has been a hot topic for a long time with the intent of designing diverse biocompatible and biodegradable *amphiphilic* block copolymers.[109] In thin films, block copolymers can adopt different morphologies as compared to when in bulk. Thin films of symmetric block copolymers form lamellae which can orient either parallel or perpendicular to the substrate.[110] On the other hand, asymmetric block copolymers which may adopt hexagonal or cubic-packed spherical morphologies in the bulk, can form parallel cylinders (stripes) or arrays of dots (spheres or perpendicular cylinders) in two dimensions of thin film.[111] It is possible to obtain a diblock copolymer thin film which is confined between two infinite, parallel plates with a vertical morphology where the lamellar structure of the bulk is realised. [112]

Cylindrical nanopatterned surfaces of *amphiphilic* polystyrene-*block*-poly(2-vinyl pyridine) (PS-*b*-P2VP) BCP thin films are stable in water. These surfaces can provide both physical and chemical patterning due to the hydrophobic and hydrophilic nature of the domains. By photo cross-linking the cylindrical domains, a more durable material that can withstand immersion in water for extended periods of time is produced.[113] Therefore, these improved properties of the PS-*b*-P2VP thin films have made it possible for the thin films to be used as biosensors after hybridization with inorganic nanoparticles such as CdS.

1.2 Bio-nano Hybrid System

The sequential information encoded within biomolecules provides the means to be used as templating units for non-specific plating procedures once self-assembly has occurred. However, biomolecular building blocks play an important role in nanomaterials synthesis by providing a set of chemically organized functional groups that can exert control over a synthetic reaction. This way, the sequenced composition of a biomolecule can control the outcome of a reaction and the desired properties such as the size of the nanomaterial. Semiconductor nanocrystals (quantum dots) are important synthetic targets because they exhibit tuneable electronic and optical properties that can be exploited for biological imaging and in the fabrication of optoelectronic devices.[114–116] Synthetic control during the preparation of these materials is typically achieved through brute-force optimization programme of reaction conditions. By using this programme, the general rules governing the production of quantum dots with defined sizes or properties which have not yet been formulated, can be known. By enrolling biomolecules as templating agents, the potential exists for programmable reactions where biological sequences could be used to control the end result of quantum dot synthesis. These findings indicate that the biomolecules can be used to systematically engineer the structures and properties of semiconductor-based

materials. Furthermore, the synergy between the dimensions of nanostructures and biomolecules provides a mean to tune the properties of materials with accurate nanoscale.

Toxicity resulting from decomposition and released from heavy metal ions and ligand has interfered with the effort to apply quantum dots as lumiphores in biological systems.[117–120] Materials that are frequently used in biological applications are synthesized in organic solutions and then transferred to aqueous solutions by a ligand exchange step that increases the polarity of the nanocrystal coating.[117] Many materials prepared in this manner do not exhibit reliable stability due to the fact that ligand exchange does not provide complete protection from water and decomposition of the particle. This phenomena shows that the "new solvent" has interacted with the nanocrystal surface. In contrast, by introducing nucleic acid templates, quantum dots are formed in water and the isolation of stable products provides an excellent starting point for obtaining materials with good stability in biological fluids. Indeed, a recent study of CdS nanocrystals or quantum dots synthesized using oligomeric DNA oligonucleotides has demonstrated that very low levels of toxicity has occurred when the cells were exposed to these hybrid biotemplated materials.[121] Thus, in addition to developing a suitable technique capable of achieving structural control over a quantum dot's structure, the use of biomaterials as based ligands may also provide a way to obtain quantum dots with improved toxicity profiles.

This principle may also be applied for the synthesis of colloidal solutions. Solution-synthesized inorganic crystals such as colloidal quantum dots have been proven to be competitive with traditional semiconductors in a variety of applications such as optical sensing,[122] photovoltaics,[123] and electronics.[124] There are also published reports that impart a more complex structure in the nanoscale. Early examples include branched tetrapods[125]

and core–shell nanoparticles[126] that would offer significant improvements in the performance of such devices. A survey of recent achievements in this area makes it apparent that the sequences and structures of biomolecules can be used to employ bottom-up control over the synthesis and properties of nanomaterials. In addition, the use of combinative methods in molecular biology, have been extremely useful as a tool for materials synthesis.

The discovery of biomineralization proteins in living organisms has inspired the use of peptides and proteins as templates to synthesize inorganic nanomaterials.[127,128] Proteins hold more globular structures compared to peptide fragments that have been used to achieve additional precise control over particle growth. Protein cages,[129,130] peptide assembled nanotubes[131] or nanorings[132,133] have been used as reaction containers. For example, ferritin is a robust iron-storage protein self-assembled from 24 subunits that has a total internal diameter of 7 nm. On the other hand, apo-ferritin lacks the iron oxide core, therefore, it serves as a nanoreactor for the mineralization of metal particles such as cobalt, nickel and palladium. By infusing metal ions into the protein cavity through hydrophilic channels and then adding a reducing agent, metal nanoparticles could be prepared with dimensions close to the protein interior.[134]

1.2.1 Advantageous Hybrid Materials

Nanomaterials have been visualized for usage in many applications including assembling new electronic devices, energy conversion and storage by combining materials with various properties. In this capacity, biological molecules serve as ideal vehicles for programmable and self-assembled heterostructure fabrications. The development of a novel material using biotemplating to enhance its performance is attained by illustrating the power of merging biomolecular with materials chemistry. For example, the use of in vitro selection of nucleic

acids and phage display of peptide sequences has yielded biomolecules that can directly synthesize metallic and semiconductor nanostructures of defined shapes and sizes. These hybrid materials have the potential to generate new materials with specific electronic or optical properties through combinatorial sequence searches. Several reports of the use of in vitro selection for the development of nanomaterials have now proven that the in vitro selection is a promising method to manipulate and optimize nanostructures.[135]

The first wave of nanobiotechnology demonstrated that biomolecules can be influenced by their reaction mechanisms to create direct nanostructured materials. The second wave of discoveries proved that such manipulations can lead to control of not only over the morphology, but also over properties, conductivity, light emission, dielectric constant, polarization, etc. In some cases, these biomolecule-based materials with self-assembly have shown to be superior to those generated without. The third wave demonstrated the transition by enhancing the properties of the materials with the purpose of improving the present devices. These materials' properties have improved the quality of photovoltaics, environmental sensing, and other electronics devices. Nanostructured materials have also been used to develop devices with high sensitivity to temperature and other environmental factors which will have to be addressed in order to ensure that robust devices can be generated. The fourth wave took the time to understand the system before exploiting biology's capacity to engineer along many length scales. The nanometer scale offers quantum confinement. The quantum dots with tens of nanometers scale is an ideally sized scale for devices used in detecting single molecules. Thus, the hundreds of nanometers to multiple microns scale offer resonances with light ranging from the ultraviolet through the visible and into the infrared. Nature's creations are important proofs that demonstrates the level of

quality that all robust, versatile, human-scale devices may reach when the system begins at the bottom of the synthesis system which is at the nanometer scale.[135]

1.3 Block Copolymer as Scaffold Templates

Microphase separation in pure block copolymers (BCPs) is a well-studied phenomenon of producing desired morphologies via phase separation that are determined by the relative lengths of the polymer blocks, ranging from spheres to lamellae, or interconnected network morphologies.[136-137] The size of each block of the polymer domain is determined by its overall chain length, thus providing a wide range of self-organized nanoscale-level templates. Most importantly, microphase-separated BCPs spontaneously self-assemble into regular arrays of domains which size can be controlled from a few to several tens of nanometers. BCPs can also act as hosts for sequestering nanoscopic inclusions of appropriate chemical affinity and geometry.[138-139] Thus, BCPs can be used as templates to provide supramolecular control over the size, particle density and spatial location of various inorganic nanoparticles. The ability to control the length, spatial and orientational organization of BCPs morphologies make these materials particularly attractive to be used as scaffold templates for engineering nanostructures.[4]

Figure 5 shows an example of BCP template that can be employed to align quantum dots array such as cadmium sulphide (CdS). The topic of assembling luminescent CdS and CdSe nanoparticles into specific domains of block copolymers has received massive attention nowadays, with several recent reports and publications dealing with this aspect. In bulk materials or surfaces, the following polymers and nanoparticles have been used for assembly: CdS NPs (2.0–3.4 nm) up to 43 wt% in hexagonally packed poly(styrene-*b*-ethylene oxide),[140-141] CdS NPs (4.4 nm) in poly(styrene-*b*-acrylic acid),[142] CdS NPs incorporated in

poly(styrene-*b*-methyl methacrylate),[143] wire-type CdS nanoparticles grown in cylindrical polymer brushes made from poly(acrylic acid-*b*-butylacrylate),[144] as well as CdS NPs incorporated with polypyrrole nanowires in porous polymer monoliths.[145] These research strategies are beneficial efforts towards developing various kinds of devices to be applied in wide areas of technology especially in biomedicine.

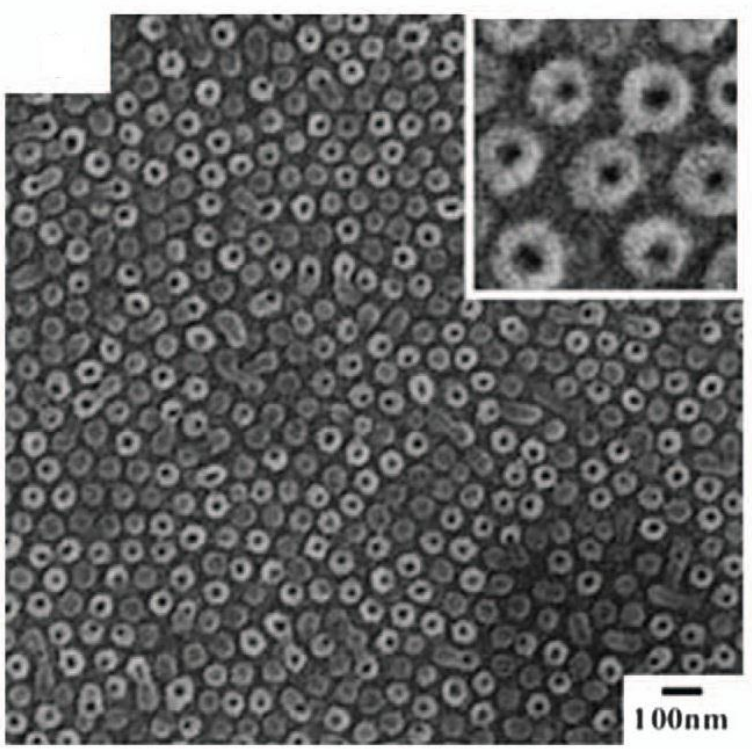

Figure 5: A scaffold perpendicular cylindrical structure of thin film template.
(a Creative Commons license - (Attribution-Noncommercial 2.5))

1.4 Characterization of Samples

1.4.1 Atomic Force Microscope (AFM)

In this current research, the surface morphology was observed at ambient conditions using a commercial AFM, equip with a Nanoscope III scanning probe microscope (Digital Instruments), California USA, in the tapping mode. The dry samples were mounted on a sample stage which was three-dimensionally driven by a piezotube scanner. Both height and phase images were recorded simultaneously. The tapping mode has operated by using

Olympus silicon microcantilever with spring constants between 39.7 N/m and 71.6 N/m and resonant frequencies of 293.8-356.0 Hz. The A_{sp} /A_0 value was set to 31.753, where A_0 is the free oscillation amplitude and A_{sp} is the set point amplitude. The scan rate was in the range of 0.48-0.55Hz. In the tapping mode, as the tip mechanically probes different domains, the phase contrast originated from local differences in the tip-surface interactions. These interactions depended not only on the intrinsic properties of the analysed material, which is the elastic modulus, but also on the mechanical properties of the tip and on the existence of tip-sample adhesion. In the case of "soft-tapping" regime; when the amplitude of the oscillating cantilever is only slightly reduced, upon interaction with the surface, it has been shown that the magnitude of the phase shift is directly related to the elastic modulus of the sample. When probing a region of higher modulus, the force interaction leads to a more positive phase shift and hence appears brighter in a phase image.[146]

1.4.2 Transmission Electron Microscope (TEM)

Transmission electron microscopy (TEM) is a microscopy technique in which a beam of electrons is transmitted through an ultra-thin specimen, interacting with the specimen as it passes through. An image is formed from the interaction of the electrons transmitted through the specimen; the image is magnified and focused onto an imaging device. TEM has been used in all areas of structure observation and biological investigations because of its ability to view the finest structures. It is also used as a diagnostic tool in hospital pathology labs beside in chemistry experiment.[147] This research has used JEM-2000FX operated at 200 keV as acceleration voltage. For a crystallographer, a metallurgist or a semiconductor research scientist, current high voltage and high resolution TEMs, have permitted the routine imaging of atoms, allowing materials researchers to monitor and design materials with custom-tailored properties.

1.4.3 Scanning Electron Microscope (SEM)

A scanning electron microscope (SEM) is a type of electron microscope that produces images of a sample by scanning it with a focused beam of electrons. The electrons interact with the electrons in the sample, producing various signals that can be detected. These signals contain information about the sample's surface topography and composition. The electron beam is generally scanned in a raster scan pattern, and the beam's position is combined with the detected signal to produce an image. SEM can achieve resolutions of higher than 1 nanometer. Specimens can be observed in high vacuum and low vacuum while in an environmental SEM, the specimens can be observed in wet condition.[148] A field emission scanning electron microscope (FESEM), has a beam cross section of close to one nanometer in diameter. This microscope, the S-4800 is Hitachi's highest resolution SEM. It features a cold cathode field emission gun. Typical magnification in this SEM can be up to two hundred thousand times, however higher magnifications of up to one million, can be obtained by a skilled operator. Two secondary electron detectors are installed. One is an in-lens detector for very high resolution. An in-lens backscatter electron detector is also available. Images can be taken with combinations of the different detectors as well as an energy filter mode. Acceleration voltages ranges from 0.1 to 30kV with a special sample bias voltage option that helps eliminate surface charging. [149] However in this study the instrument has operated at 1.5 kV.

1.4.4 Ultraviolet-visible Spectrophotometry (UV-Vis)

Ultraviolet-visible spectrophotometry (UV-Vis or UV/Vis) refers to absorption spectroscopy or reflectance spectroscopy in the ultraviolet-visible spectral region. This means it uses light in the visible and adjacent (near-UV and near-infrared (NIR)) ranges. The absorption or reflectance in the visible range directly affects the perceived colour of the chemicals involved. In this region of the electromagnetic spectrum, molecules undergo electronic transitions. This

technique is complementary to fluorescence spectroscopy, in that fluorescence deals with transitions from the excited state to the ground state, while absorption measures transitions from the ground state to the excited state. Absorption spectroscopy refers to spectroscopic techniques that measure the absorption of radiation, as a function of frequency or wavelength, due to its interaction with a sample. The sample absorbs energy, i.e., photons, from the radiating field. The intensity of the absorption varies as a function of frequency, and this variation is the absorption spectrum. Absorption spectroscopy is performed across the electromagnetic spectrum.[150]

Absorption spectroscopy is employed as an analytical chemistry tool to determine the presence of a particular substance in a sample and, in many cases, to quantify the amount of the substance that is present. Infrared and ultraviolet-visible spectroscopy is particularly common in analytical applications. Absorption spectroscopy is also employed in studies of molecular and atomic physics, astronomical spectroscopy and remote sensing. Ultraviolet and visible spectrometers have been in general use for the last 35 years and over this period have become the most important analytical instrument in the modern day laboratories. In many applications, other techniques could be employed but none is the rival to UV-Visible spectrometry for its simplicity, versatility, speed, accuracy and cost-effectiveness.[150]

Many molecules absorb ultraviolet or visible light. The absorbance of a solution increases as the attenuation of the beam increases. Absorbance is directly proportional to the path length, *b*, and the concentration, *c*, of the absorbing species. Beer's Law states that

$$A = \varepsilon bc$$

Where, ε is a constant of proportionality, called the absorptivity.

Different molecules absorb radiation of different wavelengths. An absorption spectrum will show a number of absorption bands corresponding to structural groups within the molecule. For example, the absorption observed in the UV region for the carbonyl group in acetone is of the same wavelength as the absorption from the carbonyl group in diethyl ketone.[153]

1.4.5 Fluorometer (Spectrofluorometer)

A fluorometer or fluorimeter is a device used to measure parameters of fluorescence: its intensity and wavelength distribution of emission spectrum after excitation by a certain spectrum of light. These parameters are used to identify the presence and the amount of specific molecules in a medium. Modern fluorometers are capable of detecting fluorescent molecule of concentrations as low as 1 part per trillion. Fluorescence analysis can be orders of magnitude more sensitive than other techniques. Applications include chemistry, biochemistry, medicine and environmental monitoring.[151]

Fluorescence spectroscopy or fluorometry or spectrofluorometry, is a type of electromagnetic spectroscopy which analyzes fluorescence from a sample. It involves using a beam of light, usually ultraviolet light, that excites the electrons in the molecules of certain compounds and causes them to emit light; typically, but not necessarily, visible light. A complementary technique is the absorption spectroscopy.[151]

1.5 Research Scope

The main objective of this research is to study the self-assembly of an organic material; apo-ferritin, by aligning it onto block copolymer thin films that functions as a template. During further work in this study, the apo-ferritin core was loaded with semiconductor nanocrystals

which are also called quantum dots. The aim is to develop a new device that can be applied in biomedicine, with respect to the astonishing properties of the quantum dots.

In Chapter 2, the focus is on finding the best external influence for the formation of regular long range ordered structure of the PS-*b*-P2VP block copolymer because it is highly desirable to obtain a perpendicular cylindrical structure. This structure is ideal to be used as the template for aligning apo-ferritin or hybrid quantum dots-apo-ferritin. In this study, three types of solvents have been chosen to induce the formation of this structure by applying the solvent annealing method. The solvents chosen for this purpose are; i) THF, which is a good solvent for both blocks, ii) acetone which is the selective solvent for P2VP block and iii) toluene which is the selective solvent for PS block. The surface morphology was observed using an AFM Instrument.

Chapter 3 discusses the process of determining the accurate duration for the solvent annealing treatment process of the PS-*b*-P2VP thin film. The arrangement of the perpendicular cylindrical structure of the PS-*b*-P2VP template has been determined by exposing the thin films in 3 h, 6 h and 9 h of acetic acid vapours and toluene vapours at 21°C. AFM has also been used to observe the surface structure and internal film properties.

In Chapter 4, the affinity adsorbance of ferritin onto PS-*b*-P2VP template surface was investigated by aligning ferritin onto the parallel cylindrical structure of the template. UV etching was used to remove the PS block with the purpose of inducing only P2VP surface on top of the template's surface since P2VP can adsorb the ferritin and PS cannot. This study has also proven that the pH value of ferritin also played an important role in the absorbance process. AFM was used to monitor the affinity of ferritin onto PS-*b*-P2VP template.

The method of synthesizing apo-ferritin containing CdS QDs has been discussed in Chapter 5. The critical point for this study was to get a good coating of apo-ferritin with CdS and non-agglomeration occurred upon CdS-Apo-ferritin array onto the PS-*b*-P2VP template. In this study, AFM, SEM and TEM were used to observe samples. Meanwhile, UV-vis and PL has been used to characterize the optical properties and to identify the chemical component contained in the sample by presenting its spectrum peak.

With the intention of obtaining useful nontoxic CdS QDs with ideal properties that can be applied as bionanosensors, this research has been conducted further and the detailed information can be found in Chapter 6. The CdS-apo-ferritin capped with P2VP micelles has been utilised as drug delivery. AFM, TEM, UV-vis and PL have been used to characterize samples.

References

[1] M. Knez, A. M. Bittner, F.Boes, C. Wege, H. Jeske, E. Maiâ, K. Kern, *Nano Letters* **2003**, *3(8)*, 1079.

[2] Information on http://en.wikipedia.org/wiki/Nanotechnology

[3] Information on http://en.wikipedia.org/wiki/Top-down_and_bottom-up_design

[4] A. Haryono, W. H. Binder, *Small* **2006**, *2(5)*, 600.

[5] G. Whitesides, B. Grzybowski, *Science* **2002**, *295*, 2418.

[6] D. N. Reinhoudt, M. Crego-Calama, *Science* **2002**, *295*, 2403.

[7] O. Ikkala, G. ten Brinke, *Science* **2002**, *295*, 2407.

[8] S. Svenson, D. A. Tomalia, *Adv. Drug Delivery Rev.* **2005**, *57*, 2106.

[9] E. Katz, I. Willner, *Angew. Chem. Int. Ed.* **2004**, *43*, 6042.

[10] C. P. Collier, T. Vossmeyer, J. R. Heath, *Annu. Rev. Phys. Chem.* **1998**, *49*, 371.

[11] M. P. Pileni, *J. Phys. Chem. B* **2001**, *105*, 3358.

[12] G. Schmid, U. Simon, *Chem. Commun.* **2005**, 697.

[13] S. Liu, T. Zhu, R. Hu, Z. Liu, *Phys. Chem. Chem. Phys.* **2002**, *4*, 6059.

[14] E. Rabani, D. R. Reichman, P. L. Geissler, L. E. Brus, *Nature* **2003**, *426*, 271.

[15] K. Soulantica, A. Maisonnat, M. C. Fromen, M. J. Casanove, B. Chaudret, *Angew. Chem. Int. Ed.* **2003**, *42*, 1945.

[16] D. V. Talapin, E. V. Schevchenko, C. B. Murray, A. Kornowski, S. Fçrster, H. Weller, *J. Am. Chem. Soc.* **2004**, *126*, 12984.

[17] Z. Y. Tang, N. A. Kotov, *Adv. Mater.* **2005**, *17*, 951.

[18] D. Xia, D. Li, Y. Luo, S. R. J. Brueck, *Adv. Mater.* **2006**, *18*, 930.

[19] X. C. Wu, L. F. Chi, H. Fuchs, *Eur. J. Inorg. Chem.* **2005**, 3729.

[20] W. P. Halperin, *Rev. Mod. Phys.* **1986**, *58*, 533.

[21] H. Weller, *Angew. Chem. Int. Ed.* **1993**, *32*, 4.

[22] M. Nirmal, L. Brus, *Acc. Chem. Res.* **1999**, *32*, 407.

[23] C. Burda, X. Chen, R. Narayanan, M. A. El-Sayed, *Chem. Rev.* **2005**, *105*, 1025.

[24] M. A. El-Sayed, *Acc. Chem. Res.* **2004**, *37*, 326.

[25] S. Eustis, M. A. El-Sayed, *Chem. Soc. Rev.* **2006**, *35*, 209.

[26] U. Simon, in: "*Nanoparticles from Theory to Application"*, G. Schmid, Ed., Wiley-VCH, Weinheim, **2004**, p.328.

[27] B. Yu, M. Meyyappan, *J. Solid State Electrochem.* **2006**, *50*, 536.

[28] A. N. Shipway, E. Katz, I. Willner, *Chem. Phys. Chem.* **2000**, *1*, 18.

[29] N. L. Rosi, C. A. Mirkin, *Chem. Rev.* **2005**, *105*, 1547.

[30] S. Mukerjee, in: "*Catalysis and electrocatalysis at nanoparticle surfaces"*, A. Wieckowski, E. R. Savinova, C. G. Vayenas, Eds., Marcel Dekker, New York, **2003**, p.501.

[31] C. P. Collier, T. Vossmeyer, J. R. Heath, *Annu. Rev. Phys. Chem.* **1998**, *49*, 371.

[32] C. B. Murray, C. R. Kagan, M. G. Bawendi, *Annu. Rev. Mater. Sci.* **2000**, *30*, 545.

[33] S. Sun, S. Anders, T. Thomson, J. E. E. Baglin, M. F. Toney, H. F. Hamann, C. B. Murray, B. D. Terris, J. *Phys. Chem. B* **2003**, *107*, 5419.

[34] J. J. Urban, D. V. Talapin, E. V. Shevchenko, C. B. Murray, *J. Am. Chem. Soc.* **2006**, *128*, 3248.

[35] M. Giersig, M. Hilgendorff, *Eur. J. Inorg. Chem.* **2005**, 3571.

[36] M. P. Pileni, *J. Phys. Chem. B* **2001**, *105*, 3358.

[37] M. P. Pileni, Y. Lalatonne, D. Ingert, I. Lisiecki, A. Courty, *Faraday Discuss.* **2004**, *125*, 251.

[38] G. Bognolo, *Adv. Colloid Interface Sci.* **2003**, *106*, 169.

[39] R. Glass, M. Mçller, J. P. Spatz, *Nanotechnology* **2003**, *14*, 1153.

[40] S. Kinge, M. Crego-Calama, D. N. Reinhoudt, *Chem. Phys. Chem.* **2008**, *9*, 20.

[41] I. H. J. Arellano, J. Mangadlao, I. Ramiro, K. Suazo, *Materials Letters* **2010**, *64(6)*, 785.

[42] J. C. Zhoua, X. Wang, M. Xue, Z. Xua, T. Hamasaki, Y. Yang, K. Wang, B. Dunn, *Materials Science and Engineering C* **2010**, *30*, 20.

[43] S. R. Hall, *Proc. R. Soc. A* **2009**, *465*, 335.

[44] P. A. Smith, C. D. Nordquist, T. N. Jackson, T.S. Mayer, *Appl. Phys. Lett.* **2000**, *77*, 1399.

[45] C. M. Niemeyer, *Angew. Chem., Int. Ed.* **2001**, *40*, 4128.

[46] Q. Gu, C. Cheng, R. Gonela, S. Suryanarayanan, S. Anabathula, K. Dai, D. T. Haynie, *Nanotechnology* **2006**, *17*, R14.

[47] P. Deymier, *Advanced Packaging* **2004**, 15.

[48] S. Sotiropoulou, Y. Sierra-Sastre, S. S. Mark, C. A. Batt, *Chem. Mater.* **2008**, *20*, 821.

[49] R. Djalali, Y. F. Chen, H. Matsui, *J. Am. Chem. Soc.* **2002**, *124*, 13660.

[50] M. Reches, E. Gazit, *Science* **2002**, *300*, 625.

[51] A. Satti, D. Aherne, D. Fitzmaurice, *Chem. Mater. (Comm.)* **2007**, *19*, 1543.

[52] G. Braun, K. Inagaki, R. R. Estabrook, D. K. Wood, E. Levy, A. N. Cleland, G. F. Strouse, N. O. Reich, *Langmuir* **2005**, *21*, 10699.

[53] C. Mao, D. J. Solis, B. D. Reiss, S. T. Kottmann, R. Y. Sweeney, A. Hayhurst, G. Georgiou, B. Iverson, A. M. Belcher, *Science* **2004**, *303*, 213.

[54] C. Mao, C. E. Flynn, A. Hayhurst, R. Sweeney, J. Qi, G. Georgiou, B. Iverson, A. M. Belcher, *Proc. Natl. Acad. Sci.* **2003**, *100*, 6946.

[55] S. W. Lee, C. Mao, C. E. Flynn, A. M. Belcher, *Science* **2002**, *296*, 892.

[56] Y. Huang, C. Y. Chiang, S.K. Lee, Y. Gao, E. L. Hu, J. D. Yoreo, A. M. Belcher, *Nano Lett.* **2005**, *5*, 1429.

[57] E. Dujardin, C. Peet, G. Stubbs, J. N. Culver, S. Mann, *Nano Lett.* **2003**, *3*, 413.

[58] W. Shenton, T. Douglas, M. Young, G. Stubbs, S. Mann, *Adv.Mater.* **1999**, *11*, 253.

[59] M. T. Kumara, B. C. Tripp, S. Muralidharan, *Chem. Mater.* **2007**, *19*, 2056.

[60] T. Scheibel, R. Parthasarathy, G. Sawicki, X. M. Lin, H. Jaeger, S. L. Lindquist, *Proc. Natl. Acad. Sci.* **2003**, *100*, 4527.

[61]M. Uchida, M. T. Klem, M. Allen, P. Suci, M. Flenniken, E. yGillitzer, Z. Varpness, L. O. Liepold, M. Young , T. Douglas, *Adv. Mater.* **2007**, *19*, 1025.

[62] T. Douglas, in: "*Biomimetic Approaches in Materials Science"*, S. Mann, Ed., VCH Publishers, New York, **1996**, p.91.

[63] F. C. Meldrum, V. J. Wade, D. L. Nimmo, B. R. Heywood, S. Mann, *Nature* **1991**, *349*, 684.

[64] K. K. W. Wong, S. Mann, *Adv. Mater.* **1996**, *8*, 928.

[65] T. Douglas, V. T. Stark, *Inorg. Chem.* **2000**, *39*, 1828.

[66] M. Okuda, K. Iwahori, I. Yamashita, H. Yoshimura, *Biotechnol. Bioeng.* **2003**, *84*, 355.

[67] T. Ueno, M. Suzuki, T. Goto, T. Matsumoto, K. Nagayama, Y. Watanabe, *Angew. Chem., Int. Ed.* **2004**, *43*, 2527.

[68] R. M. Kramer, C. Li, D. C. Carter, M. O. Stone, R. R. Naik, *J. Am. Chem. Soc.* **2004**, *126*, 13282.

[69] I. Yamashita, J. Hayashi, M. Hara, *Chem. Lett.* **2004**, *33*, 1158.

[70] K. Iwahori, K. Yoshizawa, M. Muraoka, I. Yamashita, *Inorg. Chem.* **2005**, *44*, 6393.

[71] K. Uto, K. Yamamoto, N. Kishimoto, M. Muraoka, T. Aoyagi, I. Yamashita, *J. Mater. Chem.* **2008**, *18*, 3876.

[72] M. Y. Paik, J. K. Bosworth, D. M. Smilges, E. L. Schwartz, X. Andre, C. K. Ober, *Macromolecules* **2010**, *43(9)*, 4253.

[73] S. B. Darling, *Prog. Polym. Sci.* **2007**, *32*, 1152.

[74] F. S. Bates, G. H. Fredrickson, *Block copolymers-designer soft materials*, *Physics Today* **1999**, *52(2)*, 32.

[75] G. E. Molau, "*Colloidal and morphological behavior of block and graft copolymers*", Plenum Press, New York **1971**, p.327.

[76] A. Noshay, J. E. McGrath, "*Block copolymers: overview and critical survey*", Academic Press, New York **1977**, p.526.

[77] R. B. Gallot, *Adv. Polym. Sci.* **1978**, *29*, 85.

[78] G. Riess, G. Hurtrez, P. Bahadur, "*Block copolymers: encyclopedia of polymer science and engineering*", Wiley-Interscience, New York, **1985**, p.324.

[79] I. W. Hamley, "Developments in block copolymer science and technology", John Wiley & Sons, New York **2004**, p.1.

[80] N. Hadjichristidis, S. Pispas, G. Floudas, *"Block copolymers: synthetic strategies, physical properties, and applications"*, Wiley-Interscience, New Jersey **2003**, p.325.

[81] T. P. Lodge, *Macromol. Chem. Phys.* **2003**, *204*, 265.

[82] C. D. Han, *"Rheology and processing of polymeric materials: vol 1, polymer rheology"*, Oxford University Press, New York **2007**, p.296.

[83] T. Hashimoto, in: "*Order–disorder transition in block copolymer"*, N. R. Legge, G. Holden, H. E. Schroeder, Eds., Hanser Publishers, Munich **1987**, p.349.

[84] E. Helfand, Z. R. Wasserman, in: *"Microdomain structure and the interface in block copolymers"*, I. Goodman, Ed., Applied Science, New York **1982**, p.99.

[85] L. Leibler, *Macromolecules* **1980**, *13*, 1602.

[86] J. K. Kim, S. Y. Yang, Y. Lee, Y. Kim, *Progress in Polymer Science* **2010**, *35*, 1325.

[87] F. S. Bates, G. H. Fredrickson, *Annu. Rev. Phys. Chem.* **1990**, *41*, 525.

[88] L. Leibler, *Macromolecules* **1980**, *13*, 1602.

[89] C. Xue, M. A. B. Meador, L. Zhu, J. J. Ge, S. Z. D. Cheng, S. Putthanarat, R. K. Eby, A. Khalfan, G. D. Bennett, S. G. Greenbaum, *Polymer* **2006**, *47*, 6149.

[90] S. Park, D. H. Lee, J. Xu, B. Kim, S. W. Hong, U. Jeong, T. Xu, T. P. Russell, *Science* **2009**, *323(5917)*, 1030.

[91] E. J. W. Crossland, M. Kamperman, M. Nedelcu, C. Ducati, U. Wiesner, D. M. Smilgies, G. E. S. Toombes, M. A. Hillmyer, S. Ludwigs, U. Steiner, H. J. Snaith, *Nano Letters* **2008**, *9(8)*, 2807.

[92] R. Zhang, H. Yokoyama, *Macromolecules* **2009**, *42*, 3559.

[93] M. Li, K. Douki, K. Goto, X. Li, C. Coenjarts, D. M. Smilgies, C. K. Ober, *Chemistry of Materials* **2004**, *16(20)*, 3800.

[94] B. Lee, J. Yoon, W. Oh, Y. Hwang, K. Heo, K. S. Jin, J. Kim, K. W. Kim, M. Ree, *Macromolecules* **2005**, *38(8)*, 3395.

[95] D. Braga, G. Horowitz, *Advanced Materials* **2009**, *2*, 1473.

[96] M. C. Iovu, R. Zhang, J. R. Cooper, D. M. Smilgies, A. E. Javier, E. E. Sheina, T. Kowalewski, R. D. McCullough, *Macromolecular Rapid Communications* **2007**, *28(17)*, 1816.

[97] E. Kaditi, G. Mountrichas, S. Pispas, *European Polymer Journal* **2011**, *47(4)*, 415.

[98] D. R. Wang, J. P. Liu, G. Ye, X. G. Wang, *Polymer* **2009**, *50*, 418.

[99] S. M. Peng, Y. Chen, C. Hua, C. M. Dong, *Macromolecules* **2009**, *42*, 104.

[100] W. S. Wang, Y. L. Guo, J. U. Otaigbe, *Polymer* **2008**, *49*, 4393.

[101] S. Strandman, A. Zarembo, A. A. Darinskii, B. Lo¨flund, S. J. Butcher, H. Tenhu, *Polymer* **2007**, *48*,7008.

[102] X. Z. Tang, Y. C. Hu, C. Y. Pan, *Polymer* **2007**, *48*, 6354.

[103] T. Li, J. P. Lin, T. Chen, S. N. Zhang, *Polymer* **2006**, *47*, 4485.

[104] J. P. Lin, J. Q. Zhu, T. Chen, S. L. Lin, C. H. Cai, L. S. Zhang, et al., *Biomaterials* **2009**, *30*,108.

[105] Y. Y. He, Z. B. Li, P. Simone, T. P. Lodge, *J. Am. Chem. Soc.* **2006**, *128*, 2745.

[106] G. Gaucher, M. H. Dufresne, V. P. Sant, N. Kang, D. Maysinger, J. C. Leroux. *J. Controlled Release* **2005**, *109*, 169.

[107] D. E. Discher, A. Eisenberg, *Science* **2002**, *297*, 967.

[108] K. Akiyoshi, N. Maruichi, M. Kohara, S. Kitamura, *Biomacromolecules* **2002**, *3*, 280.

[109] Z. Hu, X. Fan, H. Wang, J. Wang, *Polymer* **2009**, *50*, 4175.

[110] A. A. Khaydarov, I. W. Hamley, T. M. Legge, S. Perrier, *European Polymer Journal* **2007**, *43*, 789.

[111] I. W. Hamley, *Nanotechnology* **2003**, *14*, R39.

[112] D. G. Walton, G. J. Kellogg, A. M. Mayes, P. Lambooy, T. P. Russell, *Macromolecules* **1994**, *27*, 6225.

[113] C. M. Grozea, N. Gunari, J. A. Finlay, D. Grozea, M. E. Callow, J. A. Callow, Z. H. Lu, G. C. Walker, *Biomacromolecules* **2009**, *10(4)*, 1004.

[114] A. P. Alivisatos, *Science* **1996**, *271*, 933.

[115] X. Michalet, F. F. Pinaud, L. A. Bentolila, J. M. Tsay, S. Doose, J. J. Li, G. Sundaresan, A. M. Wu, S. S. Gambhir , S. Weiss, *Science* **2004**, *307*, 538.

[116] I. L. Medintz, H. T. Uyeda, E. R. Goldman, H. Mattoussi, *Nat. Mater.* **2005**, *4*, 435.

[117] A. M. Derfus, W. C. W. Chan, S. N. Bhatia, *Nano Lett.* **2004**, *4*, 11.

[118] G. Oberdorster, V. Stone and K. Donaldson, *Nanotoxicology* **2007**, *1*, 2.

[119] E. Chang, N. Thekkek, W. W. Yu, V. L. Colvin, R. Drezek, *Small* **2006**, *2*, 1412.

[120] C. Kirchner, T. Liedl, S. Kudera, T. Pellegrino, A. M. Javier, H. E. Gaub, S. Sto¨lzle, N. Fertig, W. J. Parak, *Nano Lett.* **2005**, *5*, 331.

[121] N. Ma, J. Yang, K. M. Stewart, S. O. Kelley, *Langmuir* **2007**, *23*, 12783.

[122] G. Konstantatos, I. Howard, A. Fischer, S. Hoogland, J. Clifford, E. Klem, L. Levina, E. H. Sargent, *Nature* **2006**, *442*, 180.

[123] I. Gur, N. A. Fromer, M. L. Geier, A. P. Alivisatos, *Science*, **2005**, *310*, 462.

[124] D. V. Talapin, C. B. Murray, *Science* **2005**, *310*, 86.

[125] L. Manna, E. C. Scher , A. P. Alivisatos, *J. Am. Chem. Soc.* **2000**, *122*, 12700.

[126] B. O. Dabbousi, J. Rodriguez-Viejo, F. V. Mikulec, J. R. Heine, H. Mattoussi, R. Ober, K. F. Jensen, M. G. Bawendi, *J. Phys. Chem. B* **1997**, *101*, 9463.

[127] J. Ziegler, R. T. Chang, D. W. Wright, *J. Am. Chem. Soc.* **1999**, *121*, 2395.

[128] R. Djalali, Y. Chen, H. Matsui, *J. Am. Chem. Soc.* **2002**, *124*, 13660.

[129] F. C. Meldrum, V. J. Wade, D. L. Nimmo, B. R. Heywood, S. Mann, *Nature* **1991**, *349*, 684.

[130] M. Allen, D. Willits, J. Mosolf, M. Young, T. Douglas, *Adv. Mater.* **2002**, *14*, 1562.

[131] M. Reches, E. Gazit, *Science* **2003**, *300*, 625.

[132] N. Nuraje, K. Su, A. Haboosheh, J. Samson, E. P. Manning, N. Yang, H. Matsui, *Adv. Mater.* **2006**, *18*, 807.

[133] S. Y. Lee, X. Gao, H. Matsui, *J. Am. Chem. Soc.* **2007**, *129*, 2954.

[134] T. Ueno, M. Suzuki, T. Goto, T. Matsumoto, K. Nagayama, Y. Watanabe, *Angew. Chem., Int. Ed.* **2004**, *43*, 2527.

[135] N. Ma, E. H. Sargent, S. O. Kelley, *J. Mater. Chem.* **2008**, *18*, 954.

[136] A. Noshay, J. E. McGrath, "*Block Copolymers, Overview and Critical Survey"*, Academic Press, New York **1977**,p.56.

[137] S. Fçrster, M. Konrad, *J. Mater. Chem.* **2003**, *13*, 2671.

[138] M. J. Fasolka, A. M. Mayes, *Annu. Rev. Mater. Res.* **2001**, *21*, 323.

[139] I. W. Hamley, *Nanotechnology* **2003**, *14*, 39.

[140] S. W. Yeh, T. L. Wu, K. H. Wei, Y. S. Sun, K. S. Liang, *J. Polym. Sci. Part B: Polym. Lett.* **2005**, *43*,1220.

[141] S. W. Yeh, T. L. Wu, K. H. Wei, *Nanotechnology* **2005**, *16*, 683.

[142] C. W. Wang, M. G. Moffitt, *Langmuir* **2004**, *20*, 11784.

[143] C. W. Wang, M. G. Moffitt, *Langmuir* **2005**, *21*, 2465.

[144] M. Zhang, M. Drechsler, A. H. E. M. Kller, *Chem. Mater.* **2004**, *16*, 537.

[145] B. J. S. Johnson, J. H. Wolf, A. S. Zalusky, M. A. Hillmyer, *Chem. Mater.* **2004**, *16*, 2909.

[146] J. Peng, D. H. Kim, W. Knoll, Y. Xuan, B. Li, Y. Han, *The J. Of Chem. Phys.* **2006**, *125*, 064702.

[147] Information on http://www.jic.ac.uk/microscopy/intro_em.html

[148] Information on http://en.wikipedia.org/wiki/Scanning_electron_microscope

[149] Information on http://ncf.colorado.edu/?p=instruments&sub=descriptions&subsub=fesem

[150] Information on http://en.wikipedia.org/wiki/Ultraviolet%E2%80%93visible_spectroscopy

[151] Information on http://en.wikipedia.org/wiki/Fluorometer

2

Influence of Temperature and Type of Solvents on the Microdomain Orientation of PS-*b*-P2VP Ultrathin Films by Solvent Annealing

2.1 Introduction

Block copolymers (BCPs) can self-assemble via microphase separation into a range of well-defined ordered nanostructures including spheres, cylinders, lamellae and double gyroids, depending on the relative volume fraction of the constituent polymers.[1-4] Several methods including electric field alignment,[5,6] solvent-annealing,[7,8] surfactant assisted assembly,[9] self-assembly on brush surfaces,[10-19] and directed assembly on chemically patterned surfaces[12,20-25] have been explored to induce perpendicular orientation of BCP microdomains in thin films.

When BCPs are fabricated into thin films with nanoscaled thicknesses, the effects of two additional interactions become significant, which are the polymer-substrate and polymer-air interactions. The phase that interacts most strongly with the substrate surface tends to stick on the substrate while the phase with the lowest surface tension tends to be exposed to air. Both forces regulate the alignment of the microdomains. When the thicknesses of films are less than the influential range of the interactions, the microdomains in the entire films will be

forced to orient along the direction of the thickness. In most cases, cylindrical or lamellar microdomains prefer to align parallel to the substrate surfaces.[26]

However, perpendicular orientation of microdomains in BCPs thin films is more desirable in preparation of nanoscaled templates for pattern transfer applications ranging from magnetic storage to optoelectronic materials, etching masks, sensors and scaffolds.[27-32] Recently, it has been demonstrated that solvent-annealing can be utilized as an important approach to induce long-range order in thin films of BCPs.[33-42] Solvent-annealing is usually adopted to replace thermal annealing for thin films since small solvent molecules may evaporate at low temperature and a tiny amount loss of small molecules would result in a great structural change in such thin films.[43] Different from thermal annealing, solvent molecules are the extra components introduced into the films and the final morphology may thus be affected by the interplays between the solvents and the polymers, which on one hand complicates the structure analysis but on the other hand provides an opportunity to create the structures that cannot be achieved by thermal annealing.[44] Use of solvent-annealing, rather than thermal annealing to induce long-range ordering in BCP thin films[45–49] not only induces orientation and ordering, but also may tune the self-assembled morphology reversibly as well.[50] The swelling of both blocks provides sufficient mobility for the chains to rearrange and allows one block to preferentially wet the substrate surface.[51]

If the chosen solvent has selectivity to one of the blocks, the resulting volume change in the swollen state may lead to an order-order transition from the bulk morphology. The newly attained phase may then be kinetically trapped upon fast evaporation of the solvent.[46,52] Relative orientation of the microdomains with respect to the substrate surface depends on the experimental variables, such as the surface field, film thickness, solvent evaporation rate,

solvent selectivity, annealing conditions, etc.[33-42] However, the detailed mechanisms involved in these treatments still remain unclear. Moreover, correlation between the initial morphologies of BCPs thin films spin-cast with different solvents and the resulting morphological developments after solvent annealing has been less considered.[32]

Not many different BCPs have been reported, due to the need to control both the surface energy difference between the two blocks and the interfacial energy difference between each block and the substrate to achieve vertical orientation of the microdomains that propagate entirely across the film thickness. Alternatively, non-equilibrium processing such as solvent-annealing can be used to achieve vertical orientation of copolymers that have a large surface energy difference between their respective blocks, such as polystyrene-*block*-poly(2-vinylpyridine)-*block*-poly(tert-butylmethacrylate) (PS-*b*-P2VP-*b*-PtBMA), polyisoprene-*block*-polylactide (PI-*b*-PLA), and polystyrene-*block*-poly(ethyleneoxide) (PS-*b*-PEO).[53] In this study, polystyrene-*block*-poly(2vinylpyridine) (PS-*b*-P2VP) diblock copolymer is selected because P2VP is an excellent candidate to incorporate nanoparticles and PS-*b*-P2VP can serve as a template to align nanoparticles.[54] The best condition and elucidate the mechanism to obtain the hexagonally close-packed pattern of perpendicular cylinders is discussed in this section.

2.2 Experimental Procedure

2.2.1 Materials

Asymmetric PS-*b*-P2VP diblock copolymer with the molecular weight of 79.0k-*b*-36.5k kg/mol and the polydispersity index of 1.05 was purchased from Polymer Source, Inc.TM. Figure 1 shows the chemical structure of PS-*b*-P2VP. Toluene, tetrahydrofuran (THF) and acetone with reagent grade were used for film casting or solvent-annealing.

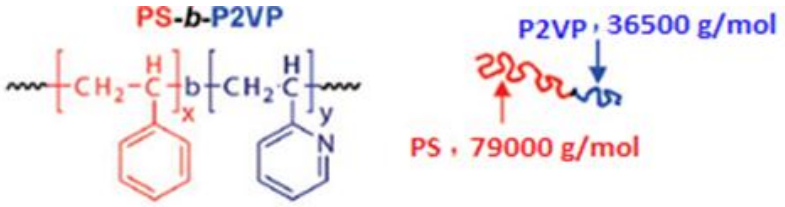

Figure 1: Chemical structure of PS-*b*-P2VP diblock copolymer.

2.2.2 Substrate Preparation

Silicon(100) wafers were cut into 1.0 cm^2 pieces and cleaned in piranha solution, i.e., the substrates were treated with a mixture of H_2O_2 and H_2SO_4 (30/70 vol%/vol%) at 100 °C for 30 minutes, rinsed with distilled water and then dried in nitrogen gas flow. They were subsequently subjected to UV treatment for 15 minutes and used immediately.[55]

2.2.3 Thin film Preparation

Ultrathin films were prepared by spin-coating 1 wt% PS-*b*-P2VP solution in the mixed solvents of toluene and tetrahydrofuran (THF) with 7:3 ratio at 5000 rpm for 20 s onto the silicon substrates.

2.2.4 Solvent Annealing Condition

The ultrathin films were annealed in the atmosphere of saturated solvent vapor using THF, acetone or toluene for 3 h at 20 or 25 °C or for 6 h at 21 °C. Namely the sample films on the substrates were placed on a slide glass on a Petri dish containing 6 ml of solvent and covered with aluminium foil with small holes on it. Then the samples were placed in the glass bottle with a lid. After 3 h or 6 h the films were taken out from the bottle to dry in the ambient atmosphere. The detail's procedure steps has presented in Figure 2.

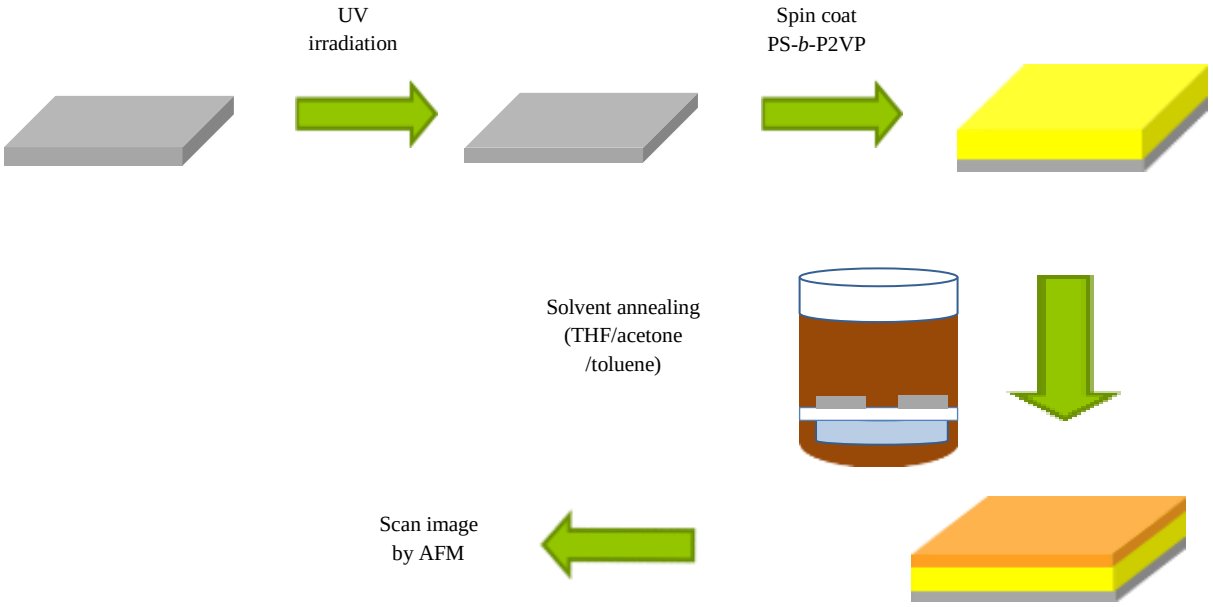

Figure 2: Experimental procedure of making cylindrical pattern of PS-*b*-P2VP block copolymer.

2.2.5 Sample Characterization

Topographical morphology of these thin films were characterized by atomic force microscopy (AFM). AFM was performed with a multimode AFM system of a Nanoscope III scanning probe microscope (Digital Instruments) in tapping mode. The tapping mode was operated by using Olympus cantilevers with spring constants ranging between 39.7 N/m and 71.6 N/m and resonant frequencies of 293.8-356.0 Hz. The oscillating cantilever of contact between tip and sample is 31.753 (A/A_o).

2.3 Results and Discussions

Many reports have shown that the type of solvents used for annealing plays an important role in the morphology of block copolymers thin films. [56–58]

Table 1: List of good and selective solvents for both block copolymers of PS-*b*-P2VP.

Solvents	**PS**	**P2VP**
Benzene, Chloroform, 1,4-dioxane, and Tetrahydrofuran (THF)	Good solvents	Good solvents
Toluene and Methylethylketone (MEK)	Selective solvents	
Acetone and Ethanol		Selective solvents

Benzene, chloroform, 1,4-dioxane and tetrahydrofuran (THF) are good solvents for both PS and P2VP blocks. Toluene and methylethylketone (MEK) are selective solvents for PS block while acetone and ethanol are selective solvents for P2VP block as shown in Table 1.[59] In this experiment, THF, acetone and toluene were selected from each category for solvent-annealing process.

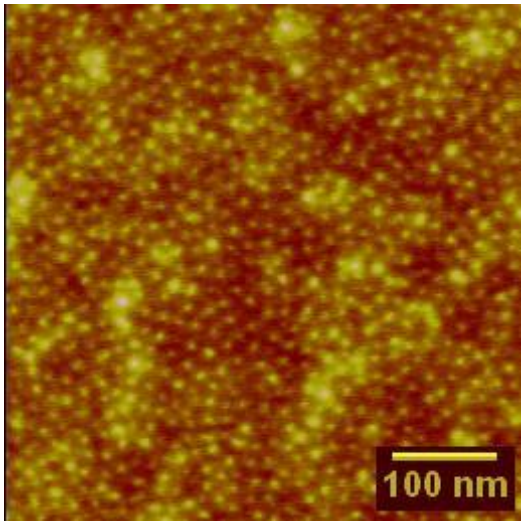

Figure 3: AFM image of PS-*b*-P2VP as-coated thin film from the solution in the mixed solvents of toluene and THF.

The PS-*b*-P2VP BCPs used in this study has a morphology of hexagonally packed P2VP cylindrical microdomains in the PS matrix in its equilibrium state in bulk. The as-coated thin

film onto the silicon substrate exhibits a dotted pattern with irregularly arranged microdomains as shown in Figure 3. Though a long-range order has not been attained, a quasi-hexagonal arrangement of the dot-like structures were observed locally, which is similar to the previous report.[32] According to the volume fraction of each component of PS-*b*-P2VP, P2VP phase should form the spherical or cylindrical microdomains, which are protruding from the surface of the thin film. If they are spherical, it must be the result of higher degree of swelling of the PS matrix phase than the P2VP phase by toluene, which is the major component of the mixed solvents and selective for PS resulting in the thinner PS matrix phase than the P2VP phase on quick removal of the solvents. The morphology of the P2VP microdomains must be spherical because some line-like structure should have been seen if they were cylindrical and irregularly arranged.

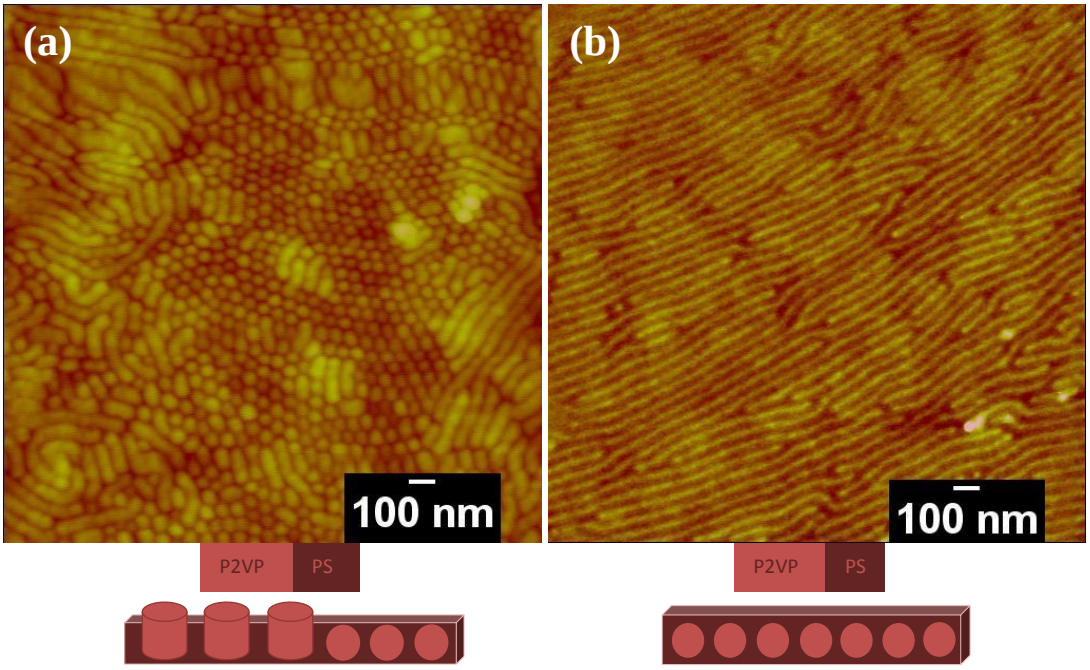

Figure 4: AFM images of PS-*b*-P2VP thin films after solvent-annealing with THF at (a) 20 °C and (b) 25 °C.

The as-coated thin films were then placed in the bottles saturated with vapour of THF, which is a good solvent for both PS and P2VP blocks at 20 or 25 °C and expected to induce a

regular arrangement of the microdomains with a long-range order. Figure 4 shows the AFM topographic images of the thin films after evaporation of THF solvent absorbed during the solvent-annealing process. The thin film solvent-annealed at 20 °C exhibits a mixed pattern with parallel lines and hexagonally close-packed dots as shown in Figure 4 (a) suggesting parallel and perpendicular cylinders to the substrate surface, respectively. The result suggests that the solvent-annealing for 3 h at 20 °C gave enough mobility to change the morphology from P2VP spheres in the as-coated film to the equilibrium morphology of P2VP cylinders. Although the orientation of the cylinders is not uniform, the regularity of the cylinder arrays has been improved. On the other hand, as shown in Figure 4 (b), the PS-*b*-P2VP thin film solvent-annealed for 3 h at 25 °C shows only parallel lines indicating the P2VP cylindrical microdomains all aligned parallel to the film surface. The difference in the two observations can be explained by the higher mobility of the BCPs chains at the higher temperature, which allowed the more relaxed microdomain structure in Figure 4 (b). The initial structure also might affect the morphology in the solvent-annealing process. If the initial morphology is P2VP spherical domains, first they will merge together to form short or perpendicular cylinders (Figure 4 (a)), then to long and parallel cylinders (Figure 4 (b)). Thus, I could observe the process of the structural rearrangement by changing the temperature.

Next, solvent-annealing of the as-coated PS-*b*-P2VP thin films with the same conditions was also performed with the saturated vapor of selective solvent for each block. The solvent-annealing with selective solvent often induces surface roughness resulting from uneven swelling of two microphases, which can be utilized for the facile placement of nanoparticles without further selective etching of one of the microphases.[60]

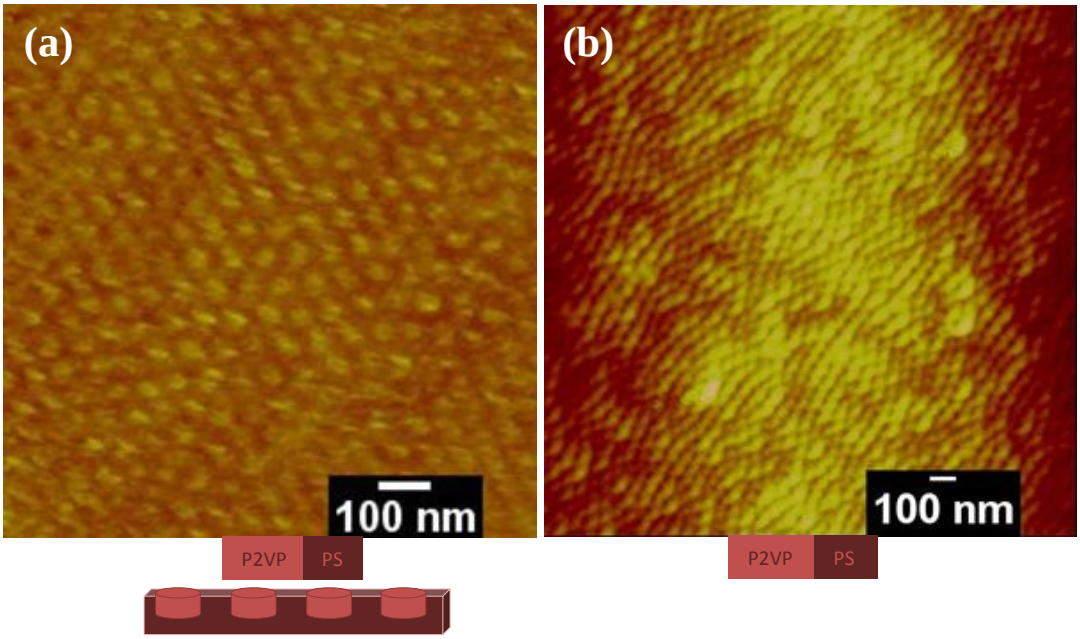

Figure 5: AFM images of PS-*b*-P2VP thin films after solvent-annealing for 3 h at 20 °C with (a) acetone, P2VP-selective solvent and (b) toluene, PS-selective solvent.

In case of PS-*b*-P2VP film treated for 3 h at 20 °C with acetone, P2VP-selective solvent, the AFM image of the thin film exhibited a pattern of hexagonal dots as shown in Figure 5 (a). Selective swelling of the P2VP phase by acetone increased the areal fraction of P2VP phase in exchange for the height contrast. The AFM image seems the P2VP phase is still protruded. The irregular shape of the dots and the partially connected structure of the dots suggest the microdomain structure is in the process of reorganization. Figure 5 (b) shows the surface of the thin film exposed to toluene, PS-selective solvent, for 3 h at 20 °C. The microdomain structure is not clear and the microdomain structure is probably also in the process of reorganization.

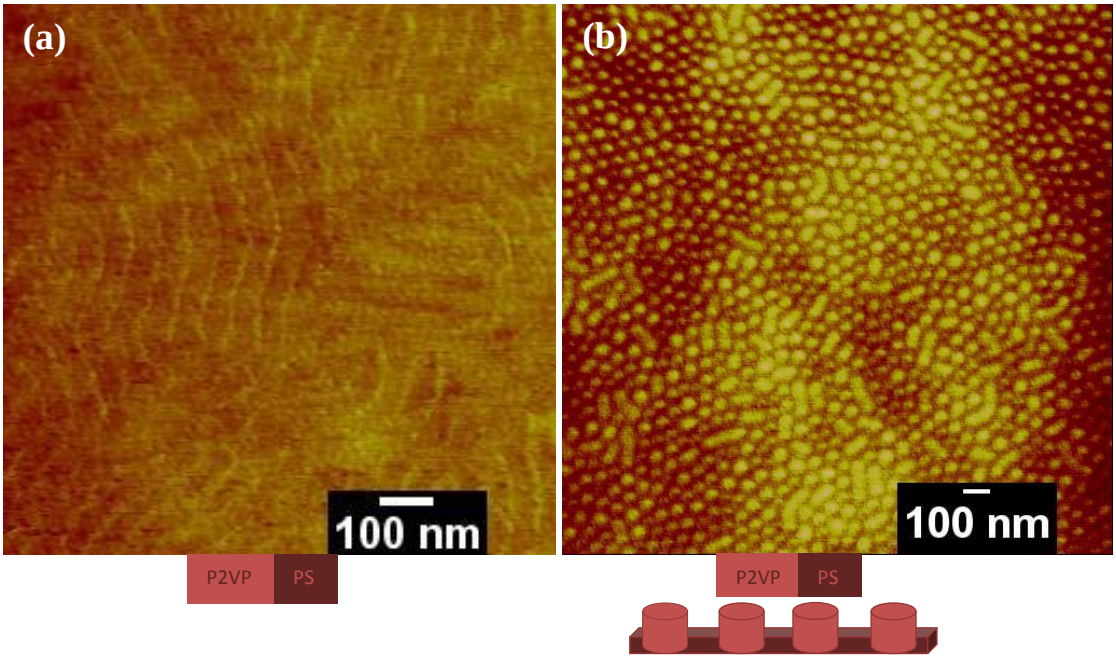

Figure 6: AFM images of PS-*b*-P2VP thin films after solvent-annealing for 3 h at 25 °C with (a) acetone, P2VP-selective solvent and (b) toluene, PS-selective solvent.

Figure 6 (a) shows the AFM height image of the thin film annealed for 3 h at 25 °C with acetone, P2VP selective solvent. The line pattern suggests the microdomain morphology of parallel cylinders or perpendicular lamellae. The extremely uneven areal fraction of dark and bright areas suggests that the height contrast is not in accordance with the areal fraction of each microphase. Taking into the account that acetone is selective solvent for P2VP and its volume fraction increased, it is natural to think that the microdomain morphology has changed to lamellae from the equilibrium morphology of cylinders in bulk. On the other hand, the film exposed to PS-selective toluene vapor for 3 h at 25 °C as shown in Figure 6 (b), the hexagonally packed dot pattern appeared suggesting perpendicularly oriented cylinders. Existence of some elongated microdomains suggests that the bright dots are not spheres but perpendicular cylinders. The P2VP microdomains are protruded with respect to the swollen PS matrix due to selective swelling of the PS domains.[60] Solvent-annealing at higher

temperature provides higher mobility to polymer molecules and the structural reorganization in shorter time. A similar result was reported by Claudia et al. 2011.[61]

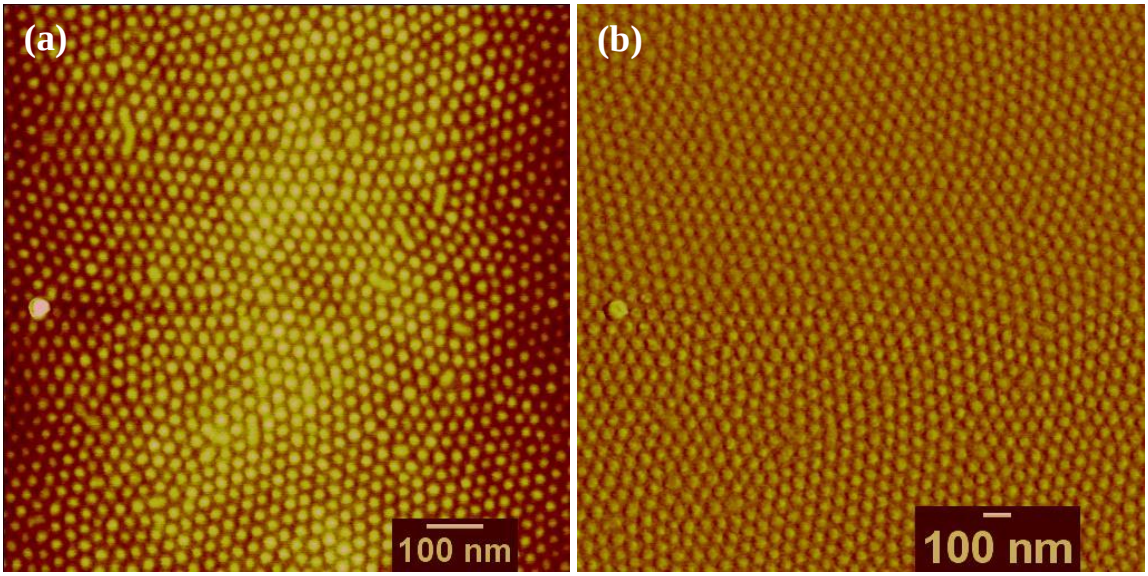

Figure 7: AFM image of PS-*b*-P2VP thin film after solvent-annealing for 6 h at 21 °C with toluene, PS-selective solvents. (a) Topographic image and (b) phase.

Much improved hexagonal dot pattern was obtained as shown in Figure 7 when the as-coated thin film of PS-*b*-P2VP was solvent-annealed for 6 h at 21 °C. The protruded P2VP domains in the topographical image in Figure 7 (a) are perpendicular cylinders and PS matrix swollen more by PS-selective toluene has lower height after removal of the solvent. The improved uniformity of the cylinder size and spacing appears can be recognized much better in the phase image as shown in Figure 7 (b). The longer annealing time allowed the polymer molecules to rearrange to form more regular structure close to the equilibrium. The spacing of the cylinders in Figure 7 was estimated to be 54 nm by using FFT of the AFM image. Solvent-annealing at lower temperature for longer time seems to give better regularity without affecting the morphology and feature sizes.

The vapor pressure of the annealing-solvent may play an important role to reorganize the microdomain structure. Solvent with lower boiling point has higher vapour pressure. The boiling points at atmospheric pressure are 110.6 °C, 66 °C and 56-57 °C for toluene, THF and acetone, respectively. Therefore, toluene with the highest boiling point must have needed the longest annealing time to attain the equilibrium morphology in the swollen state.

The equilibrium morphology of the swollen thin film with the annealing solvent should depend on the partition of the solvent to each microphase of PS-*b*-P2VP and interface interaction between each swollen microphase and the substrate surface. In the case of this study, acetone changed the microdomain morphology from cylinders to lamellae by changing the apparent volume fraction of the swollen PS and P2VP microphases. THF probably did not change the volume fraction of each microphase and the morphology, and did not neutralize the interfacial interaction either. To obtain the perpendicular orientation of P2VP cylinders of PS-*b*-P2VP in the thin film in equilibrium by solvent-annealing, it is necessary to neutralize the interaction of the two microphases against the substrate surface. Although toluene is a selective solvent for PS, the partition of the solvent in the swollen thin film must have been just in the range to neutralize the interface interaction of the two microphases without changing the morphology. For better understanding, it is necessary to investigate the interfacial interaction between the swollen polymer with the annealing solvent and the substrate and the study is deserved for future.

2.4 Conclusion

Solvent-annealing with selective solvent is an effective technique to control microdomain morphology and orientation in BCPs thin films on substrates. The type of annealing solvent and temperature play important roles to control the interfacial interaction between the swollen

BCPs thin films and the substrates in equilibrium. They also determine the necessary annealing time to attain the equilibrium by giving the kinetic effect in terms of the mobility of the BCPs molecules. I have demonstrated that PS-*b*-P2VP was successfully patterned to form perpendicular cylinders on silicon surface by solvent-annealing at room temperature with toluene which is selective solvent for PS block.

There have two reasons of causing BCP reorganization. First, at 20 °C BCPs molecules in low mobility state because of toluene is solvent with high boiling point; hence need more kinetic energy from surrounded temperature. Therefore, when the temperature has increased to 25 °C, the BCPs molecules could be moving to well organize structure of perpendicular cylinder. The other reason is cause of the mobility of BCPs molecules has occurred due to low BCPs concentration that has contained little molecules. Thus, the solvent has enough energy (driving force) to mobile BCPs molecules in present of kinetic effect.

References

[1] I. W. Hamley, *"The physics of block copolymers"*, Oxford University Press, New York **1998**.

[2] G. H. Fredrickson, F. S. Bates, *Annu Rev Mater Sci.* **1996**, *26*, 501.

[3] T. Hashimoto, M. Shibayama, M. Fujimura, H. Kawai, in: *"Block copolymers, science and technology"*, D. J. Meier, Ed., Harwood Academic, London **1983**, p.63.

[4] M. J. Fasolka, A. M. Mayes, *Annu Rev Mater Res.* **2001**, *31*, 323.

[5] K. Amundson, E. Helfand, D. D. Davis, X. Quan, S. S. Patel, S. D. Smith, *Macromolecules* **1991**, *24*, 6546.

[6] T. L. Morkved, M. Lu, A. M. Urbas, E. E. Ehrichs, H. M. Jaeger, P. Mansky, T. P. Russell, *Science* **1996**, *273*, 931.

[7] S. H. Kim, M. J. Misner, T. P. Russell, *AdV. Mater.* **2004**, *16*, 2119.

[8] S. H. Kim, M. J. Misner, T. Xu, M. Kimura, T. P. Russell, *AdV. Mater.* **2004**, *16*, 226.

[9] J. G. Son, X. Bulliard, H. Kang, P. F. Nealey, K. Char, *AdV. Mater.* **2008**, *20*, 3643.

[10] R. D. Peters, X. M. Yang, T. K. Kim, B. H. Sohn, P. F. Nealey, *Langmuir* **2000**, *24*, 4625.

[11] R. D. Peters, X. M. Yang, Q. Wang, J. J. de Pablo, P. F. J. Nealey, *Vac. Sci. Technol. B* **2000**, *18*, 3530.

[12] S. O. Kim, H. H. Solak, M. P. Stoykovich, N. J. Ferrier, J. J. de Pablo, P. F. Nealey, *Nature* **2003**, *424*, 411.

[13] R. D. Peters, X. M. Yang, T. K. Kim, P. F. Nealey, *Langmuir* **2000**, *24*, 9620.

[14] S. Ji, G. Liu, F. Zheng, G. S. W. Craig, F. J. Himpsel, P. F. Nealey, *AdV. Mater.* **2008**, *20*, 3054.

[15] P. Mansky, Y. Liu, E. Huang, T. P. Russell, C. Hawker, *Science* **1997**, *275*, 1458.

[16] D. Y. Ryu, K. Shin, E. Drockenmuller, C. J. Hawker, T. P. Russell, *Science* **2005**, *308*, 236.

[17] I. In, Y. H. La, S. M. Park, P. F. Nealey, P. Gopalan, *Langmuir* **2006**, *22*, 7855.

[18] E. Han, I. In, Y. La, S. Park, Y. Wang, P. F. Nealey, P. Gopalan, *AdV. Mater.* **2007**, *19*, 4448.

[19] J. Bang, J. Bae, P. Lo¨wenhielm, C. Spiessberger, S. A. Given-Beck, T. P. Russell, C. J. Hawker, *AdV. Mater.* **2007**, *19*, 4552.

[20] E. W. Edwards, M. F. Montague, H. H. Solak, C. J. Hawker, P. F. Nealey, *AdV. Mater.* **2004**, *16*, 1315.

[21] E. W. Edwards, M. Muller, M. P. Stoykovich, H. H. Solak, J. J. de Pablo, P. F. Nealey, *Macromolecules* **2007**, *40*, 90.

[22] Y. H. La, E. W. Edwards, S. M. Park, P. F. Nealey, *Nano Lett.* **2005**, *5*, 1379.

[23] M. P. Stoykovich, E. W. Edwards, H. H. Solak, P. F. Nealey, *Phys. ReV. Lett.* **2006**, *97*, 147802.

[24] M. P. Stoykovich, M. Muller, S. O. Kim, H. H. Solak, E. W. Edwards, J. J. de Pablo, P. F. Nealey, *Science* **2005**, *308*, 1442.

[25] S. M. Park, G. S. W. Craig, Y. H. La, H. H. Solak, P. F. Nealey, *Macromolecules* **2007**, *40*, 5084.

[26] W. H. Huang, P. Y. Chen, S. H. Tung, *Macromolecules* **2012**, *45*, 1562.

[27] C. T. Black, K. W. Guarini, K. R. Milkove, S. M. Baker, T. P. Russell, M. T. Tuominen, *Appl. Phys. Lett.* **2001**, *79*, 409.

[28] C. T. Black, *Appl. Phys. Lett.* **2005**, *87*, 163116.

[29] K. W. Guarini, C. T. Black, K. R. Milkove, R. L. J. Sandstrom, *Vac. Sci. Technol. B* **2001**, *19*, 2784.

[30] J. Y. Cheng, C. A. Ross, V. Z. H. Chan, E. L. Thomas, R. G. H. Lammertink, G. J. Vancso, *AdV. Mater.* **2001**, *13*, 1174.

[31] M. Park, C. Harrison, P. M. Chaikin, R. A. Register, D. H. Adamson, *Science* **1997**, *276*, 1401.

[32] X. Li, J. Peng, Y. Wen, D. H. Kim, W. Knoll, *Polymer* **2007**, *48*, 2434.

[33] S. Niu, R. F. Saraf, *Macromolecules* **2003**, *36*, 2428.

[34] G. Kim, M. Libera, *Macromolecules* **1998**, *31*, 2569.

[35] P. Alexandridis, R. J. Spontak, *Curr. Opin. Colloid Interface Sci.* **1999**, *4*, 130.

[36] K. Fukunaga, H. Elbs, R. Magerle, G. Krausch, *Macromolecules* **2000**, *33*, 947.

[37] Y. Xuan, J. Peng, L. Cui, H. Wang, B. Li, Y. Han, *Macromolecules* **2004**, *37*, 7301.

[38] J. Peng, D. H. Kim, W. Knoll, Y. Xuan, B. Y. Li, Y. C. Han, *J. Chem. Phys.* **2006**, *125*, 064702.

[39] J. Peng, Y. Xuan, H. F. Wang, B. Y. Li, Y. C. Han, *Polymer* **2005**, *46*, 5767.

[40] Y. Cong, Z. X. Zhang, J. Fu, J. Li, Y. C. Han, *Polymer* **2005**, *46*, 5377.

[41] J. C. Zhao, S. C. Jiang, X. L. Ji, L. J. An, B. Z. Jiang, *Polymer* **2005**, *46*, 6513.

[42] X. Han, H. Liu, Y. Dong, Y. H. Chin, *J. Chem Eng.* **2005**, *13*, 498.

[43] S. H. Tung, N. C. Kalarickal, J. W. Mays, T. Xu, *Macromolecules* **2008**, *41(17)*, 6453.

[44] S. Park, B. Kim, J. Xu, T. Hofmann, B. M. Ocko, T. P. Russell, *Macromolecules* **2009**, *42(4)*, 1278.

[45] J. K. Bosworth, M. Y. Paik, R. Ruiz, E. L. Schwartz, J. Q. Huang, A. W. Ko, D. M. Smilgies, C. T. Black, C. K. Ober, *ACS Nano* **2008**, *2(7)*, 1396.

[46] S. Park, D. H. Lee, J. Xu, B. Kim, S. W. Hong, U. Jeong, T. Xu, T. P. Russell, *Science* **2009**, *323(5917)*, 1030.

[47] V. Olszowka, M. Hund, V. Kuntermann, S. Scherdel, L. Tsarkova, A. Boker, *ACS Nano* **2009**, *3(5)*, 1091.

[48] S. H. Kim, M. J. Misner, T. Xu, M. Kimura, T. P. Russell, *Advanced Materials* **2004**, *16(3)*, 226.

[49] T. H. Kim, J. Hwang, W. S. Hwang, J. Huh, H. C. Kim, S. H. Kim, J. M. Hong, E. L. Thomas, C. Park, *Advanced Materials* **2008**, *20(3)*, 522.

[50] M. Y. Paik, J. K. Bosworth, D. M. Smilges, E. L. Schwartz, X. Andre, C. K. Ober, *Macromolecules* **2010**, *43(9)*, 4253.

[51] K. A. Cavicchi, K. J. Berthiaume, T. P. Russell, *Polymer* **2005**, 46, 11635.

[52] J. Peng, D. H. Kim, W. Knoll, Y. Xuan, B. Li, Y. Han, *The Journal of Chemical Physics* **2006**, *125*, 064702.

[53] S. X. Ji, C. C. Liu, J. G. Son, K. Gotrik, G. S. W. Craig, P. Gopalan, F. J. Himpsel, K. Char, P. F. Nealey, *Macromolecules* **2008**, *41*, 9098.

[54] S. Akasaka, H. Mori, T. Osaka, V. H. Mareau, H. Hasegawa, *Macromolecules* **2009**, *42*, 1194.

[55] I. In, Y. H. La, S. M. Park, P. F. Nealey, P. Gopalan, *Langmuir* **2006**, *22*, 7855.

[56] Y. Xuan, J. Peng, L. Cui, H. F. Wang, B. Y. Li, Y. C. Han, *Macromolecules* **2004**, *37(19)*, 7301.

[57] H. Elbs, C. Drummer, V. Abetz, G. Krausch, *Macromolecules* **2002**, *35(14)*, 5570.

[58] J. K. Bosworth, M. Y. Paik, R. Ruiz, E. L. Schwartz, J. Q. Huang, A. W. Ko, D. M. Smilgies, C. T. Black, C. K. Ober, *ACS Nano* **2008**, *2(7)*, 1396.

[59] T. Matsuyama, Y. Kawata, *Jpn. J. Appl. Phys.* **2005**, *44(5B)*, 3524.

[60] J. G. Son, W. K. Bae, H. Kang, P. F. Nealey, K. Char, *ACS Nano* **2009**, *3(12)*, 3927.

[61] M. C. Grozea, I. T. S. Li, D. Grozea, G. C. Walker, *Macromolecules* **2011**, *44*, 3901.

3

Controlling Ordered Structures of PS-*b*-P2VP Block Copolymer Thin Film by Tuning Solvent's Annealing Time

3.1 Introduction

PS-*b*-P2VP is an *amphiphilic* block copolymer that exhibits large surface energy differences, which makes it a representative model system for block copolymers with large surface energy differences. In particular, nanometer-sized micellar monolayer films can be prepared from block copolymer micelle solutions using Langmuir-Blodgett self-assembly, dip coating or spin-coating methods, which are versatile as templates for nanostructured materials, where the stability of the morphology is critical in future applications.[1-9] The formation of long-range order in BCPs via solvent-annealing treatment is frequently selected [10–14] because this treatment induces order orientation as well as the self-assembled morphology may be reversibly tuned as well.

For a given A-B block copolymer, a solvent may be classified as good or selective, depending on the extent to which it preferentially swells the microdomains of the copolymer morphology.[17–19] In general, good solvents are distributed near in between the A and B microdomains and decrease the A/B interaction parameter (χ). In other words, neutral solvents can shield the unfavorable contact of blocks. For example, when using A-selective solvent, the A blocks are swollen while the B block tends to collapse the conformation.

Investigations on the solvent selectivity effects have tended to focus on either the melt[18] or dilute solutions,[20-22] where the selectivity drives micellization in the latter. Hence, the effects of solvent selectivity on the solvent-annealing of block copolymer thin films are still not extensively studied.[23]

Marvin et al. 2010 used GISAXS to probe the film's interior during the solvent annealing process in combination with using a film thickness monitor,[24] so that a correlation between swelling ratio, solvent and annealing time can be made.[25] They showed that sufficient chain mobility must be available to the polymer and the appropriate volume fraction ratio must be attained in order for the ordering and morphology change to occur during solvent treatment.[26] Recently, solvent vapor annealing has become widespread. Kim et al. 2004 showed that nearly defect-free cylinder orientated polystyrene-*block*-poly(ethylene oxide) can be obtained by controlling the rate of solvent annealing.[27] Moreover, cylindrical nanopatterned surfaces of a polystyrene-*block*-poly(2-vinyl pyridine) (PS-*b*-P2VP) are stable in water. These surfaces provide both physical and chemical patterning due to the hydrophobic and hydrophilic nature of the domains. By photo cross-linking the cylindrical domains, a more durable material that can withstand immersion in water for extended periods of time is produced. [28]

In symmetric diblock copolymers, quantization of the film thickness often takes place. When the thickness of the film is not proportional to the equilibrium lamellar spacing, either holes or islands are nucleated on the film surface to adjust the local film thickness to the preferred quantized values. When the interaction with the surface is significantly reduced, the incommensurability thickness may lead to perpendicular orientation of the lamellae with respect to the boundary surfaces.[31-32] However, when the interaction between one block and

the substrate surface (the surface field) is very strong, a stable brush can be formed. In the case of a dense brush, the homopolymer or the same blocks cannot penetrate into the brush deeply, which may lead to autodewetting of the materials. It has been reported that PS homopolymer dewets PS brush layer attached to the substrate surface under certain conditions.[33] Large disordered droplets of block copolymers also autophobically dewet the dense brush layer of the ordered copolymer chains in block copolymer thin films, slightly above the order-disorder transition temperature.[34-35]

Surface and interface have a strong influence on the T_g of thin film coated on a substrate with a surface that has the effect of reducing T_g; whereas the interface increases the T_g according to the degree of interaction between a substrate and thin film.[38] Keddie et al. 1994 reported the first direct evidence for the change of T_g with decreasing film thickness for thin polystyrene (PS) films coated on Si wafer.[10-11, 39] When the film thickness was below 40 nm, there was an apparent reduction in the T_g and the T_g depression was not dependent on the molecular weight (M_w) of the sample. It was suggested that this reduction in T_g is caused by the presence of a rubbery layer at the polymer/air interface (the polymer's surface).[26] The existence of a lower T_g layer at the polymer surface has been ascertained in various experiments and simulations, so this suggestion seems to be very plausible.[40–42]

On the other hand, from the study of thin poly(methyl methacrylate) (PMMA) films coated on Si wafers bearing native oxide surface, the T_g was found to increase with decreasing film thickness.[43] It is not very surprising that thin PMMA film should have a more favorable interaction with a native oxide surface bearing Si wafers than thin PS film. A study on the T_g of thin poly(2-vinyl pyridine) (P2VP) film coated on Si wafer also revealed that T_g increases with decreasing film thickness.[44] Based on its chemistry, interactions between P2VP and the

native oxide surface of the Si wafer are more favorable than those between PMMA and the same substrate, thus a stronger interaction would be expected.[45] In this study, I applied Poly(styrene-*block*-2vinylpyridine) (PS-*b*-P2VP) that formed cylindrical structures via solvent annealing with various solvents, and investigated how the solubility of the solvent affects the alignment or morphology of the self-assembled structures in the thin film. In this study, I have also identified the best method to obtain perpendicular cylindrical patterned PS-*b*-P2VP to be used as templates and to act as a host for nanoparticles guest.

3.2 Experimental Procedure

3.2.1 Materials

Polystyrene-*block*-poly(2vinyl pyridine) (PS-*b*-P2VP) with a polydispersity index of 1.05 was purchased from Polymer Source, Inc. The number average molecular weights of PS and P2VP blocks were 79,000 g/mol and 36,500 g/mol, respectively.

3.2.2 Substrate Preparation

Silicon (Si) substrates (~1 cm x ~1 cm) with a native silicon oxide layer on the surface were cleaned with a mixed solution of concentrated H_2SO_4 and H_2O_2 (30%) (70/30 v/v) at 100 °C for 30 minutes. They were thoroughly rinsed with distilled water and dried under a stream of nitrogen gas. Next, they were subjected to further etching under UV light for 15 minutes to introduce a positive surface on the silicon wafer.

3.2.3 Film Preparation

Figure 1 below shows the method of thin film formation. The micellar films were prepared by spin coating the 1 wt% of PS-*b*-P2VP in a toluene and THF solution with a ratio of 7:3 on silicon substrates at 5000 rpm. The films were dried at ambient room temperature. The films

were exposed to a saturated of toluene or acetic acid vapor in different closed bottles at 21 °C for different periods of time (3 h, 6 h and 9 h), and then the samples were removed to ambient atmosphere and promptly dried.

Figure 1: The experimental procedure of making PS-*b*-P2VP thin film

3.2.4 Characterization

Atomic Force Microscopic (AFM) images were obtained using a Digital Instruments Nano Scope III scanning probe microscope in the tapping mode, using Olympus cantilevers with spring constants ranging between 39.7 N/m and 71.6 N/m and resonant frequencies of 293.8-356.0 Hz.

3.3 Results and Discussions

3.3.1 The Morphology of As-spun PS-*b*-P2VP Thin Films

Toluene as the selective solvent for the PS block, has been chosen to be used to dilute PS-*b*-P2VP BCP mixed with THF which is a neutral solvent for both blocks. The mixed solvents have been chosen in order to obtain the nanometer-sized micelles consisting of high solubility of PS corona and low soluble P2VP core which is formed above the critical micelle concentration (CMC). A micellar film of diblock copolymers can be easily formed via spin coating. The AFM height image of the as-spun 1 wt% PS-*b*-PVP micellar thin film in toluene:THF (70:30) solution on a silicon substrate surface is as shown in Figure 2. The brighter and darker areas in the image correspond to the P2VP microdomains and the PS

matrix, respectively. Even though a long-range order was not induced, a closely packed quasi-hexagonal irregular dot-like structure has been observed.

The initial perpendicular orientation may be the result of solvent concentration gradients, as reported by Kim and Libera 1998 for fast evaporation during spin coating. This metastable structure has some stability with regard to gentle vapor processing.[46]

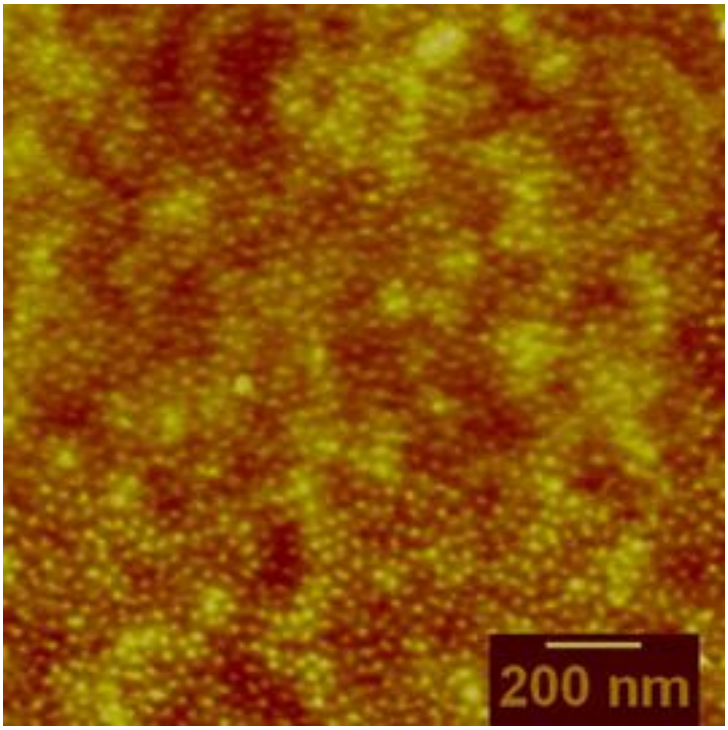

Figure 2: As-spun PS-*b*-P2VP thin film

Preferential interaction and swelling of the minor component of an asymmetric BCP in a thin film configuration, with a selective solvent can lead to a reconstruction of the film morphology. In such a reconstruction process, the minor component segregates to the surface and surrounds a scaffold of the major component. At the initial positions of minor-component domains, nanopores oriented normally to the film plane, penetrating through the entire film form.[47- 48] The molecular weight ratio between PS and P2VP is about 2:1, thus, in this system, it is expected that the PS would be the matrix and the P2VP would be the cylinders.

The darker areas in the AFM image correspond with the PS matrix, while the brighter areas correspond to the P2VP domain as mentioned earlier. The solubility of the blocks and the solvent evaporation rate are responsible for the normal orientation of the cylinders to the surface. Solvent-annealing with PS selective solvent has affected the copolymer swells with the solvent. The solvent imparts mobility to the copolymer, thus the block can reorganize. The film thickness of the as-spun was measured using AFM with stepheight analyzing software for thickness ranging between 19.04 nm - 21.7 9 nm or at the mean value of 19.96 nm.

3.3.2 The Morphology Change of PS-*b*-P2VP Thin Films under Solvent Annealing

3.3.2.1 PS-*b*-P2VP Thin Films under Toluene Vapor in several Different Time Duration

Toluene is a selective solvent for PS, therefore, PS block would typically swell while protruded island of P2VP was formed. Annealing in this solvent causes a formation of equilibrium transition detected at 3 h of solvent annealing to 6 h of solvent annealing. However, order-order phase transition has been formed starting with a cylindrical structure at 6 h solvent annealing to a spherical structure at 9 h solvent annealing. In this study, I have intended to investigate the optimum time for solvent annealing. Therefore, the PS-*b*-P2VP thin films have been annealed under toluene vapor for 3 h, 6 h and 9 h. The results presented in Figure 3 (a) shows that the annealing time of 3 hours was not long enough to mobilize the PS molecules to swell purposely in order to obtain the regular structure. Meanwhile, annealing for 6 hours using toluene has induced the regular structure of a perpendicular cylinder of P2VP with PS matrix, as shown in Figure 3 (b). This result was obtained because PS molecules has swollen well to induce the formation of the perpendicular cylindrical pattern of P2VP. On the other hand, in the case of solvent-annealing for 9 hours (Figure 3 (c)), the surface structure has transformed into the spherical domain orientation which was due to

the over-swollen PS matrix. Therefore, from these results, I have concluded that the optimum time for solvent-annealing to obtain a cylindrical formation would be for 6 hours.

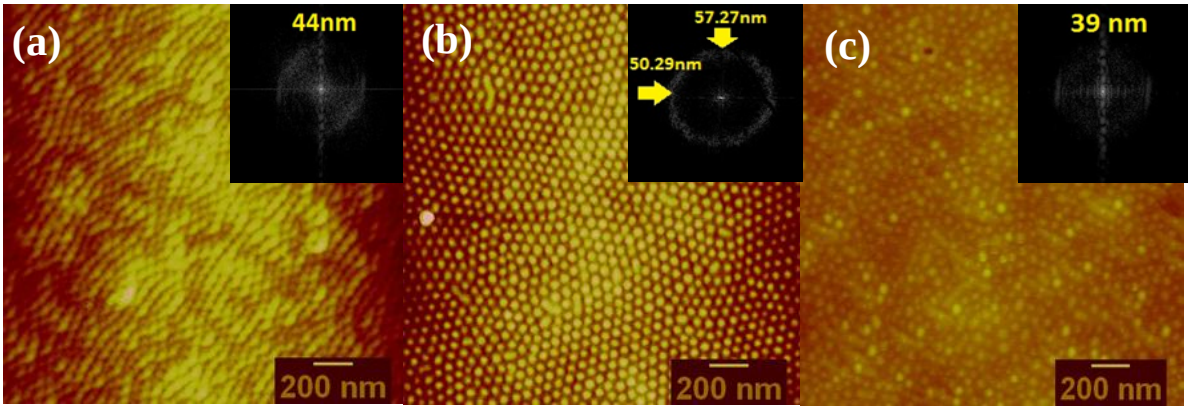

Figure 3: The height images of PS-*b*-P2VP thin films after subjected to evaporation with toluene for (a) 3 h (b) 6 h and (c) 9 h.

I also understood that, after 6 hours of solvent annealing, both blocks would be swollen. Hence, the selective toluene solvent was not strong enough to swell both microdomains in the low region of PS-*b*-P2VP for 9 hours of solvent annealing. So, in this region, the reduction of χ parameter, which is the Flory-Huggins interaction parameter between PS and P2VP species, χ_{PSP2VP} has occurred; therefore, the segregation has transformed the structure into an irregular structure. Meanwhile, for 6 hours of solvent annealing, the P2VP had continued to swell.

My results indicated that over sufficient annealing time, the decreasing thickness of the thin film would lead to changes in the morphology; from a cylinder to a sphere structure. This has happened because the BCP, which was still in a swollen state, has re-adsorbed the molecules due to the delayed removal of the thin film to a dry state that can stop the molecules' arrangement process. Therefore, the morphology spontaneously changes once these swelling have been achieved. Moreover, the block copolymer had swelled unevenly, causing the

transition to a spherical morphology. The FFT images, as shown in the top left corner of each AFM images of each sample in Figure 3, show that for a regular structure, the D-spacing is larger than in an irregular structure.

Switching the morphology between a spherical and a cylindrical morphology is possible by alternating the solvent annealing process with toluene with different time duration.[10,49] Hence, it would be more accurate to talk in terms of solvent vapor processing rather than a simple anneal.[26] Thin films previously annealed in toluene vapor for 3 hours, 6 hours and 9 hours were placed in different solvent-annealing capped-bottles. The results showed that by doing so, it has organized the BCP structure from an unorganized structure morphology into perpendicular cylinders and then into a spherical structure, respectively. The mean thicknesses of the films are 24 nm, 17.1 nm and 22.2 nm for 3 h, 6 h and 9 h of solvent-annealing in toluene vapor, respectively.

The AFM images of the 3 h solvent-annealed thin films showed an unorganized structure and spherical morphologies for the 9 h solvent-annealed thin films showed a kinetically trapped (metastable) spherical morphology which is expected. The relaxation state going back towards the thermodynamically stable cylindrical morphology was expected from the block volume fraction of the thin film that has been annealed for 6 hours. The thickness of 23.9 nm and 22.21 nm were obtained from the 3 hours and 9 hours of solvent annealing, respectively, with an unorganized structure and a spherical formation. Meanwhile, the thickness of a stable cylindrical formation was 17.1 nm as previously mentioned for the 6 hours annealing. This happened because the molecules of the stable structure has been mobilized and some of them might have evaporated together with toluene molecules while forming the stable structure of the perpendicular cylinder. I know that in this study, my as-spun films have a mean thickness

value of about 20 nm. Hence, it can be concluded that both blocks have been affected by anisotropic shrinkage due to the evaporation of the film.[26]

Moreover, in a dry state, the thin films have swelled to 119.5 % and 111.05 % of the original thickness of solvent-annealing for 3 hours and 9 hours, respectively, because the swollen polymer was sufficiently plasticized for self-reorganization to occur. In this mechanism, it is understood that the selective attraction of blocks to the air and substrate interfaces is expected to induce unorganized orientation and spherical morphologies, as observed from the AFM images in Figures 3 (a) and 3 (c). Meanwhile, for the 6 hours of solvent-annealing, the thin film underwent the reverse process whereby the thickness of the thin film had decreased down to 85% from its original thickness. The interaction between the selective solvent and the BCP molecules has caused them to be simultaneously evaporated during the formation of the ordered structure of perpendicular cylinder. This mechanism has affected the thin film thickness by decreasing it compared to the as-spun thin film. This discrepancy has been attributed to an uniaxial contraction on the fast drying evaporation of the thin films in the ambient environment[10] and the adequate annealing time needed.

3.3.2.2 The Morphology Change of PS-*b*-P2VP Thin Films under Acetic Acid Vapor

During this test, the capped-bottle has been evaporated with the selective solvent for P2VP which is acetic acid. The thin films were exposed to acetic acid for 3 h, 6 h and 9 h, which have resulted in the segregation of P2VP to the surfaces and the walls of the nanopores formed[3] from the P2VP domains with PS matrix (Figure 4). The preferential attraction of the P2VP block to the acetic acid has induced an irregular structure after solvent-annealing for 3 h, as shown in Figure 4 (a). However, the morphology has switched to a worm-like structure or nanopores structure of the BCP template in the case of solvent-annealing for 6 h and 9 h

with acetic acid (Figures 4 (b) and 4 (c)). The thickness of the thin films was found to have changed from 26.2 nm, 22.8 nm and 41.5 nm after being solvent-annealed for 3 h, 6 h and 9 h, respectively. The thickness has also increased as compared to the as-spun thin film which was about 20 nm.

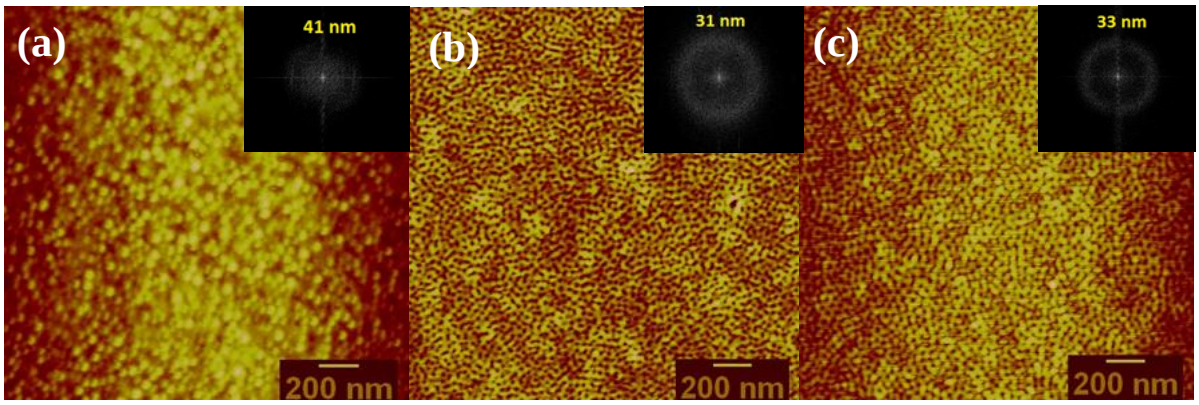

Figure 4: The morphology of PS-*b*-P2VP thin films that have been treated with acetic acid for (a) 3 h, (b) 6 h and (c) 9 h.

In this case, the topography AFM image of the 3 h (Figure 4 (a)) solvent-annealed thin film has shown the formation of an unorganized structure due to deficient mobilization of P2VP molecules to orient the order of the morphology. On the other hand, the thin film morphology suddenly changed into an organized worm-like structure (Figure 4 (b)) even though it did not attain a long-range ordered structure. This mechanism took place because the PS block could not be swollen by acetic acid, since the acetic acid is the selective solvent for P2VP block. Therefore, the mobility of PS molecules was restricted and they tended to collapse rather than swell in the PS matrix. Only the P2VP block has been swollen but the swelling process is not enough to obtain a long-range order structure as compared to toluene. Although the duration of evaporation was increased to 9 h, the result, as shown in Figure 4 (c), obviously has exhibited no change of structure for the PS-*b*-P2VP thin film. The D-spacing from the FFT

images, as shown in the top left corner of each AFM images, were 41 nm, 31 nm and 33 nm for PS-*b*-P2VP thin films after solvent-annealing for 3 h, 6 h and 9 h, respectively.

In the high magnification image by AFM for thin film with 9 h of solvent annealing (shown in Figure 5), the image revealed a dot-like structure of P2VP with PS matrix. The formation is not exactly in a close hexagonal packed pattern, even though it is an organized structure. This happened because the acetic acid was not strong enough to transform the thin film into a long-range order structure. For this condition of solvent annealing with P2VP selective solvent, the PS matrix at glassy state did not obtained any transformation of structure after 6 h and more of solvent annealing. This is because the PS is a dominant block, therefore the acetic acid, acting as the P2VP's selective solvent can only segregate the P2VP block. The acetic acid cannot be adsorbed into PS matrix and thus, the PS domain cannot move.

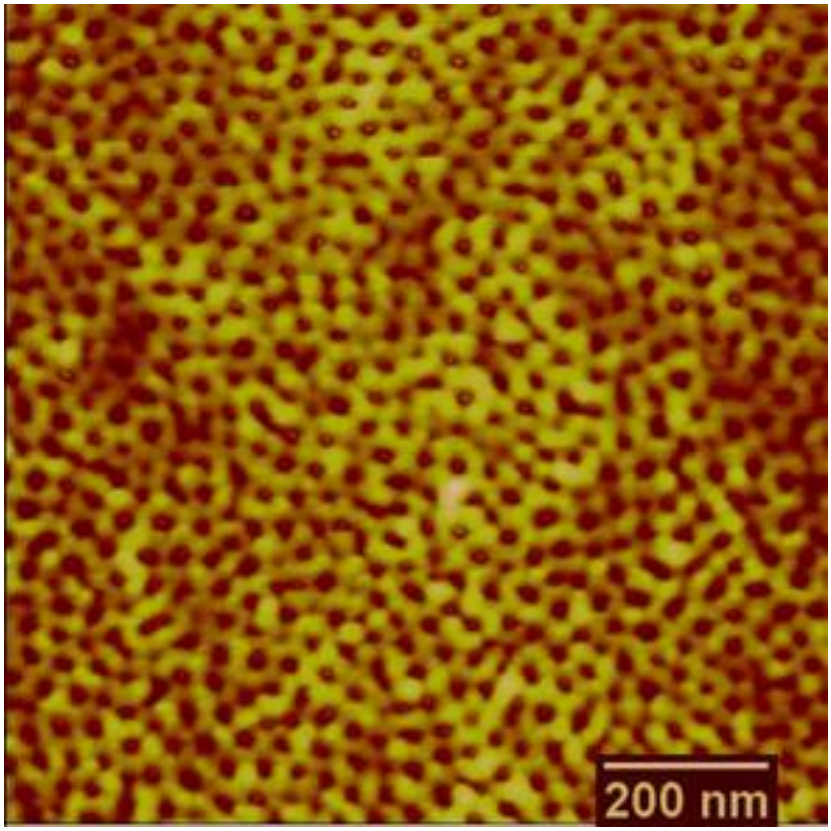

Figure 5: The high magnification image by AFM for thin film with 9 h of solvent annealing.

This phenomenon may be understood in terms of the solvent selectivity for the two blocks. In order for the block copolymer to have sufficient mobility to self-assemble via solvent vapor annealing, both blocks must be sufficiently swollen such that the glass transition temperature (T_g) of the block drops below the annealing temperature.[50] An extension of Dimarzio et al. 2009 thermodynamic model explaining the glass transition temperature depression due to a diluent was conducted by Chow.[51] He showed that for small molecule solvents, the size and concentration of the diluents were the main determinants affecting the drop in the glass transition temperature.[52] Further evidence of the glass temperature depression under solvent vapor uptake and its role in block copolymer thin film kinetics was recently provided by Di et al. 2009.[53]

The T_g of PS was measured to be 100 °C[54-56] while the T_g of P2VP is known to be approximately 100 °C,[44] hence, both values are significantly higher than room temperature. Marvin et al. 2010 have expected that the acetic acid would be swelling the P2VP block far beyond the value needed for plasticization, before the P2VP block swells sufficiently for its T_g to be suppressed below room temperature. Alongside the mobility increase, a sufficiently high P2VP volume fraction must also be achieved to act as the driving force for the phase transition.[26] Unfortunately, my results showed the opposite of this assumption which might be due to the way of handling the solvent-annealing treatment; different method with different conditions.

3.3.3 The Morphology Change of PS-*b*-P2VP Thin Films under Thermal Annealing

As initially stated, I have prepared thin films on silicone substrates via spin casting with a PS-*b*-P2VP solution. 1 wt% PS-*b*-P2VP BCP (79.0k-*b*-36.5k kg/mol) solution in mixed solvents of toluene and tetrahydrofuran (THF) with a ratio of 7:3 was used. I applied thermal

annealing to the thin films at 80 °C, 100 °C, 150 °C, 200 °C and 250 °C for 24 hours. As reported by Keddie et al. 1994,[55] the T_g values of PS changes with decreasing film thickness of below 40 nm; there is apparently reduced T_g value of PS thin film. Also T_g is not dependent on the molecular weight of the PS homopolymer. On the other hand, in the case of P2VP thin films, the T_g value increases with decreasing film thickness,[44] based on the chemical interactions between P2VP and the native oxide surface of Si substrate.[45]

The results of PS-*b*-P2VP thin films treated by thermal annealing are shown in Figure 6. It is apparent that no long-range ordered structure was present when these thin films were annealed at 80 °C with the thickness of 13.79 nm; this is lower than the T_g of both blocks. Even with thermal annealing at the T_g value of 100 °C, with 17.7 nm of thickness, there was no formation of a regular structure. Hence, it was concluded that there will be no structure and there only seemed to be swollen areas for thin films that have been annealed at 150 °C, 200 °C and 250 °C. I measured the thickness of these thin films which were 18.3 nm, 24 nm/14 nm and 17 nm/8.5 nm for thin films that have been heat treated for a day at 150 °C, 200 °C and 250 °C, respectively.

The P2VP domain has been fixed at the silicon substrate (Si) and the PS domain has shown weak segregation due to the strong affinity of Si to oxygen to P2VP domain, while PS has been attracted to the air for obtaining an irregular structure and there was also the enthalpy effect to be considered.

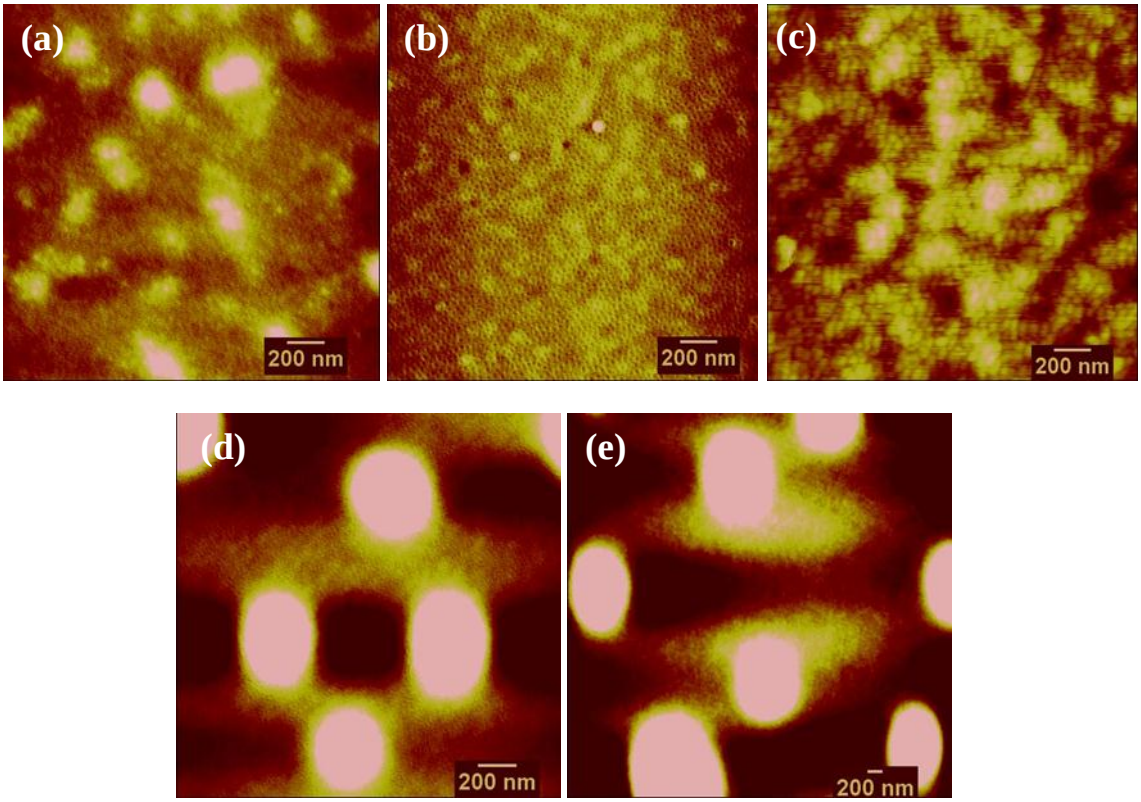

Figure 6: AFM images of PS-*b*-P2VP thin films after thermal annealing treatment at (a)80 °C, (b)100 °C, (c) 150 °C, (d) 200 °C and (e) 250 °C.

My results indicated that the thermal annealing method is not an acceptable method for obtaining a regular structure of the PS-*b*-P2VP thin film. In contrast, the solvent-annealing treatment has given long-range order orientation by applying the capable solvent to mobilize BCP molecules with sufficient time during the treatment process.

3.4 Conclusion

Solvent vapor treatment is a powerful processing technique that allows direct control over the morphology and ordering within the block copolymer's thin films. I have demonstrated the ability of PS-*b*-P2VP to directly obtain the morphology of self-assembled domains with hexagonally packed cylinders or spheres by using toluene, which is the selective solvent for PS block. Moreover, the ability to treat the thin films with sufficient duration time offers an

additional advantage for the solvent annealing method in the case of introducing long-range order structure.

In order to exploit the benefits of solvent annealing completely, the mechanism must be fully understood. I have shown that for the annealing process to take effect, the polymer must be sufficiently swollen in order to obtain high order structure of perpendicular cylindrical pattern. Thus, the block copolymer must be sufficiently plasticized for the polymer chains to be mobiled enough to reorganize. For the order-order transition to occur, the additional variable of solvent selectivity enables the tuning of the block volume fraction, and thus, the morphologies are formed. In response to toluene annealed thin film at 6 h to 9 h period, the quick relaxation away from the kinetically trapped spherical morphology was observed in contrast to the as-spun annealed films. The evaporation of the solvent resulted in the compression of the film thickness, but the morphology is otherwise maintained in the dried films for 6 h of solvent-annealing by toluene.

Thermal annealing treatment did not induce structure with regular in the thin films. This is due to the fact that PS-*b*-P2VP does not have high enough mobility to attain the regular morphology by thermal annealing treatment. Well-ordered P2VP cylinders were obtained perpendicularly to the substrate's surface by using toluene while a parallel cylinder (worm-like) without long-range order has formed by solvent annealing with acetic acid. These differences originated from the strength of the selectivity of the solvents. The strength of the selectivity of toluene is strong enough to swell both PS and P2VP blocks. Thus, both components were well swollen and had enough mobility to attain the long-range order in the swollen state. On the other hand, PS was less swollen and did not have enough mobility

during solvent annealing by acetic acid since the selectivity of acetic acid caused only the P2VP block to swell.

1. In a solvent-annealed thin film, a high order with perpendicular cylinder was achieved for solvent-annealing with toluene for a reasonable of exposure time which was for 6 h. On the one hand, the cylindrical structure has transited to a spherical structure, when the film was evaporated under toluene vapors for 9 h. On the other hand, the unorganized structure was attained when the thin film was solvent-annealed for 3 h. In this study, I proposed that the improved high order in solvent-annealing process occurs by accurate time of evaporation and sufficient surrounding temperature which are important parameters to control, in order to obtain high ordered morphology of the thin film.

2. In the case of solvent-annealing by acetic acid, the result from the experiment has demonstrated that the duration time of 3 h, 6 h and 9 h at 21 °C did not resulted in a long-range order structure. However, when the thin film was exposed in acetic acid vapor for 6 h and 9 h, a parallel cylindrical morphology that seemed to be a worm-like structure was attained. Nonetheless, the structure has not exhibited any changes even though the duration time of vapor exposure was increased.

3. Meanwhile, the thermal annealing of PS-*b*-P2VP thin film has not induced the regular morphology due to immobilized BCP molecules even with heating at below or over the glass transition temperature (T_g) of the PS and P2VP blocks.

4. After analyzing the thickness of these thin films, in the case of solvent-annealing treatment, it can be understood that the thin film thickness was decreased compared to the as-spun thin film when the thin film has obtained high order structure, while it tended to increase the thickness when irregular structure was exhibited. The swollen process of forming regular structure due to the chain of PS-*b*-P2VP being rearranged in the as-spun structure by swelling

the microdomian of the BCP with the toluene's molecules together. I have assumed that some of the BCP's molecules have evaporated with toluene's molecules. Therefore, the thickness of thin film has decreased than thickness of as-spun thin film.

5. On the other hand, for thermal annealing treatment, the thicknesses of the thin films have mostly decreased for all temperatures during the heating process. Moreover, there was a terraced area which has been forming when the thin films were heated at 200 °C and 250 °C. The driving force for the heat treatment did not performed well to transit the as-spun structure with spherical hexagonal closed packed to a regular structure, although it has been operating in the variable temperature of heating environment.

6. The kind of treatment and the type of solvents may play important roles in the formation of the desired order structure.

References

[1] G. Ka¨stle, H. G. Boyen, F. Weigl, G. Lengl, T. Herzog, P. Ziemann, et al., *Adv. Funct. Mater.* **2003**, *13*,853.

[2] J. P. Spatz, S. Mo¨sser, C. Hartmann, M. Mo¨ller, T. Herzog, M. Krieger, et al., *Langmuir* **2000**,*16*, 407.

[3] B. H. Sohn, S. I. Yoo, B. W. Seo, S. H. Yun, S. M. Park, *J. Am Chem. Soc.* **2001**, *123*, 12734.

[4] S. H. Yun, B. H. Sohn, J. C. Jung, W. C. Zin, J. K. Lee, O. Song, *Langmuir* **2005**, *21*, 6548.

[5] W. Hwang, M. H. Ham, B. H. Sohn, J. Huh, Y. S. Kang, W. Jeong, et al., *Nanotechnology* **2005**, *16*, 2897.

[6] C. C. Weng, K. F. Hsu, K. H. Wei, *Chem. Mater.* **2004**, *16*, 4080.

[7] Y. Chan, Y. Mi, *Polymer* **2004**, *45*, 3473.

[8] X. Li, K. H. A. Lau, D. H. Kim, W. Knoll, *Langmuir* **2005**, *21*, 5212.

[9] X. Li, S. J. Tian, Y. Ping, D. H. Kim, W. Knoll, *Langmuir* **2005**, *21*, 9393.

[10] J. K. Bosworth, M. Y. Paik, R. Ruiz, E. L. Schwartz, J. Q. Huang, A. W. Ko, D. M. Smilgies, C. T. Black, C. K. Ober, *ACS Nano* **2008**, *2(7)*, 1396.

[11] S. Park, D. H. Lee, J. Xu, B. Kim, S. W. Hong, U. Jeong, T. Xu, T. P. Russell, *Science* **2009**, *323(5917)*, 1030.

[12] V. Olszowka, M. Hund, V. Kuntermann, S. Scherdel, L. Tsarkova, A. Boker, *ACS Nano* **2009**, *3(5)*, 1091.

[13] S. H. Kim, M. J. Misner, T. Xu, M. Kimura, T. P. Russell, *Advanced Materials* **2004**, *16(3)*, 226.

[14] T. H. Kim, J. Hwang, W. S. Hwang, J. Huh, H. C. Kim, S. H. Kim, J. M. Hong, E. L. Thomas, C. Park, *Advanced Materials* **2008**, *20(3)*, 522.

[15] K. A. Cavicchi, K. J. Berthiaume, T. P. Russell, *Polymer* **2005**, *46*, 11635.

[16] J. Peng, D. H. Kim, W. Knoll, Y. Xuan, B. Li, Y. Han, *The Journal of Chemical Physics* **2006**, *125*, 064702.

[17] T. P. Lodge, K. J. Hanley, B. Pudil, V. Alahapperuma, *Macromolecules* **2003**, *36*, 816.

[18] K. J. Hanley, T. P. Lodge, C. I. Huang, *Macromolecules* **2000**, *33*, 5918.

[19] C. I. Huang, B. R. Chapman, T. P. Lodge, N. P. Balsara, *Macromolecules* **1998**, 31, 9384.

[20] J. S. Pedersen, I. W. Hamley, C. Y. Ryu, T. P. Lodge, *Macromolecules* **2000**, 33, 542.

[21] A. Choucair, C. Lavigueur, A. Eisenberg, *Langmuir* **2004**, *20*, 3894.

[22] Y. Yu, A. Eisenberg, *J. Am. Chem. Soc.* **1997**, *119*, 8383.

[23] J. Peng, D. H. Kim, W. Knoll, Y. Xuan, B. Li, Y. Han, *The Journal of Chemical Physics* **2006**, *125*, 064702.

[24] D. M. Smilgies, R. Li, Z. Di, C. Darko, C. M. Papadakis, D. Posselt, *Materials Research Society Symposium Proceedings* **2009**, 1147.

[25] S. Dourdain, A. Rezaire, A. Mehdi, B. M. Ocko, A. Gibaud, *Physica B: Condensed Matter* **2005**, *357(1–2)*, 180.

[26] M. Y. Paik, J. K. Bosworth, D. M. Smilges, E. L. Schwartz, X. Andre, C. K. Ober, *Macromolecules* **2010**, *43(9)*, 4253.

[27] S. H. Kim, M. J. Misner, T. Xu, M. Kimura, T. P. Russell, *AdV.Mater.* **2004**, *16*, 226.

[28] C. M. Grozea, N. Gunari, J. A. Finlay, D. Grozea, M. E. Callow, J. A. Callow, Z. H. Lu, G. C. Walker, *Biomacromolecules* **2009**, *10(4)*, 1004.

[29] G. Coulon, V. R. Deline, T. P. Russell, P. F. Green, *Macromolecules* **1989**, *22*, 2581.

[30] E. Huang, S. Pruzinsky, T. P. Russell, *Macromolecules* **1999**, *32*, 5299.

[31] S. H. Anastasiadis, T. P. Russell, S. K. Satija, C. F. Majkrzak, *Phys. Rev. Lett.* **1989**, *62*, 1852.

[32] X. Li, J. Peng, Y. Wen, D. H. Kim, W. Knoll, *Polymer* **2007**, *48*, 2434.

[33] J. H. Maas, M. A. Cohen Stuart, F. A. M. Leermakers, N. A. M. Besseling, *Langmuir* **2000**, 16, 3478.

[34] R. Limary, P. F. Green, *Macromolecules* **1999**, 32, 8167.

[35] I. W. Hamley, E. L. Hiscutt, Y. W. Yang, C. Booth, *J. Colloid Interface Sci.* **1999**, *209*, 255.

[36] H. W. Shen, A. Eisenberg, *J. Phys. Chem. B* **1999**, *103*, 9473.

[37] P. Bhargava, J. X. Zheng, P. Li, R. P. Quirk, F. W. Harris, S. Z. D. Cheng, *Macromolecules* **2006**, *39*, 4880.

[38] C. H. Park, J. H. Kim, M. Ree, B. H. Sohna, J. C. Junga, W. C. Zina, *Polymer* **2004**, *45*, 4507.

[39] E. J. W. Crossland, M. Kamperman, M. Nedelcu, C. Ducati, U. Wiesner, D-M. Smilgies, G. E. S. Toombes, M. A. Hillmyer, S. Ludwigs, U. Steiner, H. J. Snaith, *Nano Letters* **2008**, *9(8)*, 2807-2812.

[40] J. Peng, D. H. Kim, W. Knoll, Y. Xuan, B. Y. Li, Y. C. Han, *J. Chem. Phys.* **2006**, *125*, 064702.

[41] J. Peng, Y. Xuan, H. F. Wang, B. Y. Li, Y. C. Han, *Polymer* **2005**, *46*, 5767.

[42] Y. Cong, Z. X. Zhang, J. Fu, J. Li, Y. C. Han, *Polymer* **2005**, *46*, 5377.

[43] J. C. Zhao, S. C. Jiang, X. L. Ji, L. J. An, B. Z. Jiang, *Polymer* **2005**, *46*, 6513.

[44] X. Han, H. Liu, Y. Dong, Y. C. Hu, *J. Chem. Eng.* **2005**,*13*, 498.

[45] S. H. Anastasiadis, T. P. Russell, S. K. Satija, C. F. Majkrzak, *Phys. Rev. Lett.* **1989**, *62*, 1852.

[46] G. Kim, M. Libera, *Macromolecules* **1998**, *31(8)*, 2569.

[47] T. Xu, J. Stevens, J. A. Villa, J. T. Goldbach, K. W. Guarini, C. T. Black, C. J. Hawker, T. P. Russell, *AdV. Funct. Mater.* **2003**, *13*, 698.

[48] Y. Wang, M. Becker, L. Wang, J. Liu, R. Scholz, J. Peng, U. Gosele, S. Christiansen, D. H. Kim, M. Steinhart, *Nano. Letters.* **2009** ,*9(6)*, 2384.

[49] J. K. Bosworth, C. T. Black, C. K. Ober, *ACS Nano* **2009**, *3(7)*, 1761.

[50] D. W. Van Krevelan, P. J. Hoftyzer, "*Properties of Polymers: Their Estimation and Correlation Length with Chemical Structure 2*", Elsevier Scientific Publishing Company, New York **1976**.

[51] E. A. Dimarzio, J. H. Gibbs, *Journal of Polymer Science Part A: General Papers* **1963**,*1(4)*, 1417.

[52] T. S. Chow, *Macromolecules* **1980**, *13(2)*, 362.

[53] Z. Di, D. Posselt, D. M. Smilgies, C. M. Papadakis, *Macromolecules* **2009**, *43(1)*, 418.

[54] J. L. Keddie, R. A. Jones, R. A. Cory, *Faraday Discuss.* **1994**, *98*, 219.

[55] J. L. Keddie, R. A. Jones, R. A. Cory, *Europhys Lett.* **1994**, *27*, 59.

[56] J. L. Keddie, R. A. Jones, *J. Isr. Chem. Soc.* **1995**, *35*, 21.

[57] S. Niu, R. F. Saraf, *Macromolecules* **2003**, *36*, 2428.

4

Alignment of Ferritin Protein Molecules on Diblock Copolymer Patterns by Using Self-Assembly

4.1 Introduction

Patterned surfaces is also called nano-templates with microdomains as feature sizes shrink from the micron scale to the nanoscale, can be formed as platforms to direct self-assembly of nanoelements or biological molecules onto this controlled patterns.[1-3] Block copolymers (BCPs) have produced extraordinary well-aligned and defect-free nano-template by controlling microdomain orientation via methods such as graphoepitaxy, directed self-assembly, chemical patterning, etc.[4-7] These nano-templates with various patterns prepared by using self-assembly microphase separation of block copolymers (BCPs).[8-13] The self-assembled domain shapes of BCPs can be tuned by adjusting the relative volume fraction of each block (f), Flory-Huggins interaction parameter χ, and the degree of polymerization N [14] as mentioned in previous chapter. Self-assembly is known as low-cost, fast, and easily scalable. Self-assembling systems are governed by a fascinating interplay between weak forces.[15] PS-*b*-P2VP is a representative model system for block copolymers with large surface energy differences.[16] Additionally, PS-*b*-P2VP has been widely studied for both scientific and technological purposes.[17-21]

In a typical BCPs, dimension of the domains range size of microdomain from 10 nm to 100 nm and can be controlled by changing molecular weight of the macromolecule,[14] while the equilibrium morphologies depend on the relative volume fraction of diblock copolymers and temperature.[22] The diblock copolymers exhibit a wide variety of morphologies ordered by microphase separation and give result in microdomain structures such as lamellar, gyroid, Fddd, hexagonally packed cylinder and a body centered lattice of spheres in the equilibrium configuration.[23-25]

Although nanostructured films of BCPs can be obtained through the simple technique of spin coating on a flat homogeneous surface, the self-assembly processes on their own are not sufficient, because the resulting nanostructures exhibit only short range order and in most cases, are strongly non-equilibrium.[15] To realize the full potential of self-assembled structures of block copolymers in thin films for lithographic application, I need to attain long-range order. To achieve long-range order, some type of guidance during the microdomain formation process is required.[26] The degree of long-range order of these domains can be controlled by a variety of factors, such as the interaction of the BCPs molecules with the substrate, the film thickness[27] and the post-deposition annealing procedures.[28,29] Several methods have been used to induced long-range order such as graphoepitaxy,[30-35] shear flow,[36] electric fields alignment[37-42] surfactant assisted assembly, [43] self-assembly on brush surfaces, [44-51] directed assembly on chemically patterned surfaces [6,52-56] and solvent annealing.[10-11, 57,26]

Ferritin has a spherical hollow protein shell with the inner and outer shell diameters of 7 nm and 12 nm, respectively. The internal cavity of ferritin protein has the ability to store iron as hydrated iron oxide. It is called apo-ferritin if iron oxide is removed from internal cavity. Various inorganic nanoparticles can be introduced into the cavity of apo-ferritin[58] to give various functions. Yamashita 2001 has assembled ferritin protein onto Si substrate with hydrophobic surface as scaffolds to produce inorganic and functional nano-structures onto a flat surface.[59] Ferritin protein is known for its ability to be adsorbed onto various polymer surfaces in different degrees.

The two- or three dimensional assemblies of these ferritin protein cage architectures on substrates has been used in many ways to obtain functional structures which may be used in biosensor, bioelectronic and nanoelectron device applications. For developing that kinds of applications, the methods that can be utilized are such as the air/water interface (LBL method), mechanical scratching, physical adsorption, SAM, peptide–substrate interaction and Bio-LBL method.[58] Therefore, ferritin protein may be able to align onto block copolymers by using its self-assembled nano-pattern as the nano-template. In this work, I focus on alignment of ferritin protein as super molecules onto the BCPs nano-template's surface with same distance as BCPs space domain, in order to make the nano-template functions.

4.2 Experimental

4.2.1 Materials

The molecular weight of the polystyrene-*block*-poly(2vinylpyridine) diblock copolymer (PS-*b*-P2VP) used as a nano-template was 79.0k-36.5k g/mol with polydispersity index of 1.05, purchased from Polymer Source Inc., Dorval, Canada. Ferritin (Aldrich) protein from horse spleen was used to align onto nano-patterned BCP.

4.2.2 Substrate Preparation

Silicon(100)(Si) wafers were used as substrates. Si wafers were cut into 1 cm^2 pieces and cleaned by piranha solution, a mixture of H_2O_2 (30%) and H_2SO_4 (70%) (v/v), at 100 °C for 30 minutes. Then rinsed with distilled water and dried in a stream of nitrogen. After the cleaning steps, the substrates were irradiated with UV light for 15 minutes and used immediately.

4.2.3 Film Preparation

The processes to form the nano-template are shown in Figure 1. PS-*b*-P2VP was spin-coated on the cleaned Si substrates from the solution of PS-*b*-P2VP at 5000 rpm for 20 s. Mixed solvents of toluene and tetrahydrofuran (THF) with ratio of 7:3 were used as solvent. I applied solvent annealing technique to as-spun samples to obtain striped patterns with P2VP parallel cylinders. The as-spun samples were exposed in saturated tetrahydrofuran (THF) solvent vapor for 3 hours. After the application of solvent annealing, I etched PS surface layer with UV-irradiation in the air for 1-5 min was performed.

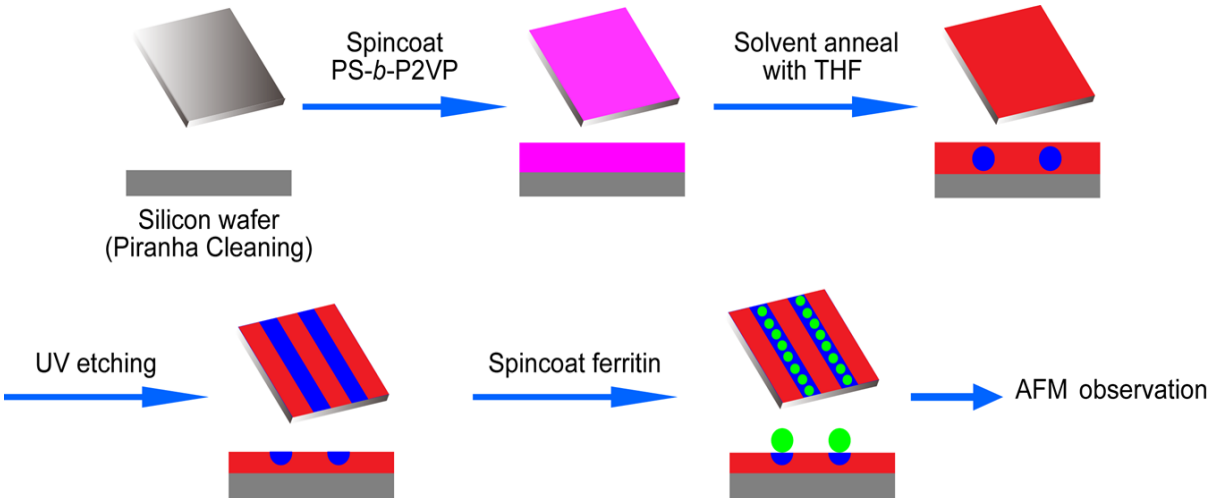

Figure 1: Alignment of ferritin onto a parallel cylindrical pattern of PS-*b*-P2VP BCP.

In order to check the affinity of PS and P2VP to ferritin, The PS homopolyer (M_n = 34.0K g/mol) and P2VP homopolymer (M_n = 51.0K g/mol) thin films also have been prepared on Si substrates by spin-cast method with toluene for PS and THF for P2VP as solvents.

4.2.4 Alignment of Ferritin Protein onto Nano-template

0.1 wt% ferritin protein aqueous solution was dropped on the patterned BCP template and left for 1 minute before spinning at 8000 rpm to control the adsorption of ferritin protein on the patterned surface. Acetic acid was dropped into ferritin protein aqueous solution with 0.12 wt% concentration in pH 3.3 with the aim to raise absorbability of ferritin protein onto BCPs PS-*b*-P2VP thin films. To check the affinity, I dropped 0.1 wt% ferritin protein aqueous solution on PS and P2VP thin films and left for 1 minute before spinning at 8000 rpm.

4.2.5 Morphology Measurement

The morphology of adsorbed ferritin on the PS-*b*-P2VP thin film template was estimated by atomic force microscopy (AFM) with a multimode AFM system of a Nanoscope III scanning probe microscope (Digital Instruments) in tapping mode. The images were obtained in the contact mode at ambient temperature.

4.3 Results and Discussions

4.3.1 Affinity of PS and P2VP to Ferritin

Figure 2 (a) and (b) show AFM height images of PS and P2VP homopolymers thin films after spin-coating with ferritin solution. It was found that more ferritin protein molecules is adsorbed on the P2VP surface rather than the PS surface. The difference in the affinity is caused by hydrophilic P2VP-homopolymer instead of hydrophobic PS-homopolymer. Moreover, THF is an oxygen-bearing solvent that contains oxygen atom on its chemical structure. The oxygen atom is highly electronegative and capable of forming hydrogen bonds.[60] The isoelectric point (pI) of horse spleen ferritin has been reported to be 4.1–5.1,[58] and at pH 3.5 which is below than ferritin's isoelectric point has carried a net positive charge,[58] I assume that, ferritin in pH 3 in acidic condition which is positive charged, can be adsorbed more onto P2VP surface due to P2VP surface has contained high amount of THF solvent that still remain on the P2VP surface since P2VP homopolymer was diluted with THF hence forming electrostatic interaction.

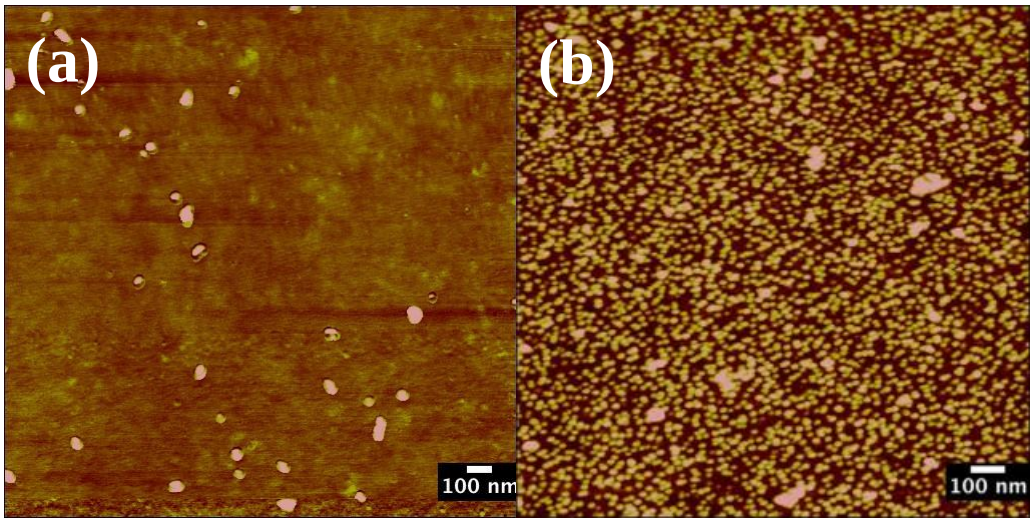

Figure 2: (a) PS-homopolymer; (b) P2VP-homopolymer with spin coated of ferritin protein.

4.3.2 Formation of Stripe Patterns in PS-*b*-P2VP Thin Films

As shown in Figure 3 (a), the as-spun PS-*b*-P2VP thin film has formed dots pattern without a long-range order. On the other hand, the stripe pattern with a long-range order (Figure 3 (b)) was formed after solvent annealing for 3 hours without terrace formation (Figure 3 (c)). The D-spacing of the pattern is 53 nm estimated from 2D-FFT image as shown in the inset of Figure 3 (b). Moreover, the template for 5 hours of solvent annealing resulted in long-range order (Figure 4 (a)) however; the terrace has been obtained that gives the effect of surface roughness as shown in Figure 4 (b). Additionally, by reducing the duration time of solvent annealing to 1.5 hours, the long-range order failed to be obtained (Figure 5).

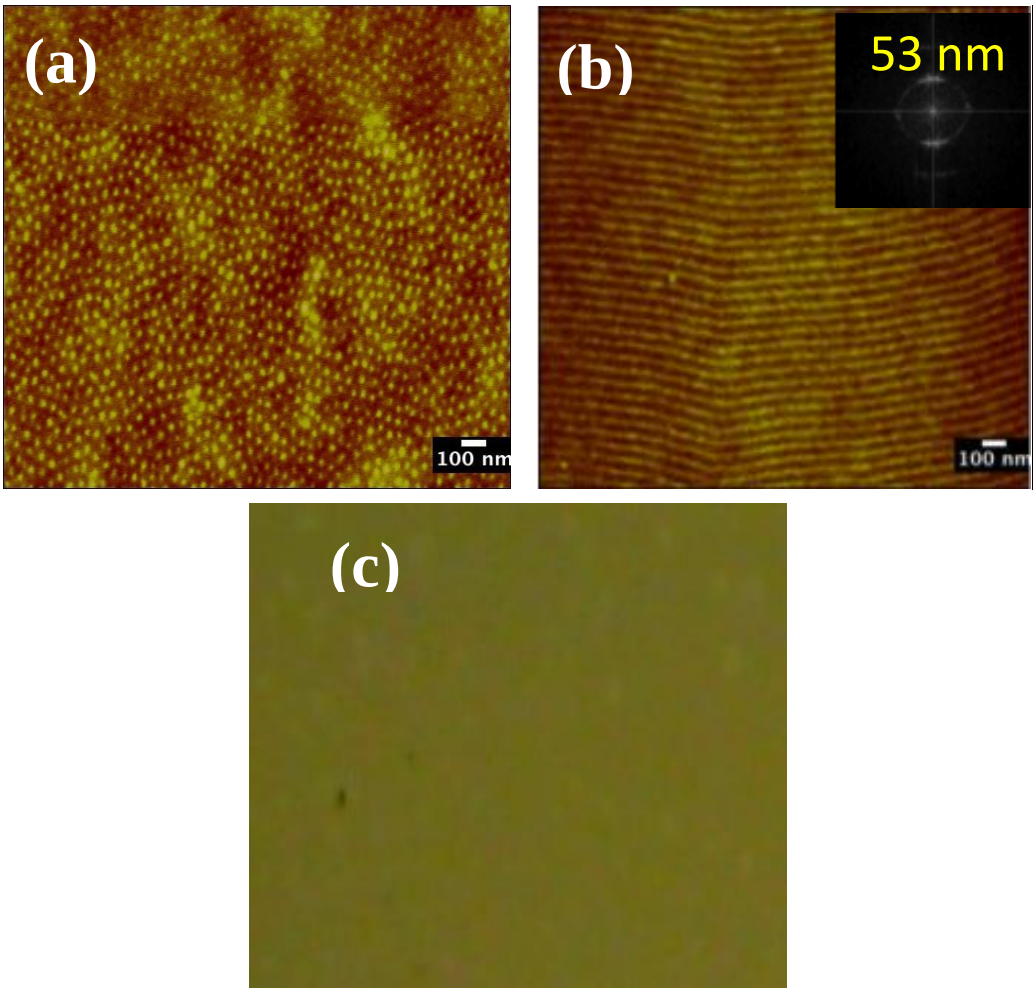

Figure 3: (a) AFM height image of as spun PS-*b*-P2VP thin film; (b) AFM height image of cylindrical P2VP microdomains with PS matrix and (c) microscope image of PS-*b*-P2VP thin film after solvent annealing for 3 hours.

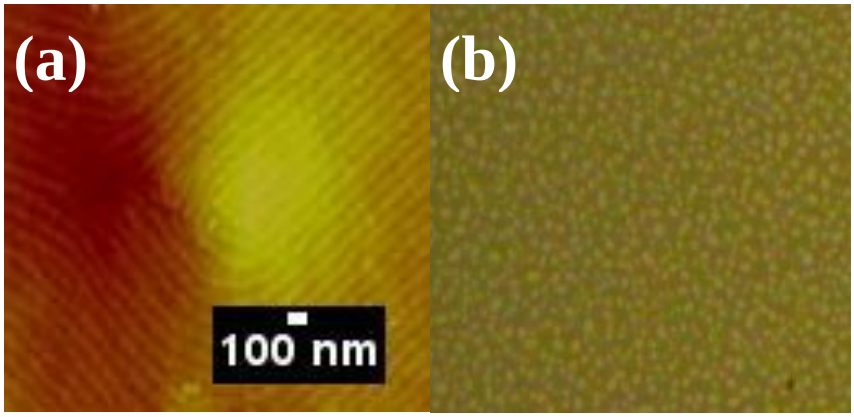

Figure 4: Images of (a) AFM height topography and (b) microscope of cylindrical P2VP microdomains of PS-*b*-P2VP thin film after solvent annealing for 5 hours.

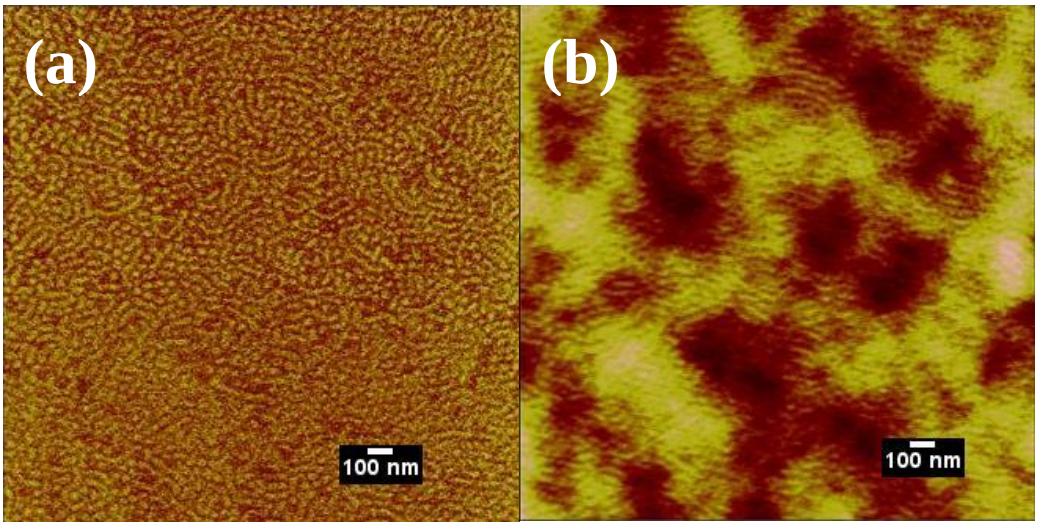

Figure 5: Images of solvent annealing for 1.5 hours of (a) phase and (b) height AFM images.

Therefore, this result showed that by furthering solvent annealing induced the terrace of the thin films and the long-range order cannot be attained with the shorter solvent annealing. This experiment has proved that the appropriate duration time of solvent annealing is extremely needed as purpose to obtain long-range ordered of PS-*b*-P2VP nano-template.

4.3.3 Effects of Surface Treatment with UV Etching on the Adsorption of Ferritin

As well known, the physicochemical process and modulation of electrostatic interaction between apo-ferritin and the surface of template can be effectively controlled by the adsorption type, density and morphology of apo-ferritin on a substrate.[58] Therefore from previous section I have discussed about ferritin affinity onto PS homopolymers and P2VP homopolymer, the result has been shown that the ferritin molecules tends to adsorb onto P2VP homopolymer thin film' surface instead of PS homopolymer thin film. I understand that after solvent annealing, the surface of this BCP template was covered with PS. In order to expose P2VP phase, I used UV etching method to remove the surface of PS layer.

Figure 6 shows the effect of irradiation time of UV etching on the adsorption of ferritin. When UV-irradiation duration time increased from 1 to 3 min (Figure 6 (a-c)), the adsorbed ferritin protein also increased. Therefore, it has been understood that ferritin protein adsorbed onto P2VP phase exposed by UV-irradiation. On the other hand, the irradiation longer than 3 minutes resulted in the distorted patterns (Figure 6 (d) and (e)) because of the excessive etching. In other words, UV-irradiation of 3 minutes in this case is the optimum for preparing the PS-*b*-P2VP nano-template to align ferritin protein.

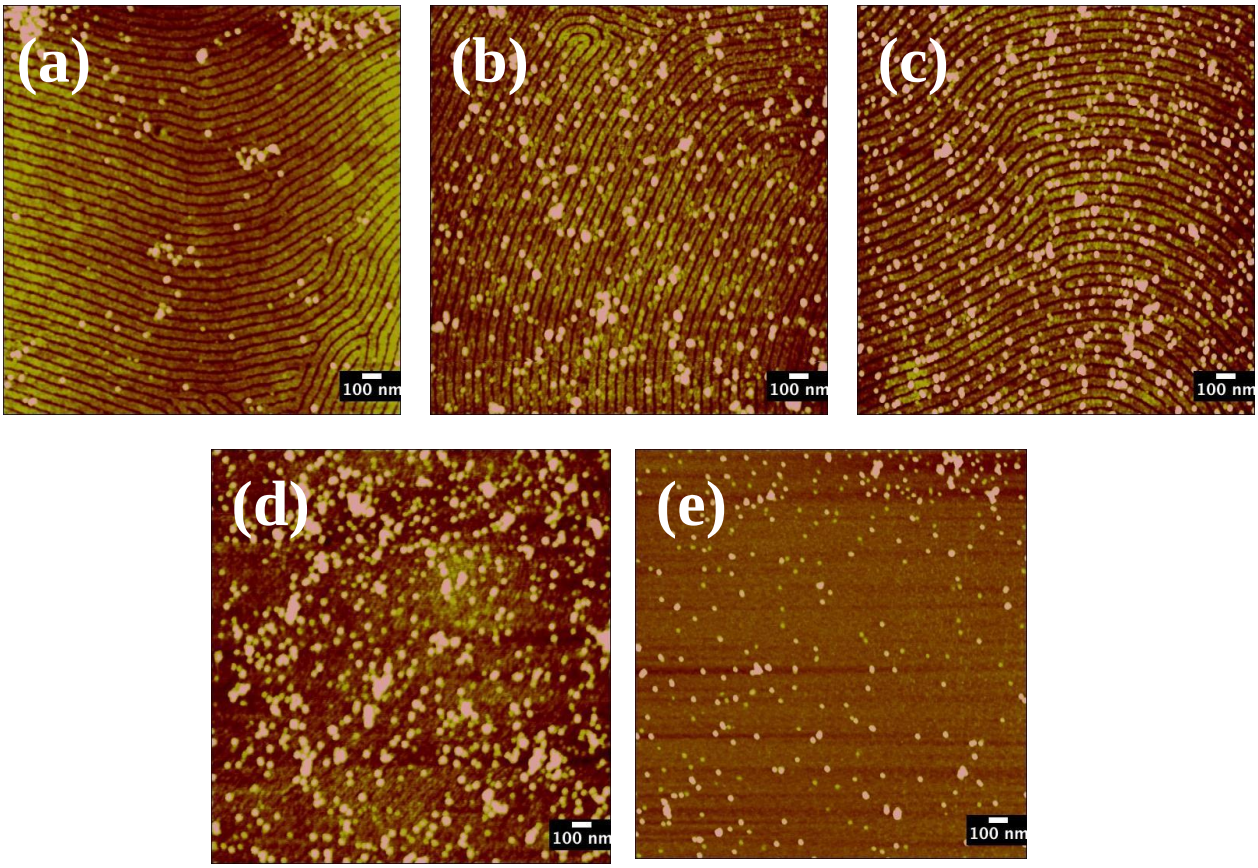

Figure 6: (a), (b), (c), (d) and (e) AFM images of PS-*b*-P2VP thin films were irradiated by UV in the air for 1 minute, 2 minutes, 3 minutes, 4 minutes and 5 minutes respectively before adsorption process with 0.1wt% ferritin protein.

Beside of hydrophilic property of P2VP homopolymer that caused the adsorption of ferritin molecules onto P2VP homopolymer, there was another factor that has been employed on this adsorption process. I understand that the THF still remains on the P2VP blocks even after UV etching and formed the P2VP surface to negative charge. Since THF contains oxygen atom and obtained highly electronegative also capable of forming hydrogen bonds [60] as discussed before. Therefore, while adsorption process; electrostatic interaction that was caused by anionic charge of P2VP and ferritin resulted in positive charge in pH 3.

Even though ferritin and apo-ferritin have the same shell but the difference between ferritin and apo-ferritin is in the presence and absence of the iron oxide within their core, respectively. Therefore, the adsorption density and adsorption constant of ferritin and apo-ferritin is differ due to the presence and absence of the iron oxide that could influence the adsorption property of the protein.[61] According to Uto et al. 2008, the values of adsorption density were larger than the theoretical values of a hexagonal close-packed monolayer of apo-ferritin on a substrate, although the apo-ferritin were adsorbed onto the thin film by an electrostatic interaction. They all mentioned that in this system, the structural relaxation after apo-ferritin adsorption has obtained an aggregation of apo-ferritin with two-dimensional movement in a dried state that caused by capillary forces.[58]

Johnson et al. 2000[62] and Uto et al. 2008[58] have found out that the electrostatic adsorption of ferritin or apo-ferritin can be described by the random sequential adsorption (RSA) model and Langmuir adsorption model, respectively. This discrepancy may be due to an adsorption

condition of apo-ferritin and ferritin is different due to the relatively higher ionic of the surface charges of apo-ferritin instead of ferritin. The Theoretical model of RSA is the model to explain about an irreversible monolayer adsorption, accounts for the electrostatic repulsion of adsorbate molecules. However, the Langmuir could be used to interpret the system with a reversible monolayer adsorption that does not account for lateral interaction at the surface. Hence, this Langmuir model can be applied to apo-ferritin adsorption in screening the electrostatic interactions by the high ionic strength. However for my study, the model might be difficult to apply cause of the template that used in this experiment has been designed with specific structure of parallel cylindrical. Meanwhile, the aforementioned models have been applied onto thin film' surface without any structure. On the other hand, the focus of this study was not about adsorption capacity of ferritin but the research has been done to find out the best method for developing the well alignment of ferritin onto the structured template of block copolymers. Also this information is important for further research for aligning the apo-ferritin molecules onto PS-*b*-P2VP template that has been discussed on the next chapter.

4.3.4 pH Dependence of Adsorption of Ferritin

Proteins which are one of the biological amphoteric molecules that contains both acidic and basic functional groups which derived from amino acid side chains. Arosio et al. 1978 have reported that the isoelectric point (pI) of horse spleen ferritin is 4.1–5.1.[58] Therefore, the charge of ferritin molecules can be easily controlled by pH condition of ferritin solution. Hence, the prediction can be done that ferritin could be adsorbed onto both cationic and anionic surfaces by electrostatic interaction between the ferritin molecule and the thin film's

precursor.

Figure 7 shows PS-*b*-P2VP templates with different pH value of ferritin protein with (a) pH 7 and (b) pH 3. The absorbability of ferritin protein is increased by maintaining ferritin protein in acidic condition at pH 3. At pH 3 that is below its pI, where ferritin carries positive charge, ferritin molecules has tended to adsorb more onto thin film' surface if compared to ferritin in pH 7. On the other hand, when at pH 7 (above its pI), ferritin carries a net negative charge, electrostatic repulsion between ferritin and P2VP could not be happened due to P2VP also carries negative charge as mentioned before. The adsorption process of ferritin's molecules onto thin film could be controlled by pH condition of ferritin solution due to obtain the appropriate surface charge of ferritin's molecules. Therefore, the result shows that the ferritin's molecules (positive charge) can be adsorbed by electrostatic interaction onto BCP template within P2VP block that has attained negative by remaining THF molecules.

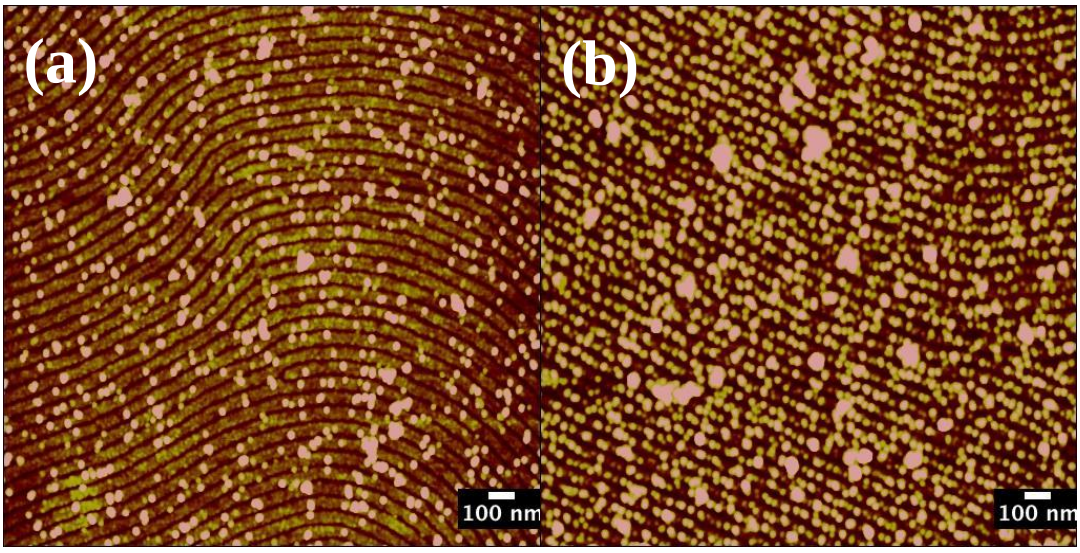

Figure 7: PS-*b*-P2VP thin film with alignment of ferritin protein (a) in pH 7 and (b) in pH 3.

For substrate without any designed structure, it can adsorb ferritin's molecules homogeneously without aggregation. However in my study, I used structured thin film to align ferritin's molecules by adsorbing ferritin's molecules onto BCPs nano-template. Most of the ferritin's molecules were adsorbed independently due to electrostatic repulsion on the ferritins molecules when they were adsorbed onto P2VP phase. Hence some aggregation still happened. The mechanism of this adsorption process is difficult to discuss deeply from the presented data. The details explanation could be discussed by an in situ analysis of the surface with techniques such as atomic force microscopy in an aqueous phase[58] and not at the dried state. However, in this study I just investigated the thin film at the dried state only. The adsorption factors including proper pH condition and UV etching treatment that applied onto ferritin solution and template before aligning process, might be useful for further research on consequence of well alignment with high density adsorption of ferritin protein on the selected block of block copolymer template by controlling the electrostatic interactions. The ferritin-immobilized film works as a two dimensional protein template for constrained synthesis and patterning of nanoparticle arrays for the next further research.

Accordingly, the ferritin adsorption that was observed in this study was caused by electrostatic interaction between the ferritin molecule and the surface of P2VP block of the thin film. The surface morphology shows a clear dependence on pH show the high adsorption density observed with ferritin adsorption at pH 3 suggested that ferritin molecules were uniformly distributed on template's surface with remarkable aggregation.[58] However, the most of the ferritin molecules has aligned well onto the PS-*b*-P2VP template. The distances of

ferritin protein after alignment process onto PS-*b*-P2VP template have been shown in Figure 8. The graph shows, the distance (d_2) of ferritin protein in range of 20 nm - 40 nm. While FFT analysis of AFM height image or d_1 gives 53 nm of spacing that is matched with PS-*b*-P2VP domain spacing.

The formation of this PS-*b*-P2VP template may inhibit the aggregation of ferritin molecules. Although some aggregates of ferritin molecule were also observed in this study but the size of aggregates was clearly smaller. From these results, the selection of suitable conditions seems to be critical in aligning process of ferritin molecules onto PS-*b*-P2VP template.

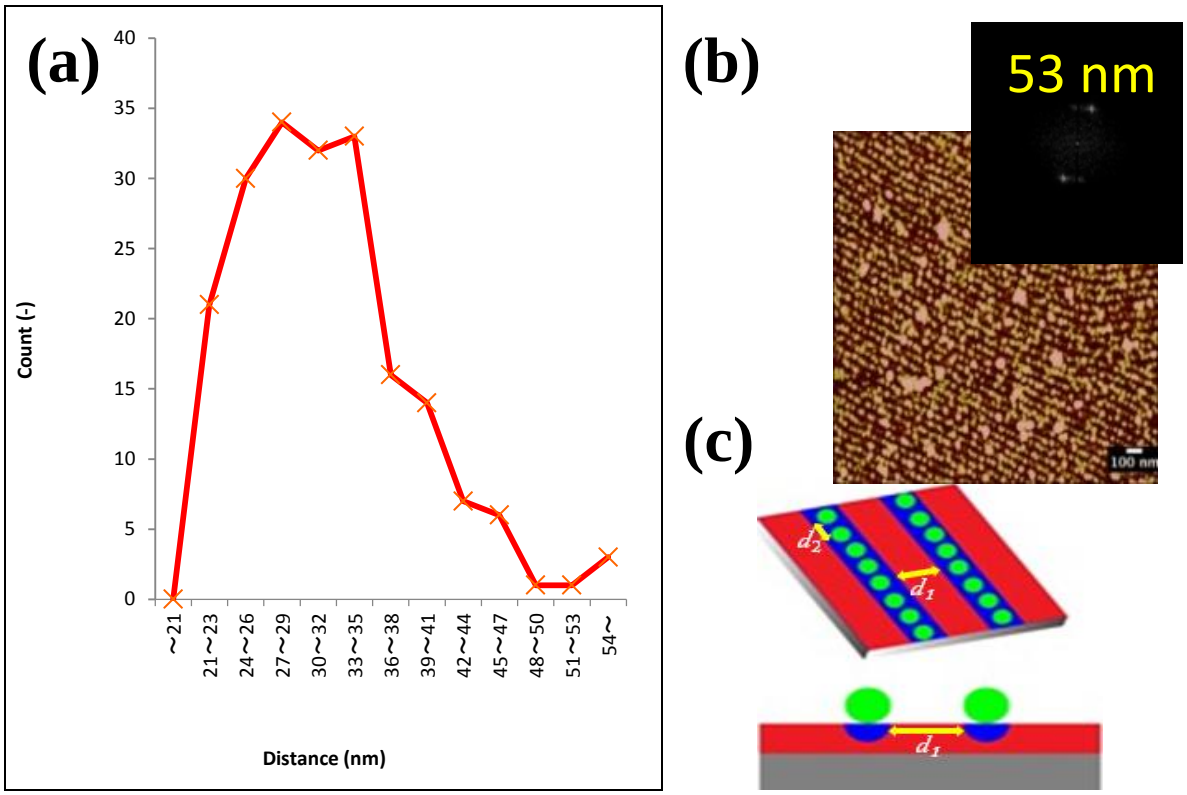

Figure 8: (a) Graph of distance (d_2) between center lines of ferritin protein in acidic condition; (b) FFT analysis of AFM height image (d_1); (c) Illustration of (d_1) and (d_2).

4.4 Conclusion

The study of adsorption behavior of ferritin on the thin film using PS-*b*-P2VP BCPs. When the pH of solution is far from the pI of ferritin (4.1– 5.1), ferritin could not be selectively adsorbed onto P2VP block surface of the thin film by electrostatic interaction. The adsorption conditions, such as the surface charge of BCPs thin film and solution pH, significantly affected their electrostatic adsorption behavior. This shows that the electrostatic interactions not caused by only on appropriate pH condition but also depends on remaining THF solvent on the P2VP surface that contains oxygen atom and obtained electronegative. These factors are important for ferritin adsorption onto this thin film.

Moreover, appropriate duration time of UV-irradiation on PS-*b*-P2VP BCP template also plays important role of self-assemblies between PS-*b*-P2VP BCP and ferritin protein. Based on these experiments, I confirmed that ferritin protein can be aligned on parallel cylindrical pattern of PS-*b*-P2VP BCP with highly adsorption capacity by self-assemblies. The method that has proposed here is to form an alignment of ferritin molecules with well array which can cater to a wide range of applications such as catalysts, transducers of sensors, quantum dots (fluorescence emitters) etc. Based on the information was obtained from this study, it will be possible to build more complex functional inorganic nanoparticle-based nanostructures with desired area and coverage that will be discussed on next chapter (Chapter 5).

Therefore, it can be concluded that this PS-*b*-P2VP BCP is a nano-patterned template that have potential to be introduced in wide range of new applications such as biosensors.

References

[1] N. Kumar, J. I. Hahm, *Langmuir* **2005**, *21*, 6652.

[2] G. Liu, J. Zhao, *Langmuir* **2006**, *22*, 2923.

[3] J. H. Park, Y. Sun, Y. E. Goldman, R. J. Composto, *Macromolecules* **2009**, *42*, 1017.

[4] J. G. Son, W. K. Bae, H. Kang, P. F. Nealey, K. Char, *American Chemical Society* **2009**, *3(12)*, 3927.

[5] J. Y. Cheng, C. A. Ross, H. I. Smith, E. L. Thomas, *Adv. Mater.* **2006**, *18*, 2505.

[6] S. O. Kim, H. H. Solak, M. P. Stoykovich, N. J. Ferrier, J. J. de Pablo, P. F. Nealey, *Nature* **2003**, *424*, 411.

[7] I. Bita, J. K. W. Yang, Y. S. Jung, C. A. Ross, E. L. Thomas, K. K. Berggren, *Science* **2008**, *321*, 939.

[8] F. S. Bates, G. H. Fredrickson, *Annu. Rev. Phys. Chem.* **1990**, *41*, 525.

[9] M. Park, C. Harrison, P. M. Chaikin, R. A. Register, D. H. Adamson, *Science* **1997**, *276*, 1401.

[10] S. H. Kim, M. J. Misner, T. P. Russell, *AdV. Mater.* **2004**, *16*, 2119.

[11] S. H. Kim, M. J. Misner, T. Xu, M. Kimura, T. P. Russell, *AdV. Mater.* **2004**, *16*, 226.

[12] J. G. Son, X. Bulliard, H. Kang, P. F. Nealey, K. Char, *AdV. Mater.* **2008**, *20*, 3643.

[13] R. D. Peters, X. M. Yang, T. K. Kim, B. H. Sohn, P. F. Nealey, *Langmuir* **2000**, *24*, 4625.

[14] Y. C. Tseng , S. B. Darling, *Polymers* **2010**, *2*, 470.

[15] S.B. Darling, *Prog. Polym. Sci.* **2007**, *32*, 1152.

[16] B. B. Sauer, G. T. Dee, *Macromolecules* **2002**, *35*, 7024.

[17] J. Heier, J. Genzer, E. J. Kramer, F. S. Bates, S. Walheim, G. J. Krausch, *Chem. Phys.* **1999**, *111*, 11101.

[18] J. J. Chiu, B. J. Kim, E. J. Kramer, D. J. J. Pine, *Am. Chem. Soc.* **2005**, *127*, 5036.

[19] J. I. Abes, R. E. Cohen, C. A. Ross, *Chem. Mater.* **2003**, *15*, 1125.

[20] X. Li, J. Peng, Y. Wen, D. H. Kim, W. Knoll, *Polymer* **2007**, *48*, 2434.

[21] H. Yokoyama, T. E. Mates, E. J. Kramer, *Macromolecules* **2000**, *33*, 1888.

[22] H. Kitano, S. Akasaka, T. Inoue, F. Chen, M. Takenaka, H. Hasegawa, H. Yoshida, H. Nagano, *Langmuir* **2007**, *23*, 6404.

[23] A. K. Khandpur, S. Forster, F. S. Bates, I. W. Hamley, A. J. Ryan, W. Bras, K. Almdal, K. Mortensen, *Macromolecules* **1995**, *28*, 8796.

[24] M. W. Matsen, M. Schick, *Phys. ReV. Lett.* **1994**, *72*, 2660.

[25] M. Takenaka, T. Wakada, S. Akasaka, S. Nishitsuji, K. Saijo, H. Shimizu, M. I. Kim, H. Hasegawa, *Macromolecules* **2007**, *40*, 4399.

[26] S. Akasaka, H. Yoshida, H. Hasegawa, E. Dobisz, D. Kercher, M. Takenaka. *Macromolecules* **2008**, *41*, 9267.

[27] D. Y. Ryu, K. Shin, E. Drockenmuller, C. J. Hawker, T. P. Russell, *Science* **2005**, *308*, 236.

[28] S. B. Darling, *Progr. Polym. Sci.* **2007**, *32*, 1152.

[29] H. C. Kim, S. M. Park, W. D. Hinsberg, *Chem. Rev.* **2010**, 110, 146.

[30] C. T. Black, K. W. Guarini, K. R. Milkove, S. M. Baker, T. P. Russell, M. T. Tuominen, *Appl. Phys. Lett.* **2001**, *79*, 409.

[31] R. A. Segalman, H. Yokoyama, E. J. Kramer, *AdV. Mater.* **2001**, *13*, 1152.

[32] D. Sundrani, S. J. Sibener, *Macromolecules* **2002**, *35*, 8531.

[33] J. Y. Cheng, A. M. Mayes, *Nat. Mater.* **2004**, *3*, 823.

[34] S. G. Xiao, X. M. Yang, E. W. Edwards, Y. H. La, P. F. Nealey, *Nanotechnology* **2005**, *16*, S324.

[35] F. Chen, S. Akasaka, T. Inoue, M. Takenaka, H. Hasegawa, H. Yoshida, *Macromol. Rapid Commun.* **2007**, *28*, 2137.

[36] D. E. Angelescu, J. H. Waller, D. H. Adamson, P. Deshpande, S. Y. Chou, R. A. Register, P. M. Chaikin, *AdV. Mater.* **2004**, *16*, 1736.

[37] T. Thurn-Albrecht, J. Scotter, G. A. Kastle, N. Emley, T. Shibauchi, L. Krusin-Elbaum, K. Guarini, C. T. Black, M. T. Tuominen, T. P. Russell, *Science* **2000**, *290*, 2126.

[38] P. Mansky, J. DeRouchey, T. P. Russell, J. Mays, M. Pitsikalis, T. Morkved, H. Jaeger, *Macromolecules* **1998**, *31*, 4399.

[39] P. Mansky, Y. Liu, E. Huang, T. P. Russell, C. Hawker, *Science* **1997**, *275*, 1458.

[40] T. Xu, A. V. Zvelindovsky, G. J. A. Sevink, K. S. Lyakhova, H. Jinnai, T. P. Russell, *Macromolecules* **2005**, *38*, 10788.

[41] K. Amundson, E. Helfand, D. D. Davis, X. Quan, S. S. Patel, S. D. Smith, *Macromolecules* **1991**, *24*, 6546.

[42] T. L. Morkved, M. Lu, A. M. Urbas, E. E. Ehrichs, H. M. Jaeger, P. Mansky, T. P. Russell, *Science* **1996**, *273*, 931.

[43] J. G. Son, X. Bulliard, H. Kang, P. F. Nealey, K. Char, *AdV. Mater.* **2008**, *20*, 3643.

[44] R. D. Peters, X. M. Yang, T. K. Kim, B. H. Sohn, P. F. Nealey, *Langmuir* **2000**, *24*, 4625.

[45] R. D. Peters, X. M. Yang, Q. Wang, J. J. de Pablo, P. F. Nealey, *J. Vac. Sci. Technol. B* **2000**, *18*, 3530.

[46] R. D. Peters, X. M. Yang, T. K. Kim, P. F. Nealey, *Langmuir* **2000**, *24*, 9620.

[47] S. Ji, G. Liu, F. Zheng, G. S. W. Craig, F. J. Himpsel, P. F. Nealey, *AdV. Mater.* **2008**, *20*, 3054.

[48] I. In, Y. H. La, S. M. Park, P. F. Nealey, P. Gopalan, *Langmuir* **2006**, *22*, 7855.

[49] E. Han, I. In, Y. La, S. Park, Y. Wang, P. F. Nealey, P. Gopalan, *AdV. Mater.* **2007**, *19*, 4448.

[50] J. Bang, J. Bae, P. Lo¨wenhielm, C. Spiessberger, S. A. Given-Beck, T. P. Russell, C. J. Hawker, *AdV. Mater.* **2007**, *19*, 4552.

[51] E. W. Edwards, M. F. Montague, H. H. Solak, C. J. Hawker, P. F. Nealey, *AdV. Mater.* **2004**, *16*, 1315.

[52] E. W. Edwards, M. Muller, M. P. Stoykovich, H. H. Solak, J. J. de Pablo, P. F. Nealey, *Macromolecules* **2007**, *40*, 90.

[53] Y. H. La, E. W. Edwards, S. M. Park, P. F. Nealey, *Nano Lett.* **2005**, *5*, 1379.

[54] M. P. Stoykovich, E. W. Edwards, H. H. Solak, P. F. Nealey, *Phys. ReV. Lett.* **2006**, *97*, 147802.

[55] M. P. Stoykovich, M. Muller, S. O. Kim, H. H. Solak, E. W. Edwards, J. J. de Pablo, P. F. Nealey, *Science* **2005**, *308*, 1442.

[56] S. M. Park, G. S. W. Craig, Y. H. La, H. H. Solak, P. F. Nealey, *Macromolecules* **2007**, *40*, 5084.

[57] C. M. Grozea, I. T. S. Li, D. Grozea, G. C. Walker. *Macromolecules* **2011**, *44*, 3901.

[58] K. Uto, K. Yamamoto, N. Kishimoto, M. Muraoka, T. Aoyagi, I. Yamashita, *J. Mater. Chem.*, **2008**, *18*, 3876.

[59] I. Yamashita, *Thin Solid Films* **2001**, *393*, 12.

[60] W. H. Huang, P. Y. Chen, S. H. Tung, *Macromolecules* **2012**, *45*, 1562.

[61] K. C. Martin, S. M. Villano, P. R. McCurdy, D. C. Zapien, *Langmuir* **2003,** *19*, 5808.

[62] C. A. Johnson, Y. Yuan, A. M. Lenhoff, *J. Colloid Interface Sci.* **2000**, *223*, 261.

5

Aligning CdS Quantum Dots in Apo-ferritin Protein and PS-*b*-P2VP Organic Templates

5.1 Introduction

Semiconductor nanocrystals, also known as quantum dots (QDs), are one of the emerging nanomaterials that offer various advantages in the development of new devices specifically in nanoscience and optical sciences. QDs properties are intermediary between bulk semiconductors and discrete molecules which have excitons confinement in all spatial dimensions. When QDs excite the energy higher than their band gap, photons are emitted by releasing the absorbed energy. The emission energy is an important optical property for QDs and it is possible to change the energy by governing the composition and particle size of the QDs that contribute to the quantum confinement effects.[1] This effect influences the QDs to emit different colour of emission under UV light depending on the size of QDs.[2] Meanwhile, the Quantum-confined Stark effect in quantum well is very important in understanding optic modulations.[3] The Stark effect exudes strong effect in nanoscale for semiconductors due to energy levels that can be adjusted by an externally applied electric field.[2] Furthermore, in order to apply QDs in biological uses, the chemical surface of the QDs is an important parameter to control to obtain suitable and applicable QDs as tissue and cell tracer. This present property of QDs has widely opened the potential of developing nanobio devices that can function as tracers. From their diffusion and movements in biological tissues, targeted abnormal tissues and cells can be tracked down.[2] This is how QDs can be employed in biomedical application.

In order to emerge in the field of nanobiotechnology, the fabrication of hybrid nanocomposites using protein nanocages is required.[2,4-9] The attractive scaffold template for fabricating hybrid bionanostructure can be developed using protein nanocages due to their unique surface structure which have various functionalities as well as the capability to self-assemble.[10] A natural nanocage with a well-defined globular morphology with the capacity of loading an inorganic core is the best option as a QDs carrier, which is perfect for biological applications. Horse spleen ferritin (HSF) is a robust iron-storage which can also act as a natural nanocage or nanoreactor.[11] The core of the HSF contains iron oxide with a diameter measured at 8 nm and shell diameter at 12 nm, obtained by arranging 24 polypeptide subunits in a spherical shape.[10] The HSF without iron oxide is called apo-ferritin and this empty core can be loaded with metal or semiconductor nanoparticles such as cobalt, nickel, palladium. CdS, CdSe QDs, etc.[12] Additionally, the outer surface of an HSF cage has the potential to assemble onto other organic surfaces such as block copolymer. Other than that, HSF can also serve as a biological scaffold template for applying a variety of functions to the QDs due to its adjustable exterior and interior surfaces.[13]

A study conducted on preparing CdS QDs has been published by B.T et al. 2011,[10] whereby a reduction agent was added to the reaction of metal ion and HSF. In doing so, metal nanoparticles can be easily loaded in the dimension close to the HSF interior via hydrophilic channel.[12] Another approach was conducted by Naik and his co-worker were they synthesized silver nanoparticles in the inner C-terminal end of human L chain ferritin and the silver nanoparticles constrained inside the protein cavity have produced monodisperse products.[14] On the other hand, the higher ordered CoPt and FePt nanoparticles have been grown in apo-ferritin, resulting in a narrow size distribution, as synthesized by Mayes et al. 2003.[15] This ferritin-encapsulated CoPt or FePt has obtained a hexagonal close-packed (hcp) structure whereby the shape of the structure depends on the ferritin nanocage and not by the particles-apoferritin system.[2] By introducing ferritin nanocage when preparing QDs, the size distribution of the system can be controlled persistently.

Ferritin can also be deposited as quasi-crystalline ferritin layers on a substrate to form iron oxide nanoparticles arrays. This is known as two-dimensional (2D) array of iron oxide nanoparticles that are embedded on a substrate, as demonstrated by Yuen et al. 2007 [16] and Yamashita 2001.[17] A spin-coating technique has been applied to obtain this result based on evaporation-induced convective assembly. The ferritin molecules' organic protein shells were removed by controlling the pyrolysis and leaving the ordered iron oxide on the silica substrate.[18] The 2D-arrays of CdS QDs can also be formed using this method if needed.

Block copolymer (BCP) without other composites like nanoparticles can form ordered structures due to competing effects and microphase separation. The microdomains of BCP composed of different blocks in tens of nanometers are formed only over distances of several tens lattice constant. The long range ordered microdomain segregation has been influenced by both internal and external controls the formation during treatment process. The internal control includes molecule weight, composition, chain architecture, etc. The external influences may include mechanical flow field,[19] electric field,[20] the influence of surface interaction,[21] chemically pattern surface,[22] temperature gradient to create a preferred orientation of microdomain, etc.[23]

Detailed mechanisms for the nanoparticles-polymer composites have been investigated via theoretical and computer simulations for the development of structural and physical properties. A Lattice Monte Carlo simulation has been performed by Huh et al. 2000 [24] to determine the phase behaviour of nanoparticles in melted-block copolymer domains.[25] When the size of the nanoparticles is comparable to the radius of gyration of block with A-B diblock, BCPs has formed a microphase transition. Another research by Aizawa's group has shown the selective loading of different metallic of Au/Ag bimetallic array onto triblock BCPs template with different functional block.[26] The BCP as the template that is used to align metallic nanoparticles, not only serve as an equivalent polymer resistant structure for subsequent pattern transfers but can also be employed as

carrier to load metallic nanoparticles to be turned into metallic nanostructures. The metal ions in an anionic metallic solution can adsorb onto PS-*b*-P2VP BCPs.[27] Due to P2VP blocks becoming protonated in an acidic condition and carrying positive charges, the anions which are metal ions with negative charges, are attracted to the cationic P2VP blocks and are embedded into the P2VP blocks. Then, the P2VP BCPs can be eliminated via oxygen plasma etching, thus leaving only the metallic nanoparticles in the shape of the P2VP blocks on the substrate.

Another study has reported producing gold nanowire in PS-*b*-P2VP BCPs. The PS-*b*-P2VP was treated with annealing at 230 °C for 24 h, followed by aligning P2VP block in nanoscale trenches of Si substrate that has been pre-patterned by e-beam lithography and dry etching to obtain a nanowires pattern. After that, the P2VP-patterned silicon substrate was immersed into 10 mM $HA\mu Cl_4$ + 0.9% HF solution for 5-10 minutes, then generated the $[AuCl_4]^-$ to load into P2VP nanowires. Finally, oxygen plasma treatment was applied to eliminate P2VP with the aim of exposing gold nanowire.[27] Moreover, segregating the nanoparticles into cylindrical P2VP microdomains has improved the microdomain's order. This assembly process should be used for several of other systems due to the surface chemistry of nanoparticles that can be tuned.[28] These studies have shown the manipulation via physical and chemical methods, while BCPs lithography can be used as an alternative nanostructure technique to develop large area of polymer patterns at 100 nm.[29]

Furthermore, a good example of manipulating genetical and chemical surface properties included bio-nanoparticles such as ferritin-inorganic materials. This idea has captured scientists' interest because of the unique functionalities of this hybrid system which can be applied as nanocarrier in the medical field.[28] These bionanoparticles can be aligned onto BCP by segregation them to the BCP interface and this system dependent on film thickness. The manipulation of BCP orientation requires external influence depending on the nature of the interfaces and the geometry of the

system. For systems such as PS-*b*-P2VP, the interfacial interactions are too strong and the large external influence cannot reorient the entire domain of thin film. Therefore, synthesized of nanocrystals[30] and bionanoparticles can be formed by modifying the surface[31] using a biomineralized method. The results of a synergy assembly system can be employed as chemical sensing, separation, catalysis, high-density data storage and photonic materials due to the system that can be controlled remarkably and has the flexibility of fabrication for nanostructure materials.

The precise assembly and patterning of nanoparticles on the surface and at the interface of BCP is essential for developing functional devices.[32] Moreover, the significance of monodispersity and homogeneity of nanoparticles is needed to create versatile nanoparticles for various applications. Therefore, the self-assembly of incorporating inorganic nanoparticles such as Cadmium Sulphide (CdS) into BCPs such as PS-*b*-P2VP microphase-separated, has been intensively studied to develop novel functional hybrid materials.[33] The focus of my study is on in vitro research on developing a biosensor that can be applied to trace abnormal human cells by combining inorganic materials (i.e. CdS) with biological materials (apo-ferritin) and the organic template of BCPs (PS-*b*-P2VP). This device needs to go through more in vivo research before it can be applied to a human body.

5.2 Experimental Procedure

5.2.1 Materials

Asymmetric polystyrene-*block*-poly(2vinylpyridine) (PS-*b*-P2VP) diblock copolymer[34] with molecular weight of 79.0k-*b*-36.5kkg/mol and polydispersity index of 1.05 from Polymer Source, Inc. was used to form thin film template, while toluene was used for solvent annealing process with the purpose of inducing perpendicular cylinder structure of PS-*b*-P2VP.

5.2.2 Substrate Preparation

Silicon(100) wafers were cut into 1.0 cm^2 pieces and cleaned via piranha cleaning procedure. The substrates were treated with a mixture of H_2O_2 (30%) and H_2SO_4 (70%) (v/v) at 100 °C for 30 minutes and then rinsed with distilled water, followed by drying in a stream of nitrogen. Then, the substrates underwent UV treatment for 15 minutes before being used immediately.[35]

5.2.3 Thin Film Preparation

Ultrathin films were prepared by spin-coating 1 wt% PS-*b*-P2VP block copolymer solution with a solvent mixture consisting of toluene and tetrahydrofuran (THF) with a ratio of 7:3. Then, the PS-*b*-P2VP solvent was spin-coated at 5000 rpm for 20 s on silicon wafers.

5.2.4 Solvent Annealing Condition

The ultrathin films were solvent vapour-annealed using toluene for 6 h at 21 °C. 25 ml volume of toluene solvents was filled in small Petri dish and covered with a piece of aluminium foil with small holes on it. This Petri dish was placed in the glass bottle that was used for the solvent annealing treatment. The films were placed on a glass slide that was placed on top of the Petri dish.

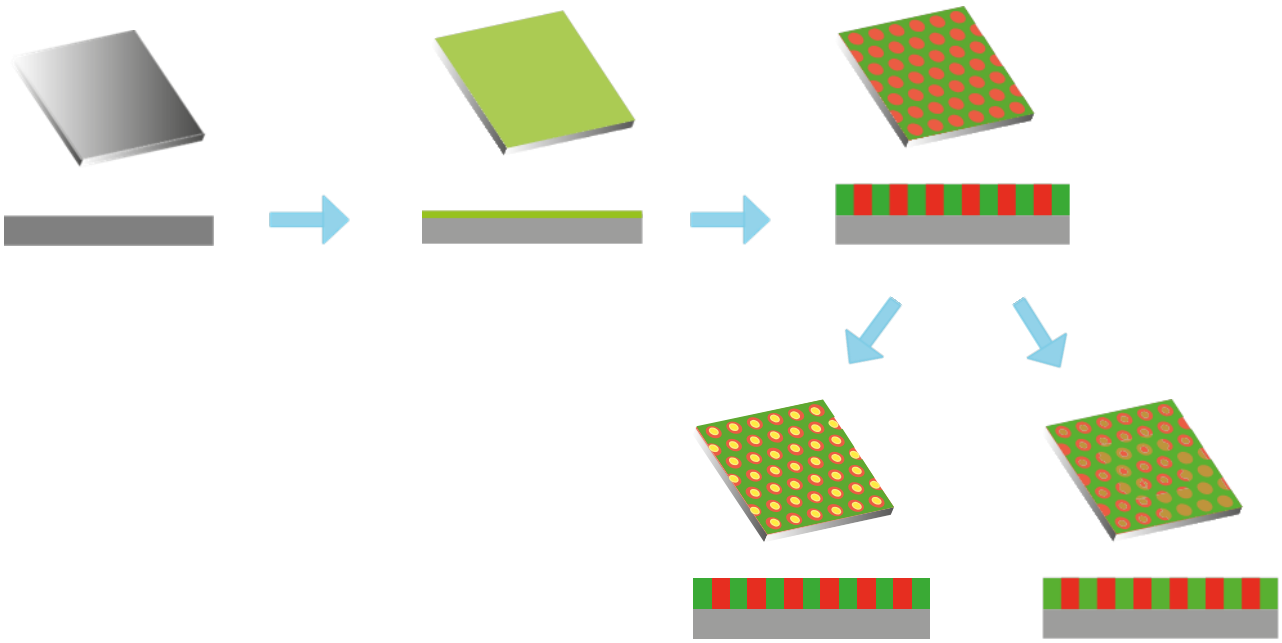

Figure 1: The experimental procedure of making arrays of CdS QDs and CdS-apoferritin onto cylindrical pattern of PS-*b*-P2VP block copolymer.

5.2.5 Preparation of CdS Quantum Dots (QDs)

CdS quantum dots were synthesized via a colloidal method using TGA as the stabilizing agent. Briefly, 0.3 mmol Cadmium Acetate was dissolved in 65 ml water and 20 µl thioglicolic acid (TGA) was added under continuous stirring. The pH value was adjusted with a pH modifier (0.1 M NaOH) to pH 9. Next, 0.02 mmol Sodium Sulphide (Na_2S) was dissolved in 35 ml water. The oxygen in the system was removed by a nitrogen flow. Under stirring condition, Na_2S was added. Then, the colloidal CdS was kept overnight at room temperature under continuous stirring.[36]

5.2.6 Preparing CdS-Apoferritin Complexes

The steps for this part were referred to Iwahari Kenji's [37] research with some adjustments during synthesis. The CdS-apoferritin was prepared by mixing 1 M of ammonium acetate, 1 M of ammonia water and 100 mM of a cadmium acetate solution with 300 ml of distilled water. Then, 0.3 mg/ml of apo-ferritin solution from horse spleen is added to the resultant reactant. Then, the reaction was allowed to stand for 10 minutes under nitrogen flow at room temperature to obtain

ammonium complex of cadmium. After that, 0.02 mmol Sodium Sulphide was added to the reaction solution. The reaction solution was allowed to stand for 24 hours at room temperature with vigorous stirring condition to yield CdS-apoferritin complexes in pH 9-10.

5.2.7 Morphology Measurement

The topographical morphology of these thin films was investigated using atomic force microscopy (AFM) and scanning electron microscopy (SEM) topography. AFM was performed with a multimode AFM system of a Nanoscope III scanning probe microscope (Digital Instruments) in tapping mode. The tapping mode was operated by using Olympus cantilevers with spring constants ranging between 39.7 N/m and 71.6 N/m and resonant frequencies of 293.8-356.0 Hz. I observed the structures of polymer films by using a Hitachi S-4800 field-emission scanning electron microscope (SEM) instrument operated at an acceleration voltage of 1.5 kV. The SEM detects the secondary electrons of the films, and therefore, contrast of SEM images depends on the amounts of the secondary electrons.

The sizes of CdS QDs and CdS-apoferritin complexes were measured using transmission electron microscopy (TEM) and small angle scattering (SAXS). TEM micrographs of the colloidal dispersions were obtained using a JEM-2000FX instrument operated at 200 kV as the acceleration voltage. The high-resolution carbon-supported copper mesh was used to support the samples of colloidal dispersions. The diameter of each particle was determined from enlarge photographs. SAXS experiments were performed for the colloidal dispersions of CdS QDs, stabilized by SDS before and after UV-irradiation, at BL-6A station in KEK-PF. The X-ray wavelength and the sample-to-detector distance were 0.15 nm and 1200 mm, respectively. PILATUS 300K was used as the detector.

The optical property of CdS QDs was measured using UV-vis Absorption spectrum and Photoluminescence spectrum. The UV-vis Absorption spectrum for the colloidal dispersions of CdS QDs as the corresponding ionic precursors was measured by Hitachi U-3010 spectrometer to determine the adsorption peak of each sample. Photoluminescence spectrum was performed using a F-7000 spectrofluorometer (Hitachi, Japan) with a quartz cell (1 cm × 1 cm). The fluorescence spectra were recorded at λ_{ex} = 335 nm.

5.3 Results and Discussions

5.3.1 Synthesis CdS QDs via the Ideal Method

I have successfully synthesized CdS quantum dots using a wet-chemical method. Usually, the metal salt reduction is chosen as a practical strategy to produce bimetallic or layered bimetallic systems from different types of quantum dots such as CdS and CdSe.[38] This wet-chemical method is one of "bottom up" approach for preparing nanoparticle that rely on the chemical reduction of metal salts, electrochemical pathways, or the controlled decomposition of metastable organometallic compounds.[39] The metal chalcogenide nanoparticles have been selected in this experiment due to the air stable precursors that promises luminescent particles as the outcome.[9] In this study, CdS quantum dots with yellow colloidal solution was obtained because it contains sulphide ions (Figure 2 (a)) and also due to its quantum size. Emission from photons that are transited from excited state to ground state, which emitted orange fluorescent emission under UV light with 365 nm of wavelength, is shown in Figure 2 (b). Figure 2 (c) shows the distribution of physical sphere structure of naked CdS QDs, obtained with large size of 100 nm at low magnification of 30k and also 60k. However, when the observation was done at higher magnification of 150k, it was found that the inside dark circle contains a group of little dots of 8-10 nm in diameter. These dots are the real naked CdS QDs and I assume that these CdS QDs have positioned themselves closely to each other which caused the formation of the large sphere shape at low magnification. The size of these naked CdS QDs has been measured by using image-J software.

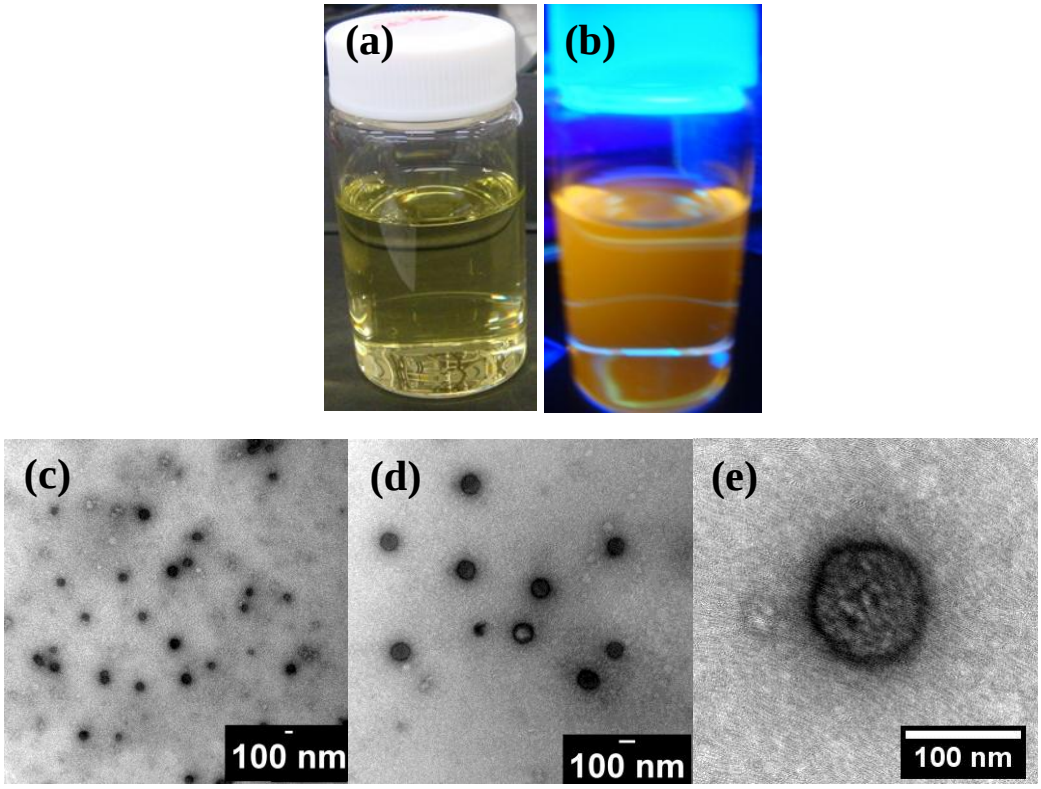

Figure 2: CdS QDs under visible light (a) and UV light (b). TEM images of CdS QDs are shown in Figure 2 (c),(d) and (e).

Essentially, nanoparticles with different sizes and shapes can be obtained by applying this method.[2] In the case of this study, the present sphere shaped CdS QDs with average size of 8 nm-10 nm have been produced after being coated with stabilizer surfactant. It is well-known that the right selection of ligand and surfactant during synthesis can assist in obtaining QDs with unique additional properties. The type and amount of surfactant and ligand strictly play an important role for QDs determination.[40-41] In order to obtain a colloidal solution, I controlled the ratio of Cd ion to S ion with 1:1 and used thioglycolic acid (TGA) as the stabilizer and left the CdS QDs growth in the embryonic stage of nucleation to give zero-valent of CdS QDs.[42]

The use of ligand in a wet-chemical synthesis is not only for adding unique function to QDs but also to achieve stabilization of zero-valent QDs. Apart from using ligand and surfactant, I can also use polymers and biological molecules as protective and stabilizer agents, which offer excellent

control over the morphologies of the nanocolloids.[43] Creating stable and re-dispersible QDs depends on the properties of the protective agents.[43] Therefore, TGA has been selected as a stabilizer to form steric stabilizing mode while polyethyleneimine (PEI) was selected as a ligand which is a type of polyelectrolyte (PET), to enhance the optical property of the CdS. Two main interactions played important roles in stabilizing the colloidal system; electrostatic and steric stabilizations. Columbic repulsion between the particles was involved during electrostatic stabilization due to the electrical double layers formed by ions adsorbed at the particle surface and corresponds by counterions.[39] However, steric stabilization was achieved when organic molecules act as protective shields on the QDs' surface.[2,39]

Manipulating Columbic interactions between positive and negative QDs can be done by tuning the nature property and length of capping ligands. This manipulation has allowed the formation of binary superlatices with defined stoichiometries of the building blocks. Carefully selected surface modifiers have opened up the possibility of introducing new principles for inducing the interaction between QDs that drive QDs to be organized into confined structures and manipulate the separation distances and interactions between homogenous and heterogeneous QDs.[2] Figure 3 (a) and 3 (b) display the CdS QDs coated with PEI under visible light and UV light, respectively. The results showed that the CdS-PEI QDs has changed to yellow luminescent caused by quantum confinement and the size of CdS-PEI was decreased by the PEI capping agent. I have used PEI to manipulate the columbic interaction between Cd^{2+} and S^{2-} that resulted in a high PL spectrum peak that correspond to energy released by the transition of photon from conduction band to valence band.

Additionally, applying suitable and multi-functional ligands for chemical surface functionalization of QDs' surface is strictly important in order to establish multifunctional QDs devices.[44] This CdS coloidal system is presented in alkaline aqueous medium with pH 10.25 and the zeta potential of PEI as studied by Miura et al. 2007, has given a negative charge when PEI is in an alkaline

condition.[45] Therefore, these CdS QDs with PEI capping agent has obtained negative charge. The result of CdS QD's emission colour changing from orange to yellow due to PEI capping agent is shown in Figure 3(c).

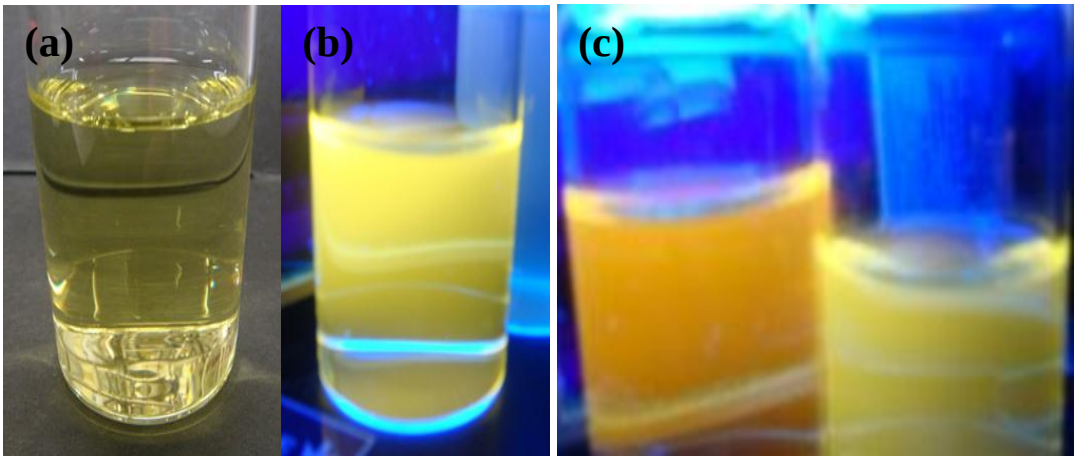

Figure 3: Rounded CdS QDs with polyethyleneimine (PEI) under visible light (a) and UV light (b). Figure 3(c) is picture of CdS QDs and coated CdS QDs with PEI under UV light.

Figure 4 (a) shows large spherical dots with average size of 500 nm-1000 nm. However, when the observation was done at high magnification as depicted in Figure 4 (c) and Figure 4 (d), I discovered that the dark spheres were not actually CdS QDs but PEI shells. The round dark circle is amino group from PEI that has formed surface-bounded amino group and obtained as linkers to CdS QDs core. These linkers have been rendered as shells for these CdS QDs. Therefore, CdS QDs was clearly observed as depicted in Figure 4 (d), as sphere dots with 8 nm-10 nm in diameter. PEI is one type of Polyelectrolytes (PET) with ionisable groups.[46–52] The PEI can dissociate, leaving charges on the chains and releasing counterions in polar solution. Therefore, PEI can interact with electrostatic interactions when it is applied to other systems.[53–55] I understand that in the case of my experiment, the electrostatic interaction was employed during synthesis.

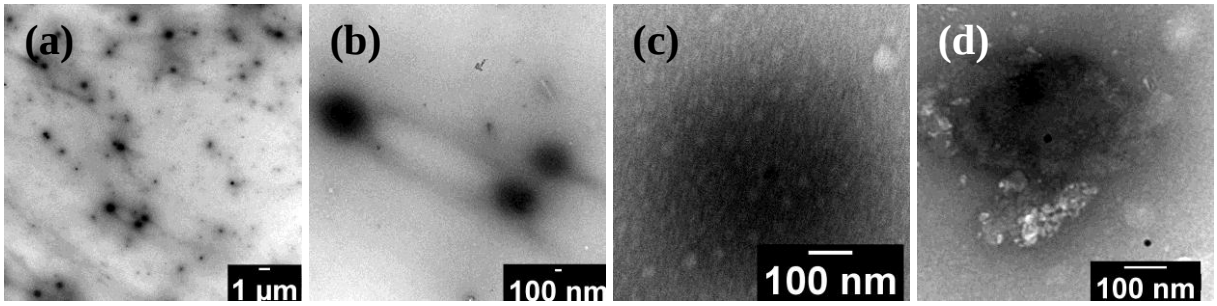

Figure 4: (a), (b), (c) and (d) are TEM images of coated CdS QDs with PEI.

5.3.2 Using Ferritin as Biotemplate for CdS QDs

I have also used bio-templates as mediators for assembling process in subsequent experiments by introducing CdS QDs inside apo-ferritin to open the opportunity of surface chemical functionalization pave of CdS QDs. As known, the template-directed synthesis can lead to controlled sizes and geometries of the QDs.[56] Meanwhile, both the stabilizer and the templates control the initial nucleation and subsequent growth steps by piloting the formation of uniform homogeneous QDs at the end.[2] There have been many reports of nanoparticles (NPs) synthesized in the cavity of apo-ferritin and many types of metal, metal oxide, magnetic and semiconductor NPs accommodated by apo-ferritin are now available. In my study, I used horse spleen apo-ferritin as nanocage to load CdS QDs inside its core. The essential mechanism in synthesizing CdS in the apo-ferritin is electrostatic interaction where the positive inner apo-ferritin cavity[57] can be loaded with negatively charged CdS, which degrade slowly in the reaction solution for 24 hours or more. The result from this experiment is shown in Figure 5 (a) where after being encapsulated in the apo-ferritin nanocage, the CdS QDs is presented as a cloudy yellow colloid. The core size of the CdS QDs has decreased, as observed from the CdS coloidal solution under UV light. It is apparent that the color of the emitted light has changed from orange, with the absence of apo-ferritin, to a yellow greenish emission (Figure 5 (b)) under UV light at 254 nm of wavelength. However, under a long wavelength (Figure 5 (c)), the particles can not emit any emission due to the reduced size of QDs which is smaller than 365nm.

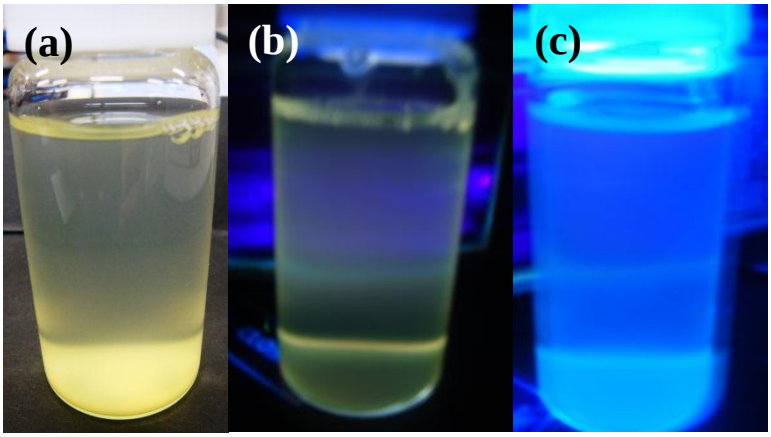

Figure 5: Colloidal solution of encapsulated CdS QDs inside apo-ferritin core (a) under visible light (b) under UV light with short wavelength (254 nm) and (c) under UV light with long wavelength (365 nm).

5.3.3 Introducing CdS QDs with PEI Ligand into Apo-ferritin

Although protein-templated QDs preparation allows the diameters to be precisely defined by the inner diameters of the proteins, uniform and discrete molecular sizes of the template proteins may sometimes cause problems for tailor-made manipulations of the optophysical properties. To overcome this shortcoming, I applied surface modification technique to enhance the CdS QDs' photon emission as previously mentioned; by encapsulating CdS QDs inside apo-ferriritin and later, capping the CdS-apo with PEI. Optical properties have been measured by UV-absorbance and photolumiescence peaks spectra. From the results as shown in Figure 6, I can compare the spectral intensity of CdS capped with PEI (CdS + PEI), encapsulated CdS inside apo-ferritin nanocage (CdS-apo) and using both agents for capping CdS QDs (CdS-apo + PEI) with standard intensity of naked CdS (CdS) that have been obtained.

From these results, it can be concluded that either by loading naked CdS inside the apo-ferritin or the loaded apo-ferritin with CdS and then capped with PEI, these CdS would have smaller core size as compared to CdS without an apo-ferritin template. This could be due to the CdS size conforming to apo-ferritin's size shape. In general, the results from photoluminescence and UV absorption

spectra, as seen in Figure 6 (a) and Figure 6 (b), have shown that the smallest CdS QDs was obtained when the CdS was loaded inside apo-ferritin. This is followed by CdS-apo capped with PEI, CdS capped with PEI and finally, the biggest CdS QDs is the naked CdS. These results have proven that CdS coated with ligand would have smaller core size which in turn produces QDs with higher band gap energy. Moreover, other than decreasing the CdS QDs' size, the PEI ligand also funtioned as an enhancer to the CdS QDs luminescence spectra.

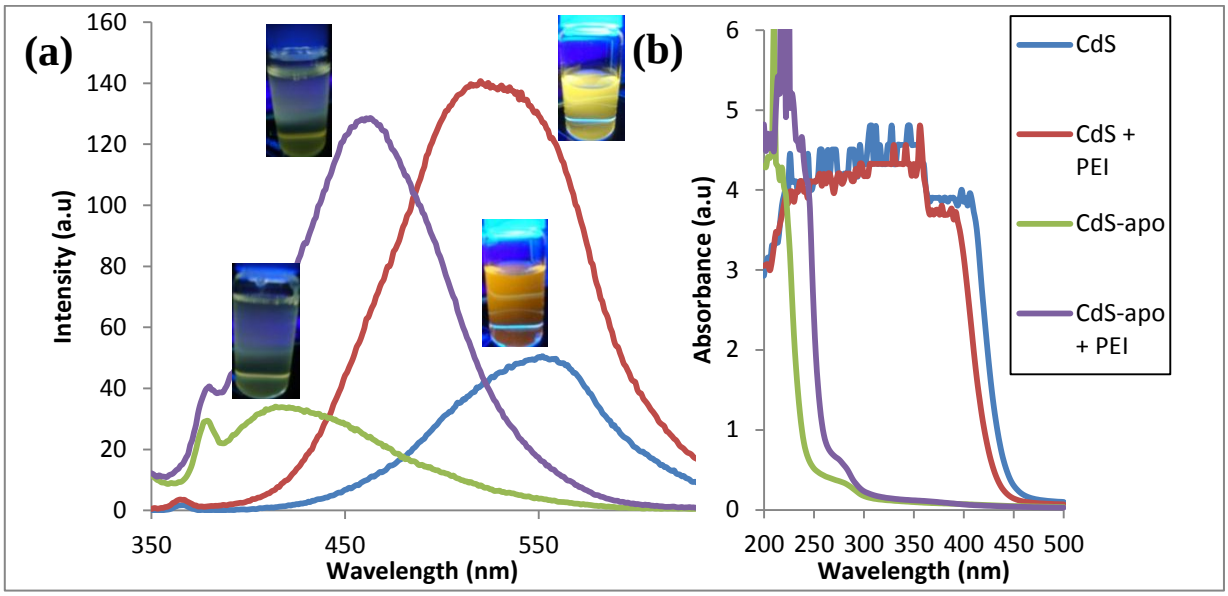

Figure 6: (a) Photoluminescence spectra and (b) absorption spectra peaks of CdS, CdS coated with PEI (CdS+PEI), CdS encapsulated with apo-ferritin (CdS-apo) and rounded PEI over CdS encapsulated with apo-ferritin (CdS-apo +PEI).

Reduction and chelation processes have occured in CdS-apoferritin system due to not only the capsulation with apo-ferritin but also effected by TGA that allowed the reconstitution of the CdS QDs' core.[58] The TGA contains mercaptan groups which strongly bond to cadmium and prevent the CdS QDs from having toxicity problem. If this CdS QDs was synthesized with narrow radii variation, the possibility of using CdS-apoferritin complex for cancer treatment is promising.[59] Interestingly, after 12 days of synthesis, the optical properties of the luminescence spectrum was measured again as shown in Figure 7. The results have clearly proven that by adding PEI and encapsulating CdS inside ferritin nanocages may produce CdS with the desired optical propeties

that are capable of acting as bionanosensors. Apart from the CdS-apo + PEI's size becoming smaller due to the size of the ferritin core, its luminescence spectrum peak has also stabilized with high peaks from the first day of syntesis and after being kept for 12 days. This result proves that photobleaching has not occured for the CdS-apo + PEI as compared to the naked CdS, CdS + PEI and CdS-apo.

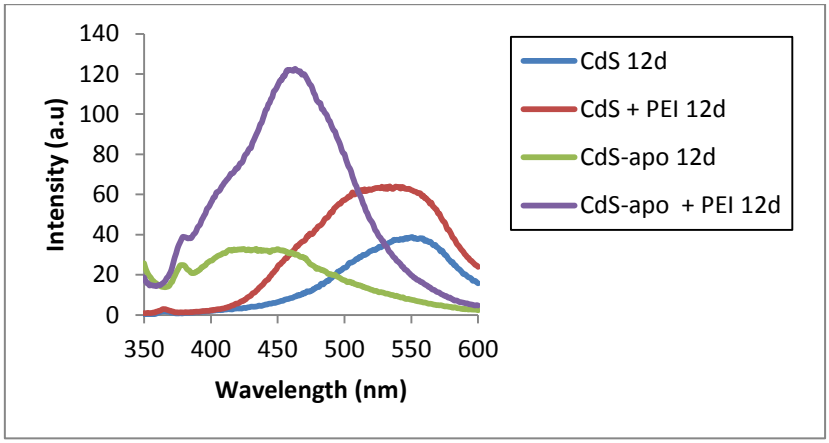

Figure 7: Photoluminescence spectra of CdS, CdS coated with PEI (CdS+PEI), CdS encapsulated with apo-ferritin (CdS-apo) and rounded PEI over CdS encapsulated with apo-ferritin (CdS-apo + PEI) after 12 days of synthesis.

TEM images are shown in Figure 8 have proven that by encapsulating CdS with apo-ferritin, a good size distribution (9 nm) of the CdS QDs was possible. Figure 8 (a), (b) and (c) are TEM images of CdS inside apo-ferritin. These images have proven that encapsulating CdS inside ferritin core would result in CdS QDs with the size and shape of the ferritin protein. Additionally, by introducing apo-ferritin, the agglomeration of dark circles around the CdS QDs was prevented. Unfortunately, eventhough CdS-apoferritin with PEI has given the best optical properties over the others, the shape of the real CdS QDs is difficult to observe due to the coverage by PEI linker that surrounded the CdS-apo QDs, as clearly shown in Figure 8 (d) and (e). I was unable to observe the CdS-apo QDs capped with PEI particles even at a high magnification (100 nm), as shown in Figure 8 (f).

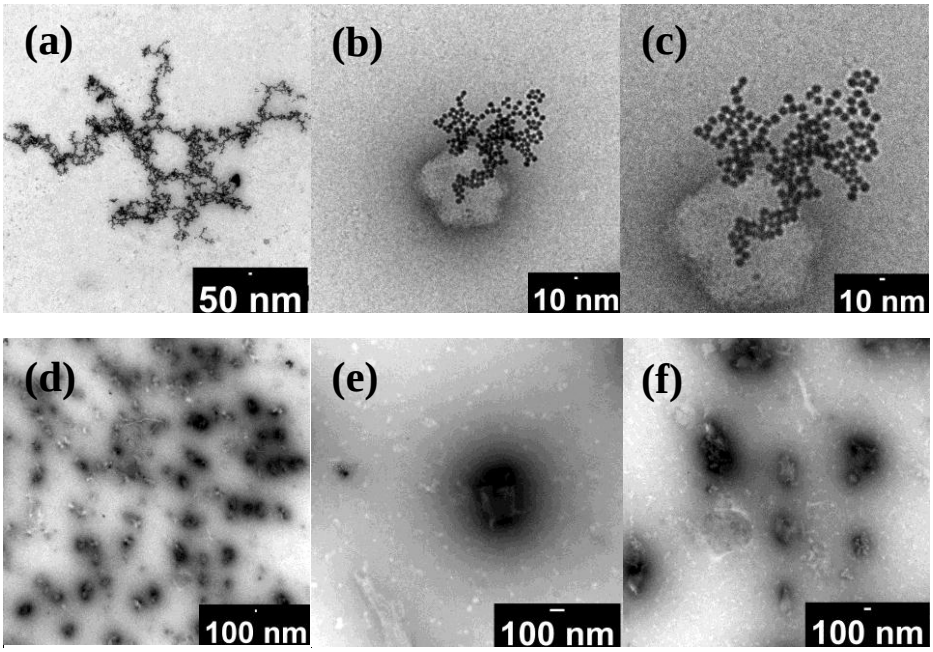

Figure 8: (a), (b) and (c) TEM images of CdS encapsulated with apo-ferritin. Figure 8 (d), (e) and (f) TEM images of rounded PEI over encapsulated CdS with apo-ferritin.

The SAXS intraparticle data was measured from the first peak of SAXS spectrum (Figure 9) by calculating the allowed peak reflection for sphere particle via the following equation:

$$q_{m,i}\ R = 5.765, 9.111, 11.22 \ldots.\ \text{(i=1,2,3,..)} \quad (1)$$

This proves that the size (diameter) of the QDs for the naked CdS, CdS coated with PEI (CdS+PEI), CdS encapsulated inside ferritin core (CdS-apo) and using both agents for capping CdS QDs (CdS-apo + PEI) are all 9.6 nm due to all peak appearing at q=1.2 nm^{-1}.

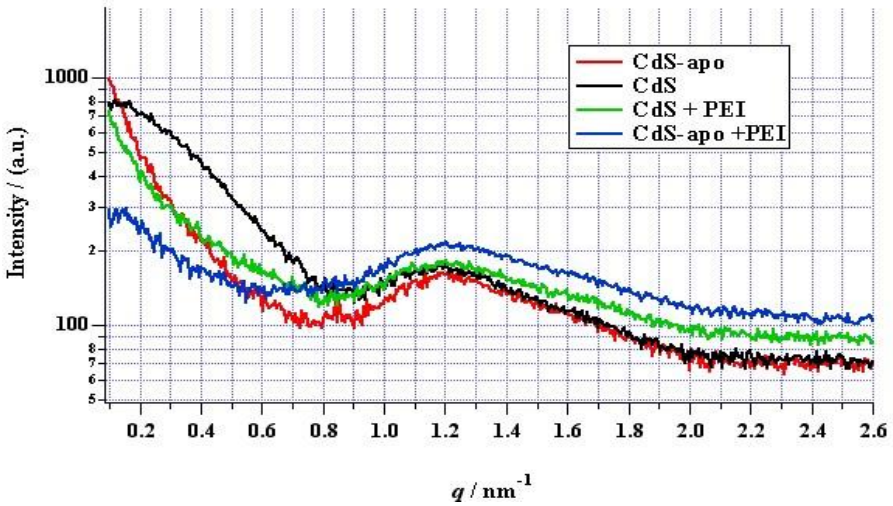

Figure 9: SAXS data of CdS, CdS coated with PEI, encapsulated CdS with apo-ferritin and rounded PEI over encapsulated CdS with apo-ferritin.

Apart from applying QDs as biosensors, they are also expected to be a key component in nano-scale electronic devices. Since the electronic energy levels of QDs are radically affected by their sizes, there is a large demand for reproducible methods of making and handling the QDs with same methode. To overcome this challenge, the apo-ferritin cage is preferable because of the size of its inner cavity which is suitable as a uniform size-restraining chemical reaction chamber for the QDs.[1] Therefore, as proven via TEM observations, by encapsulating CdS inside ferritin core, I can control the size of the CdS QDs with beautiful particles distributions. Moreover, its UV absorption peak has appeared at the smallest wavelength as compared to the other QDs.

The fundamental absorption, which corresponds to electron excitation from the valence band to conduction band, can be used to determine the value of the optical band gap.[60] The connection between the band gap (E_g) and maximum wavelength (λ_{max}) can be written as:

$$E_g = \frac{hc}{\lambda_{max}} \qquad (2)$$

where, E_g is the band gap of the material, h is Planks constant, c is speed of light and λ_{max} is the absorbance peak wavelength.[1] Base on this equation, the band gap is inversely proportional to

wavelength (λ_{max}). Equation 3 is used for analyse the optic absorbance spectrum in order to determine the band gap energy for difficult spectra and unclear peaks.

$$(\alpha hv)^2 = K(hv - E_g) \tag{3}$$

where, α is absorbance constant, hv is photon discrete energy and E_g is the band gap. The absorbance constant value can be calculated using Equation 4 below.

$$\alpha = \frac{1 - \log I_t / I_O}{t \log e} = \frac{A}{t \log e} \tag{4}$$

where, t is the thickness of the quartz cuvette cell, I_t and I_o are transmission and incidence light intensity, respectively and A is sample's absorbance from UV -vis measurement.

Band gap energy is illustrated as a graph of $(\alpha hv)^2$ versus photon energy, as shown in Figure 10. For the band gap energy in the absence of PEI, the Photon Energy is 2.90 eV and this value increased to 2.99 eV in the presence of PEI through calculation using Equation 3 and Equation 4. Meanwhile, using the same calculations, the Photon Energy for encapsulated CdS with apo-ferritin in the absence of PEI is 5.3 eV which decreases to 4.8 eV in the presence of PEI.

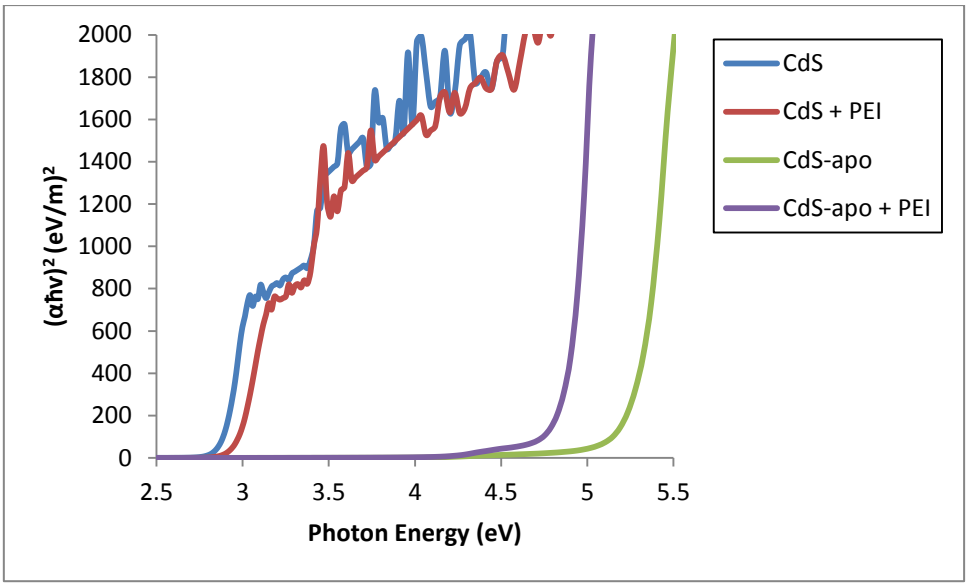

Figure 10: Band gap energy of CdS, CdS coated with PEI, encapsulated CdS with apo-ferritin and rounded PEI over encapsulated CdS with apo-ferritin.

5.3.4 Using PS-*b*-P2VP Template for QDs array

Polystyrene (PS) based block copolymers with poly- (2-vinylpyridine) (P2VP) can act as templates to load the metallic precursors or NPs into selective domains of micro separated block copolymer nanostructures.[61-66] This leads to the formation of NP with well-defined size control and interparticle spacing without NP aggregations.[2] On the other hand, the structural information at molecular or cell levels[67-70] of biological material such as DNA strands,[71-72] peptides,[73-75] viruses[78-79] and protein can be utilized as templates for assembling nanoparticles. These templates provide a platform to organize particles through covalent and non-covalent interactions.[2] Therefore, CdS-apoferritin in the desire size can be aligned to PS-*b*-P2VP template to form an organize network .

Firstly, the as-spun thin film of PS-*b*-P2VP was solvent-annealed for 6 h at 20 °C. The protruded P2VP domains in the topographical image in Figure 11 (a) are perpendicular cylinders and PS matrix swollen more by PS-selective toluene has lower height after the removal of the solvent. The improved uniformity of the cylinder size and spacing can be recognized much better in the phase image as shown in Figure 11 (b). The longer annealing time allowed the polymer's molecules to rearrange to form a more regular structure close to equilibrium as discussed in chapter 2. The spacing of the cylinders was estimated to be 57 nm using FFT of the AFM image. Solvent annealing at lower temperature for longer period seems to give better regularity without affecting the morphology and feature sizes. Figure 11 (c) is shows the SEM image of the same PS-*b*-P2VP template.

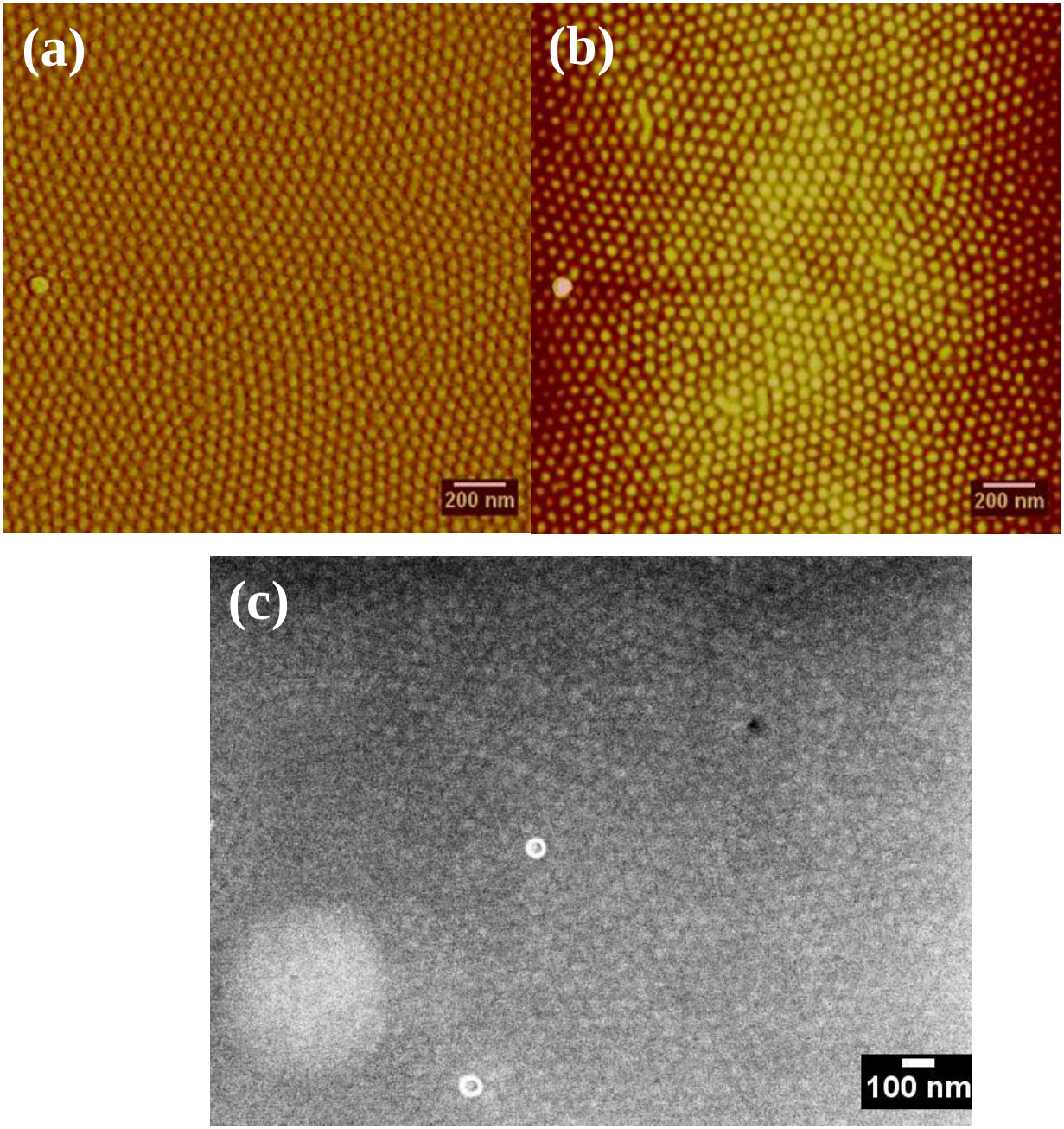

Figure 11: Topography images of PS-*b*-P2VP thin film template (a) AFM phase image (b) AFM height image and (c) SEM image.

In order to introduce NPs into the BCP domain, there are two kinds of approaches that are regularly applied to form nanoparticle-block copolymer hybrid. Firstly, the in situ approach can be prepared via reduction metal ions in one block of BCP. The BCP has been used as nanopatterned reactive medium before being removed by plasma, chemical reducing agents, hydrogen gas exposure, thermal decomposition, etc.[80] Therefore, only metal ions are left on the substrate and the BCP is

formed as a scaffold template to induce organized structure of NPs. On the other hand, the ex situ approach has been done by introducing nanopatterned BCP as supported rays for NPs where the metallic NPs are capped with ligand monolayer.[81] Hence, the metallic NPs can be solubilized into one block of BCP. In this study, I decided to choose the ex situ approach by applying TGA as a ligand monolayer before aligning it onto the PS-*b*-P2VP BCP. I chose to use naked CdS instead of the rounded CdS with PEI due to PEI forming linkers around the CdS core that resulted in large CdS with PEI shells. These could lead to aggregation when arraying the CdS-PEI onto the PS-*b*-P2VP template.

Moreover, in order to assemble QDs onto BCP thin film, the parameter that needs to be controlled is surface wettibility and this interfacial self-assembly can be used to establish 2D assemblies.[2] Surface wettability is increased[61,82-84] by applying TGA monolayer rounded CdS QDs, has rendered the CdS QDs for self-assembling at selected microdomain that is P2VP. Furthermore, the aqueous CdS has rendered the CdS to be easily adsorbed onto P2VP microdomain due to P2VP being a hydrophilic homopolymer. Furthermore, the polarity of the TGA surface drives this assembly process.[2] This direct chemical binding of QDs onto BCP surfaces is the way to generate ordered particle arrays.[85-86] This assembling process has described that direct binding between QDs and BCP depends on three major factors which are; i) the chemical nature of the BCP domain that the QDs have prefered to array on, ii) the chemical structure of the capping agents used to obtain unique property and to stabilize the QDs and iii) the interaction between the surface of the BCP and the QDs.[87-88] Noncovalent bonds also play important role while assembling QDs onto BCP surface. This bond is weak and reversible which could lead to the formation of supramolecular interactions.

By considering the interactions between the ligands that capped QDs with TGA, I would be able to control the distances between QDs. The hydrophilic surfactant (TGA) that are used would not only

render the QDs to be soluble, but it also offers stability because the highly charged surfaces often create electrostatic layers. Entropic, van der Waals, steric and dipolar forces as well as electric charges on the sterically charged QDs determine the stoichiometry of the structures.[2] The TGA has produced CdS with highly anionic property that causes it to assemble with the cationic P2VP domain via electrostatic interaction. On the other hand, CdS QDs are negatively charged and the P2VP is positively charged, therefore, nonbonded interactions has drawn to hydrogen bonding.[89-90] Due to its specific, directional and reversible characteristics, hydrogen bonding has been widely used for supramolecular self-assembly of polymers and inorganic molecules.[91-92] Nevertheless, a typical single hydrogen bond strength (530 kJ/mol) is much lesser than covalent bonds (250800 kJ/mol).[96] However, significant favorable interactions can be obtained through the formation of multiple hydrogen bonds which would create self-healing polymeric materials, which is an emerging goal in materials science.[94-95] Hydrogen bonding has been selected for the selective segregation of QDs in P2VP microdomains. The naked CdS with an average size of 8-10 nm was aligned onto P2VP microdomain as shown in Figure 12.

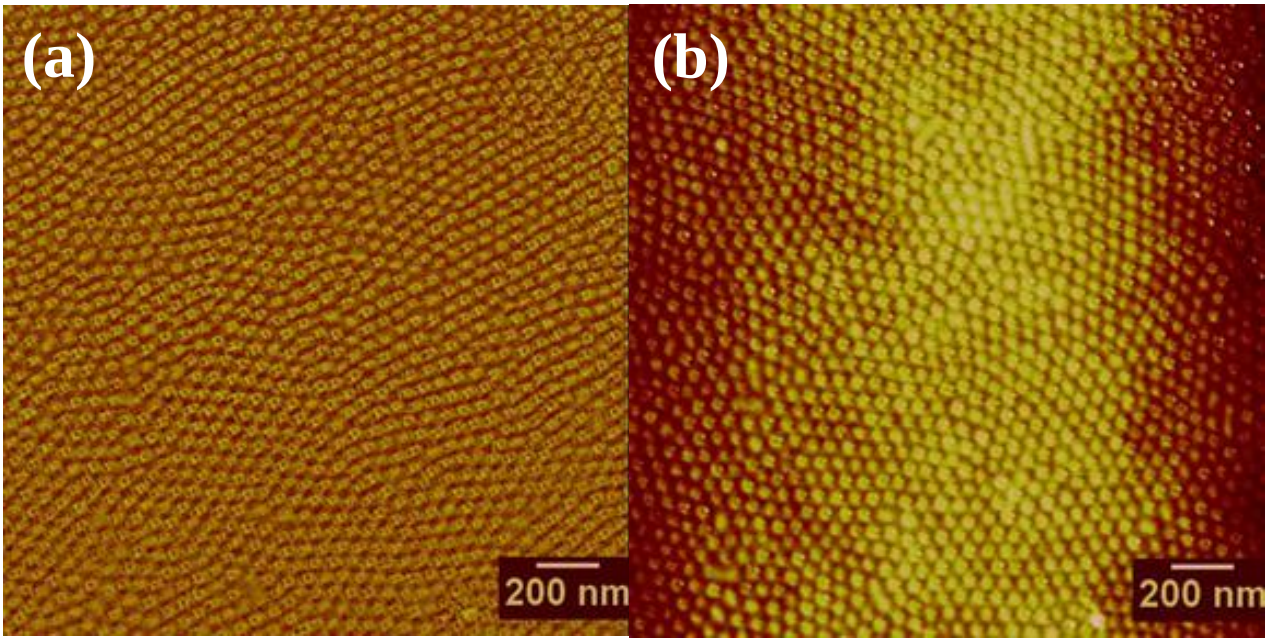

Figure 12: AFM images of PS-*b*-P2VP template with CdS QDs arrays (a) phase image and (b) height image.

Usually, nanocylinder lithography is applied for QDs pattern to serve as a template.[96] Furthermore, QDs assembly can be achieved on the surface of prefered P2VP microdomain, which form intricate surface patterns via nanoscale phase segregation of the polymer blocks based on the hydrophilic/hydrophobic balance. [97] QDs preferentially adsorb on the low surface tension area and would often aggregate with pronounced fractal dimensionality.[98] This experiment was conducted using CdS QDs organized onto P2VP microdomain surfaces that have been functionalized with carboxylic acid and mercaptan groups. Ligand molecules on the surface of inorganic CdS QDs play an important role in the synthesis and application of QDs due to their dramatic influence over surface properties.[99-101] Tailoring of QDs surfaces with ligands is therefore a key factor for stabilizing QDs in aquous as well as for controlling hierarchical assembly of QDs in order to obtain functional materials.[93]

Chemical templates have been demonstrated as having high potentials towards creating versatile nanoparticle assemblies. For example, biological templates such as DNA strands and proteins are utilized for 1D organization of nanoparticles.[102] Here, different supramolecular interactions such as electrostatic interactions and hydrogen bonding are crucial for attaching nanoparticles to the surface scaffolds.[2] As the charge transport in the nanoparticle thin films is very sensitive to the tunneling conditions, this effect may be utilized for sensor applications, for example, gas and (bio)sensors.[103-108]

Rounded PEI over encapsulated CdS with apo-ferritin has obtained aggregation, as seen from TEM observation. For that reason, the encapsulated CdS with apo-ferritin has been selected to be introduced onto PS-*b*-P2VP template via the formation of hybrid host-guest system. The AFM image is shown in Figure 13, where the perpendicular cylinder P2VP has swollen after loading with CdS-apo into P2VP microdomain and D-spacing became smaller to 25 nm. These subchains of P2VP were streched in order to wrap around the CdS-apo QDs arrays that were introduced into

P2VP microdomain. The AFM phase image in Figure 13 (a) shows the dark dots of CdS-apo QDs in the middle of the bright cylinder P2VP microdomains has obtained convex shape based from the height image of AFM in Figure 13 (b). The height of protruded islands of P2VP microdomains is increased compared to P2VP without loaded CdS-apo QDs. The mechanical response as observed in the AFM phase images of P2VP microdomains depends on the existence of CdS QDs.

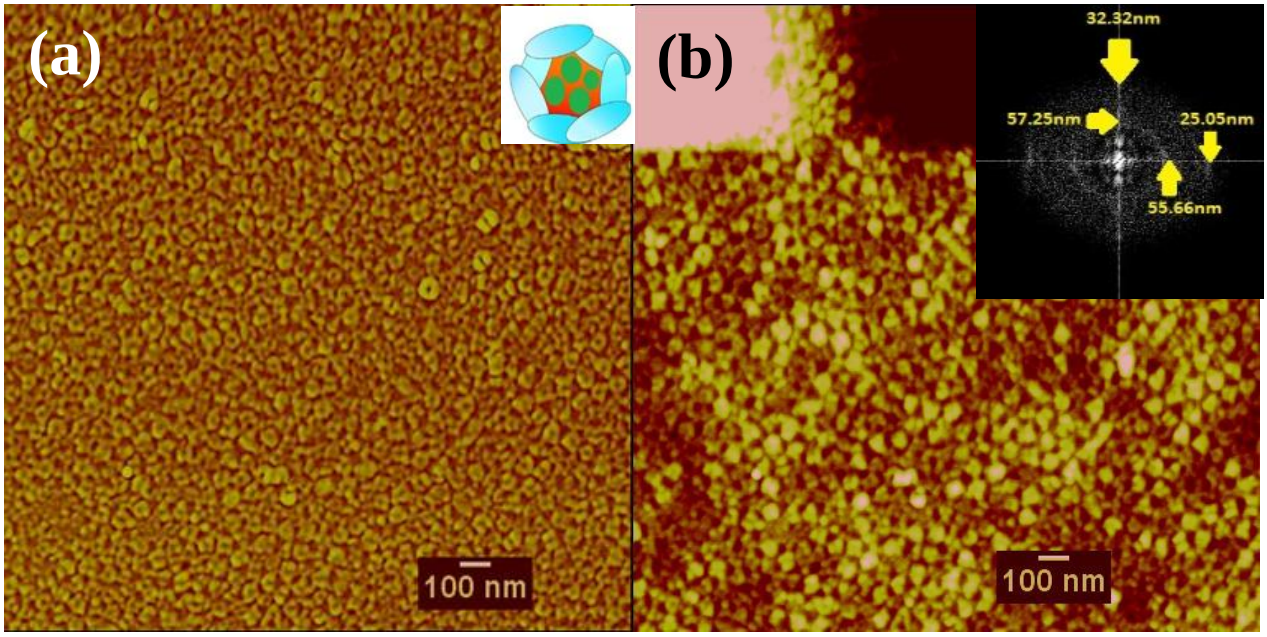

Figure 13: Phase (a) and height (b) images of PS-*b*-P2VP template with encapsulated CdS QDs with apo-ferritin arrays.

The electrostatic interactions and hydrogen bonding have been involved for assembling these CdS-apo QDs. The positively charged internal surface of apo-ferritin attracts and stabilizes negatively charged CdS coated with TGA molecules. Moreover, the linker ferritin molecules which form intermolecular H bonds, are effective assembly mediators.[109,39] The chemical recognition and specificity of biomolecules are important for this purpose.

5.4 Conclusion

The ultimate goal of self-assembly should be to provide a flexible and easy approach for creating complicated architectures starting from one or more types of nanostructures, and this is still at the boundary of the current research.

Encapsulated CdS QDs inside ferritin core is presented as the smallest particles among the others due to the absoption UV spectrum and rendered to increase CdS QDs band gap energy. By applying polyethilenemine (PEI), the photoluminescence spectrum was enhanced. It also prevented photobleaching even after 12 days especially for encapsulated CdS QDs inside ferritin core. Moreover, the self-assembly of CdS QDs on PS-*b*-P2VP block copolymer has been introduced by ex situ approach to form hybrid CdS-PS-*b*-P2VP. Furthermore, swelling effect occurred when CdS-apo QDs were arrayed onto the PS-*b*-P2VP template.

References

[1] L. E. Brus, *J. Chem. Phys.* **1984**, *80*, 4403.

[2] S. Kinge, M. Crego-Calama, D. N. Reinhoudt, *Chem. Phys. Chem.* **2008**, *9*, 20.

[3] M. Bruchez, M. Moronne, P. Gin, S. Weiss, A. P. Alivisatos, Science **1998**, *281*,2013.

[4] A. R. Kovsh, A. E. Zhukov, D. A. Lifshits, A.Y. Egorov, V. M. Ustinov, M. V. Maximov, Y. G. Musikhin, N. N. Ledentsov, P. S. Kop'ev, Z. I. Alferov, D. Bimberg, *Electronics Letters* **1999**, *35(14)*, 1161.

[5] G. J. Jacobs, L. C. Barbosa, C. L. Cesar, *SPIE International Symposium on Advanced materials and structures Proceeding* **2005**, *5734*, 124.

[6] B. C. Lagerholm, L. A. Ernst, M. P. Bruche, A. S. Waggoner, B. Ballou, *Bioconjugate Chem.* **2004**, *15(1)*, 79.

[7] W. Y. William, E. Chang, R. Drezek and V. L. Colvin, *Biochem. Biophys. Res. Commun.* **2006**, *348*, 781.

[8] W. C. W. Chan, D. J. Maxwell, X. Gao, R. E. Bailey, M. Han, S. Nie, *Curr. Opin. Biotechnol.* **2002**, *13*, 40.

[9] C. B. Murray, D. J. Norris, M. G. Bawendi, *J. Am. Chem. Soc.* **1993**, *115(19)*, 8706.

[10] B. T. Huy, Min-Ho Seo, Jae-Min Lim, Dong-Soo Shin,Yong-Ill Lee, Sang-Su Kim, Kiwan Jang, Taekwon Song, *Journal of the Korean Physical Society* **2011**, *59(5)*, 3293.

[11] N. Ma, E. H. Sargent, S. O. Kelley, *J. Mater. Chem.* **2008**, *18*, 954.

[12] T. Ueno, M. Suzuki, T. Goto, T. Matsumoto, K. Nagayama, Y. Watanabe, *Angew. Chem. Int. Ed* **2004**, *43(19)*, 2527.

[13] Y. Hu, D. Samanta, S. S. Parelka , S. W. Hong, Q. Wang , T. P. Russell, T. Emrick, *Adv. Funct. Mater.* **2010**, *20*, 3603.

[14] R. M. Kramer, C. Li, D. C. Carter, M. O. Stone, R. R. Naik, *J. Am. Chem. Soc.*, **2004**, *126(41)*, 13282.

[15] E. Mayes, A. Bewick, D. Gleeson, J. Hoinville, R. Jones, O. Kasyutich, A. Nartowski, B. Warne, J. Wiggins, K. K. W. Wong, *IEEE Trans. Magn.* **2003**, *39*, 624.

[16] Z. Yuan, D. N. Petsev, B. G. Prevo, O. D. Velev, P. Atanassov, *Langmuir* **2007**, *23*, 5498.

[17] I. Yamashita, *Thin Solid Films* **2001**, *393*, 12.

[18] K. Iwahori, I. Yamashita, *Journal of Cluster Science* **2007**, *18(2)*, 358.

[19] H. Xu, S. S. Sheiko, D. Shirvanyants, M. Rubinstein, K. L. Beers, K. Matyjaszewski, *Langmuir* **2006**, *22(3)*, 1254.

[20] T. L. Morkved, M. Lu, A. M. Urbas, E. E. Ehrichs, H. M. Jaeger, P. Mansky, T. P. Russell, *Science* **1996**, *273 (5277)*, 931.

[21] J. Hahm and S. J. Sibener, *Langmuir* **2000**, *16(11)*, 4766.

[22] E. W. Edwards, M. P. Stoykovich, H. H. Solak, J. J. de Pablo, P. F. Nealey, *Macromolecules* **2006**, *39(10)*, 3598.

[23] C. J. Yoon Park, E. L. Thomas, *Polymer* **2003**, *44*, 6725.

[24] J. Huh, V. V. Ginzburg, A. C. Balazs, *Macromolecules* **2000**, *33*, 8085.

[25] A. Haryono, W. H. Binder, *Small* **2006**, *2(5)*, 600.

[26] M. Aizawa, J. M. Buriak, *J. Am. Chem. Soc.* **2006**, *128*, 5877.

[27] J . Chai, D. Wang, X. Fan, J. M. Buriak, *Nat. Nanotechnol.* **2007**, *2(8)*, 500.

[28] Y. Lin, A. Böker, J. He, K. Sill, H. Xiang, C. Abetz, X. Li, J. Wang, T. Emrick, S. Long, Q. Wang, A. Balazs, T. P. Russell, *Nature* **2005**, *434*, 55.

[29] J. Y. Cheng, C. A. Ross, E. L. Thomas, H. I. Smith, G. J. Vancso, *Appl. Phys. Lett.* **2002**, *81*, 3657.

[30] A. P. Alivisatos, *J. Phys. Chem.* **1996**, *100*, 13226.

[31] K. S. Raja, Q. Wang, Bionanoparticles and nanotechnology, in: "*Encyclopedia of Nanoscience and Nanotechnology* ", J.A. Schwars, C.I. Contescu, K. Putyera, Eds., Vol B, Marcel Dekker Inc., New York **2004**, p. 321.

[32] M. Boncheva, G. M. Whitesides, *MRS Bull.* **2005**, *30*, 736.

[33] Z. Cui, "*Nanofabrication Principles, Capabilities and Limits"*, Springer India, New Delhi **2012**, p.312.

[34] S. Akasaka, H. Mori, T. Osaka, V. H. Mareau, H. Hasegawa, *Controlled introduction of metal nanoparticles into a microdomain structure macromolecules* **2009**, *42*, 1194.

[35] I. In, Y. H. La, S. M. Park, P. F. Nealey, P. Gopalan, *Langmuir* **2006**, *22(18)*, 7855.

[36] S. A. Shamsudin, S. Radiman, M. S. Ghamsari, K. S. Khoo, *AIP Conference Proceeding* **2009**, *1136*, 292.

[37] K. Iwahori, *U.S. 7* **2011**,*897*,408 B2.

[38] N. Chandrasekharana, P. V. Kamat, *Res. Chem. Intermed.* **2002**, *28*, 847.

[39]R. Richards, H. Bnnemann, Synthetic approaches to metallic nanomaterials, in: "*Nanofabrication Towards Biomedical Applications*", C. S.S.R. Kumar, J. Hormes, C. Leuschner, Eds., Wiley-VCH, Weinheim, **2005**, p. 3.

[40] Y. Sun, Y. Xia, *Science* **2002**, *298(5601)*, 2176.

[41] T. Teranishi, R. Kurita, M. Miyake, *J. Inorg. Organomet. Polym.* **2000**, *10*, 145.

[42] T. Leisner, C. Rosche, S. Wolf, F. Granzer, L. Woste, *Surf. Rev. Lett.* **1996**, *3*, 1105.

[43] H. Bçnnemann, R. Richards, *Eur. J. Inorg. Chem.* **2001**, *10*, 2455.

[44] G. Kickelbick, U. Schubert, Organic functionalization of metal oxide nanoparticles, in: "*Advances in Nanophase Materials and Nanotechnology"*, M.I. Baraton, Ed., American Scientific Publishers, Stevenson Ranch, CA, USA **2003**, p. 91.

[45] A. Miura, Y. Uraoka, T. Fuyuki, S. Kumagai, S. Yoshii, N. Matsukawa, I. Yamashita, *Surface Science* **2007**, *601*, L81.

[46] S. Förster, M. Schmidt, *Adv. Polym. Sci.* **1995**, *120*, 51.

[47] J. L. Barrat, J. F. Joanny, *Adv. Chem. Phys.* **1996**, *94*, 1.

[48] K. S. Schmitz, "*Macro-ions in Solution and Colloidal Suspension"*, Wiley VCH, New York **1993**.

[49] C. Tanford, "*Physical Chemistry of Macromolecules"*, Wiley, New York, **1961**.

[50] F. Oosawa, "*Polyelectrolytes"*, Marcel Dekker, New York **1971**.

[51] M. Hara, "*Polyelectrolytes: Science and Technology"*, Marcel Dekker, New York **1993**.

[52] T. Radeva, "*Physical Chemistry of Polyelectrolytes"*, Marcel Dekker, New York **2001**.

[53] M. Doi, S.F. Edwards, "*The Theory of Polymer Dynamics"*, Clarendon Press, Oxford **1989**.

[54] P.G. de Gennes. "*Scaling Concepts in Polymer Physics"*, Cornell University Press Ithaca, New York **1979**.

[55] M. Rubinstein, R.H. Colby, "*Polymer Physics"*, Oxford University Press, New York **2003**.

[56] D. Wang, H. Mçhwald, *J. Mater. Chem.* **2004**, *14*, 459.

[57] K. Iwahori, I. Yamashita, *Journal of Physics: Conference Series* **2007**, *61*, 492.

[58] S. H. Choi, J. W. Kim, S. H. Chu, Y. Park, G. C. King, P. T. Lillehei, S. J. Kim, J. R. Elliott, *12th SPIE International Symposium on Smart Structures and Smart Materials Proceedings* **2005,** *5763,* 213.

[59] J. F. Hainfeld, *Proc. Nat. Acad. Sci.* **1992**, *89*, 11064.

[60] S. R. Kuldeep, D. Patidar, Y. Janu, N. S. Saxena, S. Kananbala, T. P. Sharma, *Chalcogenide Letter* **2008**, *5(6)*, 105.

[61] Y. Lin, H. Skaff, A. Bçker, A. D. Dinsmore, T. Emrick, T. P. Russell, *J. Am. Chem. Soc.* **2003**, *125*, 2690.

[62] S. Liu, T. Zhu, R. Hu, Z. Liu, *Phys. Chem. Chem. Phys.* **2002**, *4*, 6059.

[63] E. Rabani, D. R. Reichman, P. L. Geissler, L. E. Brus, *Nature* **2003**, *426*, 271.

[64] K. Soulantica, A. Maisonnat, M. C. Fromen, M. J. Casanove, B. Chaudret, *Angew. Chem. Int. Ed.* **2003**, *42(17)*, 1945.

[65] D. V. Talapin, E. V. Schevchenko, C. B. Murray, A. Kornowski, S. Fçrster, H. Weller, *J. Am. Chem. Soc.* **2004**, *126(40)*, 12984.

[66] D. Xia, D. Li, Y. Luo, S. R. J. Brueck, *Adv. Mater.* **2006**, *18*, 930.

[67] C. M. Niemeyer, *Angew. Chem. Int.* Ed. **2001**, *40(22)*, 4128.

[68] S. G. Zhang, *Nat. Biotechnol.* **2003**, *21*, 1171.

[69] A. M. Bittner, *Naturwissenschaften* **2005**, *92*, 51.

[70] C. M. Niemeyer, U. Simon, *Eur. J. Inorg. Chem.* **2005**, *18*, 3641.

[71] M. G. Warner, J. E. Hutchison, *Nat. Mater.* **2003**, *2*, 272.

[72] H. Nakao, H. Shiigi, Y. Yamamoto, Y. Yamamoto, S. Tokonami, T. Nagaoka, S. Sugiyama, T. Ohtani, *Nano Lett.* **2003**, *3*, 1391.

[73] J. D. Hartgerink, E. Beniash, S. I. Stupp, *Science* **2001**, *294*, 1684.

[74] J. D. Hartgerink, E. Beniash, S. I. Stupp, *Proc. Natl. Acad. Sci. USA* **2002**, *99(8)*, 5133.

[75] M. Reches, E. Gazit, Science **2003**, *300(5619)*, 625.

[76] L. Li, S. I. Stuppe, *Angew. Chem. Int. Ed.* **2005**, *44*, 1833.

[77] W. Shenton, T. Douglas, M. Young, G. Stubbs, S. Mann, *Adv. Mater.* **1999**, *11*, 253.

[78] C. Mao, D. J. Solis, B. D. Reiss, S. T. Kottmann, R. Y. Sweeney, A. Hayhurst, G. Georgiou, B. Iverson, A. M. Belcher, *Science* **2004**, *303(5655)*, 213.

[79] T. Douglas, M. Young, *Nature* **1998**, *393*, 152.

[80] J. Chai, J. M. Buriak, *ACSNANO* **2008**, *2(3)*, 489.

[81] S. W. Yeh, K. H. Wei, Y. S. Sun, U. S. Jeng, K. S. Liang, *Macromolecules* **2005**, *38*, 6559.

[82] Y. Lin, A. Bçker, H. Skaff, D. Cookson, A. D. Dinsmore, T. Emrick, T. P. Russell, *Langmuir* **2005**, *21(1)*, 191.

[83] Y. Lin, H. Skaff, T. Ermick, A. D. Dinsmore, T. P. Russell, *Science* **2003**, *299(5604)*, 226.

[84] B. Binks, J. H. Clint, *Langmuir* **2002**, *18(4)*, 1270.

[85] W. H. Binder, *Angew. Chem. Int. Ed.* **2005**, *44*, 5172.

[86] C. B. Murray, C. R. Kagan, M. G. Bawendi, *Ann. Rev. Mater. Sci.* **2000**, *30*, 545.

[87] V. L. Colvin, A. N. Goldstein, A. P. Alivisatos, *J. Am. Chem. Soc.* **1992**, *114*, 5221.

[88] S. Westenhoff, N. A. Kotov, *J. Am. Chem. Soc.* **2002**, *124*, 2884.

[89] S. C. Zimmerman, P. S.Corbin, in: "*Molecular Self Assembly: Organic versus Inorganic Approaches; Structure and Bonding*", M. Fujita, Ed., Springer-Verlag, New York 2000, p.63.

[90] W. H. Binder, R. Zirbs, *Adv. Polym. Sci.* **2007**, *207*, 1.

[91] S. C. Warren, L. C. Messina, L. S. Slaughter, M. Kamperman, Q. Zhou, S. M. Gruner, F. J. DiSalvo, U. Wiesner, *Science* **2008**, *320(5884)*, 1748.

[92] Y. Zhao, K. Thorkelsson, A. J. Mastroianni, T. Schilling, J. M. Luther, B. J. Rancatore, K. Matsunaga, H. Jinnai, Y. Wu, D. Poulsen, J. M. J. Frechet, A. P. Alivisatos, T. Xu, *Nat. Mater.* **2009**, *8*, 979.

[93] S. G. Jang, E. J. Kramer, C. J. Hawker, *J. Am. Chem. Soc.* **2011**, *133*, 16986.

[94] B. J. Blaiszik, S. L. B. Kramer, S. C. Olugebefola, J. S. Moore, N. R. Sottos, S. R. White, *Ann. Rev. Mater. Res.* **2010**, *40*, 179.

[95] P. Cordier, F. Tournilhac, C. Soulie-Ziakovic, L. Leibler, *Nature* **2008**, *451*, 977.

[96] S. P. Li, W. S. Lew, Y. B. Xu, A. Hirohata, A. Samad, F. Baker, J. A. C. Bland, *Appl. Phys. Lett.* **2000**, *76*, 748.

[97] I. A. Ansari, I. W. Hamley, *J. Mater. Chem.* **2003**, *13*, 2412.

[98] L. S. Li, J. Jin, S. Yu, Y. Zhao, C. Zhang, T. Li, *J. Phys. Chem. B* **1998**, *102*, 5648.

[99] M. C. Daniel, D. Astruc, *Chem. Rev.* **2004**, *104*, 293.

[101] J. Shan, H.Tenhu, *Chem. Commun.* **2007**, *44*, 4580.

[102] S. Mann, W. Shenton, M. Li, S. Connolly, D. Fitzmaurice, *Adv. Mater.* **2000**, *12*, 147.

[103] M. E. Franke, T. J. Koplin, U. Simon, *Small* **2006**, *2(1)*, 36.

[104] E. E. Foos, A. W. Snow, M. E. Twigg, M. G. Ancona, *Chem. Mater.* **2002**, *14*, 2401.

[105] N. Krasteva, I. Besnard, B. Guse, R. E. Bauer, K. Muellen, A. Yasuda, T. Vossmeyer, *Nano Lett.* **2002**, *2(5)*, 551.

[106] A. N. Shipway, I. Willner, *Chem. Commun.* **2001**, *20*, 2035.

[107] I. Willner, A. N. Shipway, B. Willner, *ACS Symp. Ser.* **2003**, *844*, 88.

[108] F. Favier, E. C. Walter, M. P. Zach, T. Benter, R. M. Penner, *Science* **2001**, *293*, 2227.

[109] F. A. Leibowitz, W. X. Zheng, M. M. Maye, C. J. Zhong, *Anal. Chem.* **1999**, *71*, 5076.

6

Introducing the Safe Capsule for CdS Quantum Dots as Bio-labelling Device

6.1 Introduction

Nanoparticles 1-10 nm in diameter with diverse surface chemistry, tuneable absorption and emission properties have shown great potential in disease diagnosis and therapy. Broad ranges of nanoscale inorganics such as water soluble quantum dots (QDs) have the potential to be applied in bio-detection, cellular imaging, photothermal therapy of tumours, optical barcoding and drug carrier. Moreover, charge, size, shape and hydrophilicity remain among the most important properties of QDs for effective delivery to the desired target.[1] Ferrari 2005 has successfully prepared fluorescent MNPs composed of silica-coated CdTe QDs and magnetic nanoparticles (FMNPs), and used as-prepared FMNPs to label biomolecules for tumor imaging and hyperthermia therapy. [1-2]

Quantum dots (QDs) are fluorescent semiconductor nanocrystals with unique optical and electrical properties. Compared to organic dyes and fluorescent proteins, QDs possess near-unity quantum yields and much greater brightness than dyes (10-100 times). QDs also show broad absorption characteristics; a narrow, continuous and tuneable emission spectra due to quantum size effects. Other properties include long fluorescence lifetime (5 to > 100 ns compared to 1-5 ns in organic dyes) and negligible photobleaching (100-1000 times less than fluorescent dyes) over minutes to hours.[3]

Surface functionalization has further expanded the potential of QDs as probes for biomedical applications.[3] Therefore, hydrophobic conditions for synthesis of high-quality QDs are required as many biomolecules have limited solubility and stability in organic solvents. Ligand exchange and surface stabilizers can be used for surface modification of QDs to improve stability in aqueous conditions as well as biocompatibility. In this process, heterobifunctional ligands such as mercaptoacetic acid containing thiol functionalities are used, which can covalently bind to QDs and improve their hydrophilicity. However, the ligand exchange method may induce agglomeration and decreases fluorescence efficiency.

Additionally, if QDs are to be used in biomedical sciences, their toxicity should be taken into considerations. Complete characterization of size, shape, charge, surface chemistry and material properties are important when correlating toxicity. QDs also may agglomerate in vitro or in vivo and may chemically degrade, making it difficult to measure toxicity level when the QDs are conjugated with other materials. Therefore, another approach to prevent these problems is by stabilizing the surface using amphiphilic polymers [4] and biomaterials such as protein and enzyme.

6.2 Experimental Procedure

6.2.1 Materials

Cadmium Acetate, thioglycolic acid (TGA), Sodium Sulphide (Na_2S), Sodium Hydroxide (NaOH), P2VP Homopolymer (M_n = 2200 M_w/M_n = 1.09), Apo-ferritin from Horse Spleen and Polyethilenimine (PEI).

6.2.2 Preparation of CdS Quantum Dots (QDs)

CdS quantum dots were synthesized via a colloidal method as detail's mentioned in previous chapter.[5] CdS-apoferritin complexes were prepared by referring to Iwahari Kenji's[6] research with some adjustments made during synthesis as mentioned in previous chapter.

The details procedure of preparing capsulated CdS with P2VP homopolymer is discussed in this chapter. Firstly, 1 M of ammonium acetate and 1 M of ammonia water was mixed with 100 mM of a cadmium acetate solution in 300 ml of distilled water. Then, 0.0363 g of P2VP homopolymer solution is added to the resulting reactant. The reaction was allowed to stand for 10 minutes under nitrogen flow at room temperature to obtain ammonium complex of cadmium with P2VP homopolymer. Next, 0.02 mmol of Sodium Sulphide was added to the reaction solution. Then, the solution was allowed to stand for 24 hours at room temperature with vigorous stirring to yield CdS-P2VP complexes in pH 9-10 before adding PEI at the end of the reaction.

6.2.3 Sample Characterization

The size of CdS-apoferritin and CdS-P2VP complexes were measured using transmission electron microscopy (TEM). TEM micrographs of the colloidal dispersions were obtained using a JEM-2000FX instrument operated at 200 kV as the acceleration voltage. The optical properties of these samples were measured using UV-vis Absorption spectrum and Photoluminescence spectrum. The UV-vis Absorption spectrum for the colloidal dispersions of CdS QDs as the corresponding ionic precursors was measured using a Hitachi U-3010 spectrometer to determine the adsorption peak of each sample. Photoluminescence spectrum was performed using a F-7000 spectrofluorometer (Hitachi, Japan) with a quartz cell (1 cm × 1 cm). The fluorescence spectra was recorded at λ_{ex} = 335 nm.

6.3 Results and Discussions

Safe bio-labelling with unique properties is the desired bio-imaging, perfect for tumour imaging and treatment. In this study, the in vitro experiment method was introduced for preparing safe bio-labelling based on CdS QDs for medical treatments. It is well known that CdS has great optical properties but it is also considered toxic due to the cadmium metal (Cd). To overcome this problem, I have introduced two kinds of capsules; apo-ferritin and hydrophilic P2VP homopolymer, to encapsulate the CdS QDs, with the purpose of determining which the best capsule is for these QDs.

Figure 1 (a) and Figure 1 (b) show the absorption spectra and the photoluminescence spectra peaks for all studied samples, respectively. The apo-ferritin encapsulated CdS (CdS-apo + PEI) and P2VP capped CdS (CdS-p2vp + PEI) are smaller in size compared to the naked CdS and CdS capped with PEI only (CdS + PEI). On the other hand, the photoluminescence spectra in Figure 1 (b) shows that the CdS-apo + PEI spectrum is the second highest peak after CdS + PEI. Based on these spectra, it is clear that CdS-apo + PEI has small size QDs with high peak photoluminescence. Therefore, I have come to the conclusion that the combination of apo-ferritin and PEI can produce CdS QDs that are water-soluble, less toxic plus small particles with a high emission peak by encapsulating the QDs inside the apo-ferritin cage. To determine the toxicity level of these QDs, further in vivo research and clinical test are extremely needed.

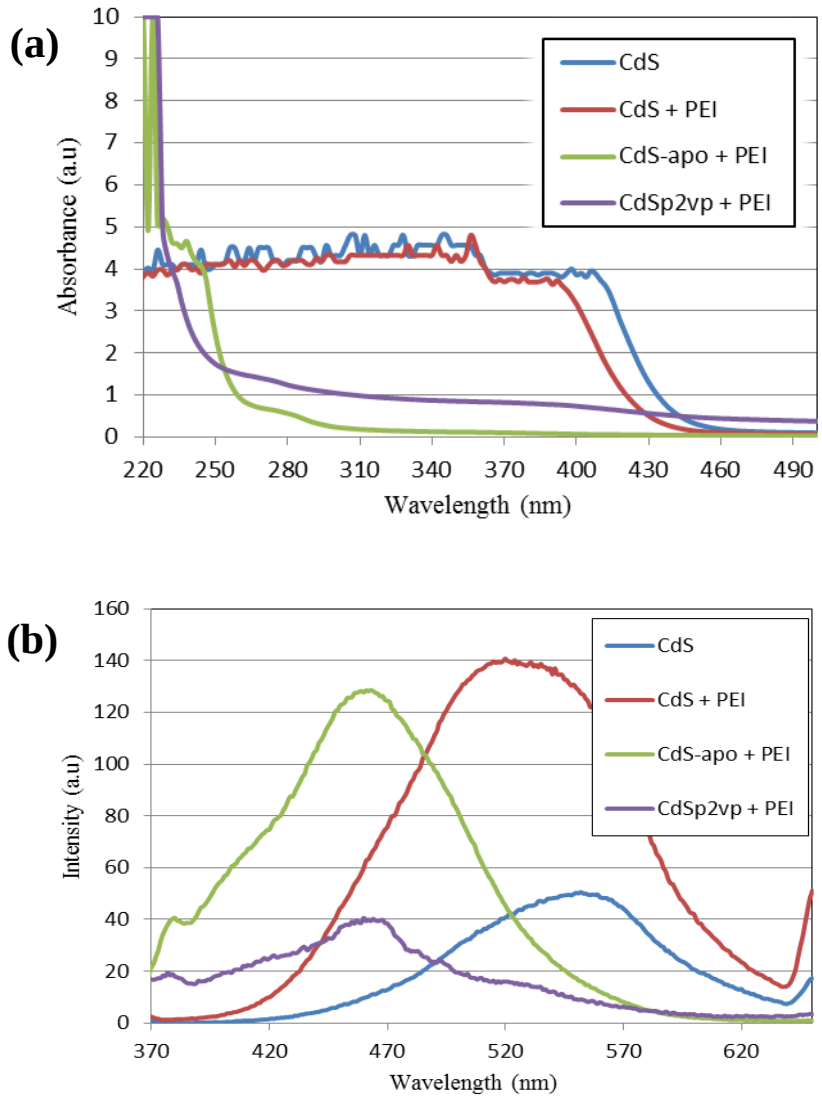

Figure 1: (a) Absorption spectra and (b) photoluminescence spectra peaks of CdS, CdS coated with PEI (CdS+PEI), rounded PEI over encapsulated CdS with apo-ferritin (CdS-apo+PEI) and rounded PEI over encapsulated CdS with P2VP homopolymer (CdSp2vp+PEI).

The fundamental absorption, which corresponds to electron excitation from the valence band to conduction band, can be used to determine the value of the optical band gap.[7] The connection between the band gap (E_g) and maximum wavelength (λ_{max}) can be written as

$$E_g = \frac{hc}{\lambda_{max}} \qquad (1)$$

where, E_g is the band gap of the material, h is Planks constant, c is speed of light and λ_{max} is the absorbance peak wavelength.

Band gap energy is illustrated as a graph of $(\alpha hv)^2$ versus *photon energy*, is shown in Figure 2. For the band gap energy in the absence of PEI, the Photon Energy is 2.90 eV and this value increased to 2.99 eV in the presence of PEI through calculations using the complex equation available in chapter 5.[8] Meanwhile, using the same calculations, the Photon Energy for encapsulated CdS with apo-ferritin in the presence of PEI is 4.8 eV which increases to 5.0 eV for capping with P2VP-homopolymer.

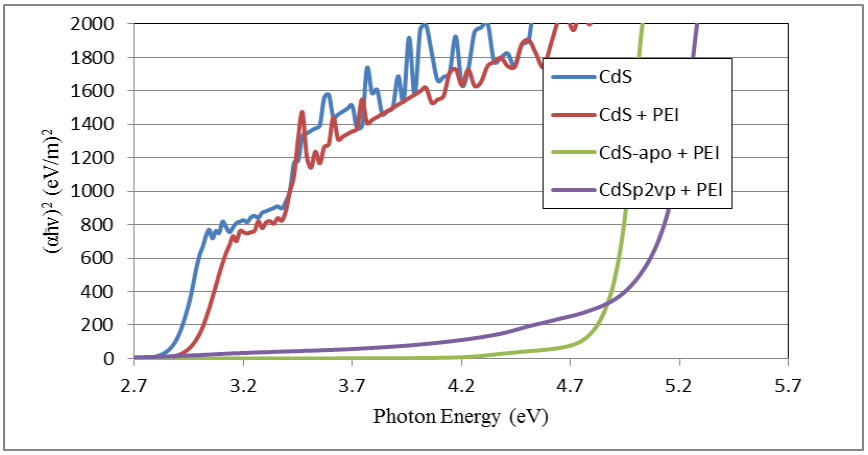

Figure 2: Band gap energy for CdS, CdS coated with PEI, rounded PEI over encapsulated CdS with apo-ferritin and rounded PEI over encapsulated CdS with P2VP homopolymer .

As the size of CdS-apo + PEI and CdS-p2vp + PEI are being too small and emission under 365 nm wavelength was hardly obtained, hence these two samples were placed under UV-light with 254 nm wavelength as shown in Figure 3 (c) and (d). Figure 3 (a) shows the CdS without any capping agent has emitted orange emission under 365 nm wavelength of UV-light. Meanwhile, the colour of the emitted light has changed from bright yellow under 365 nm wavelength (Figure 3 (b)), with the absence of capsules, to a yellow greenish emission for

encapsulation with apo-ferritin (Figure 3 (c)) and to a bluish yellow for encapsulation with P2VP homopolymer (Figure 3 (d)) under UV light at 254 nm. The size of core CdS QDs with presence capsules has obtained blue shifted and this result is fitted to optical properties results, where encapsulation with P2VP homopolymer's size is smaller than encapsulation with apo-ferritin. On the other hand, these two samples are smaller than naked CdS QDs and also CdS QDs with PEI.

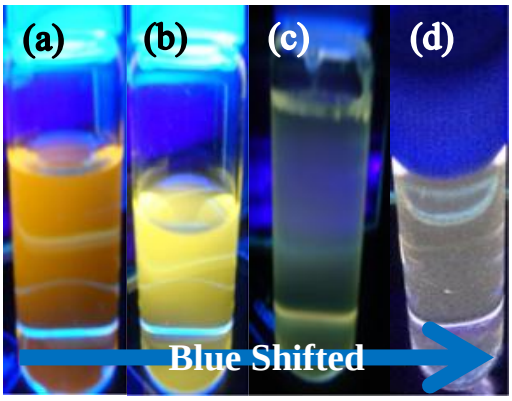

Figure 3: Colloidal solution under UV light for CdS, CdS coated with PEI, rounded PEI over encapsulated CdS with apo-ferritin and rounded PEI over encapsulated CdS with P2VP homopolymer .

In chapter 5, I have discussed that by capping CdS QDs with PEI was resulted CdS QDs with bigger size due to presence PEI linker surrounded CdS QDs core can be obsereved with TEM. Therefore, only TEM images of encapsulated CdS with apo-ferritin and capsulated CdS with P2VP homopolymer witout PEI have selected to be discussed in this section. The TEM images as shown in Figure 4 have proven that encapsulating CdS inside ferritin core would result in CdS QDs with the size and shape of the ferritin protein. Additionally, by introducing apo-ferritin, the aggregation of dark circles around the CdS QDs (Figure 4 (a)) was prevented if compared to QDs encapsulated with P2VP homopolymer (Figure 4 (b)), even though the size of the QDs much smaller than those encapsulated with apo-ferritin.

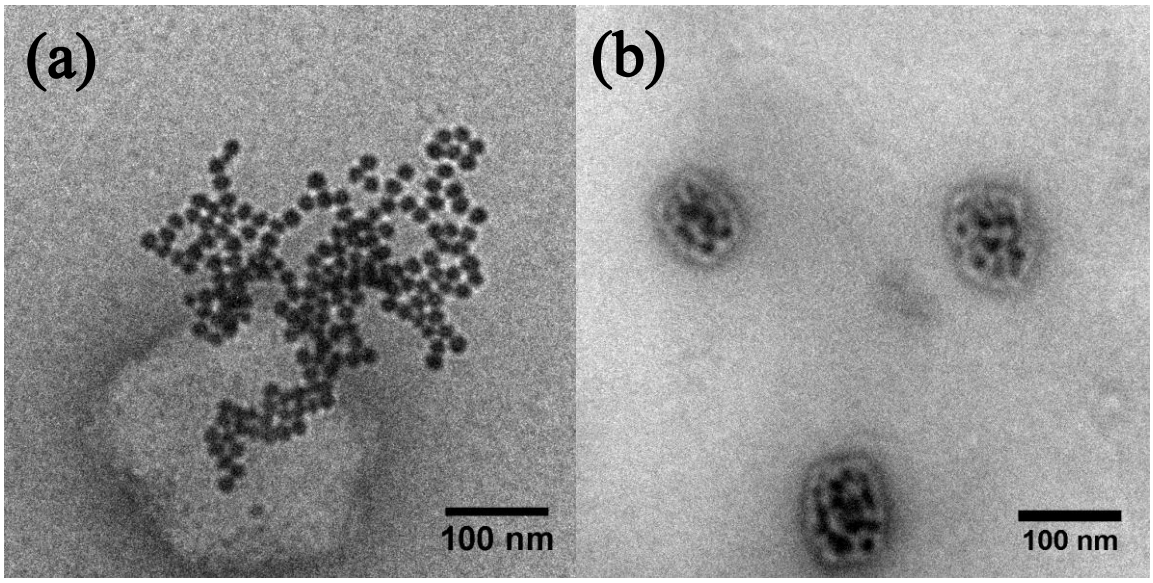

Figure 4: TEM images of (a) encapsulated CdS with apo-ferritin and (b) capsulated CdS with P2VP homopolymer.

6.4 Conclusion

CdS QDs encapsulation process has resulted in CdS QDs with small particle size compared to CdS QDs without capsule. Therefore, the developed QDs with high band gap energy have the possibility of being employed as bio-labelling due to the water solubility and non-toxicity properties. Although nanoparticle-based molecular imaging applications are moving towards clinical applications, formulation challenges such as aggregation and storage in clinical settings remain a challenge. [3]

The possibility of using apo-ferritin as capsules for nanoparticles might just be the solution for the aggregation problem. More detailed studies of these systems are currently under investigation.

References

[1] J. Ruan, K. Wang, H. Song, X. Xu, J. Ji, D. Cui, *Nanoscale Research Letters* **2011**, *6*, 299.

[2] M. Ferrari, *Nat. Rev. Cancer* **2005**, *5*, 161.

[3] S. K. Nune, P. Gunda, P. K. Thallapally, Y. Y. Lin, M. L. Forrest, Cory J Berklan, *Expert Opin Drug Deliv.* **2009**, *6*, 1175.

[4] Haeng-Deog Koh, Mohammad Changez, Jae-Suk Lee, *Macromol. Rapid Commun.* **2010**, *31*, 1798.

[5] S. A. Shamsudin, S. Radiman, M. S. Ghamsari, K. S. Khoo, *AIP Conference Proceeding* **2009**, *1136*, 292.

[6] K. Iwahori, *U.S. 7* **2011**,*897*,408 B2.

[7] L.E. Brus, *J. Chem. Phys.* **1984,** *80*, 4403.

[8] S. A. Shamsudin, N. F. Omar, S. Radiman, *IFMBE Conference Proceeding* **2011**,*35*, 92.

Summary

In this research, I found out that the self-assemblies of hybrid system can be done by aligning CdS quantum dots onto block copolymer thin films with either parallel or perpendicular cylindrical structure. The CdS quantum dots also has been capped with ferritin shell purposely to introduce safe capsule for CdS quantum dots before applying it in biomedical field and before further, clinical test is extremely needed.

Chapter 1 briefly mentioned about the system and materials that have been used in this research including nanoparticles, biomaterials and template of block copolymer. Furthermore, this chapter also mentioned the instruments that have characterized the samples with details specifications. Finally, the end part of this chapter has informed about objectives of every next chapters.

In Chapter 2, the effect of temperature and type of solvent on the microdomain orientation during solvent-annealing of block copolymer ultrathin films on silicon substrates was investigated using asymmetric polystyrene-*block*-poly(2-vinylpyridine) (PS-*b*-P2VP) diblock copolymer. When the solvent-annealing was performed with THF at 20 °C, the ultrathin film exhibited a mixed orientation of cylinders parallel and perpendicular to the substrate while at 25 °C only parallel cylinders were observed by AFM. The solvent annealing with acetone gave a dot pattern at 20 °C and a line pattern at 25 °C. On the other hand, in the case of solvent-annealing with toluene perpendicular cylinders were observed at 25 °C while at 20 °C the morphology was not clear and much improved hexagonal dot pattern was obtained when

the as-spun thin film of PS-*b*-P2VP was solvent-annealed for 6 h at 21 °C. The orientation and morphology of microdomains as well as the kinetics in PS-*b*-P2VP ultrathin films on solvent-annealing is significantly affected by temperature and type of solvent. By controlling temperature and selecting the solvent, perpendicular cylinders can be formed predominantly on the substrates.

In Chapter 3, selective solvents for each block were chosen to induce specific blocks of the PS-*b*-P2VP block copolymer thin film with the purpose of comparing the degree of block swelling affected by solvent vapours onto the thin film. A solvent with high boiling point which will slowly evaporate, allowing the block copolymer to assemble properly, has been chosen for this study. Therefore, toluene and acetic acid were selected as the selective solvents for PS and P2VP, respectively. Annealing in toluene causes a formation of equilibrium transition detected at 3 h of solvent annealing to 6 h of solvent annealing. However, order-order phase transition has been formed starting with a cylindrical structure at 6 h solvent annealing to a spherical structure at 9 h solvent annealing. In this study, I have intended to investigate the optimum time for solvent annealing. Meanwhile, for the 3 h solvent-annealed thin film with acetic acid has shown the formation of an unorganized structure due to deficient mobilization of P2VP molecules to orient the order of the morphology. On the other hand, the thin film morphology suddenly changed into an organized worm-like structure for 6h and 9h even though it did not attain a long-range ordered structure. This mechanism took place because the PS block could not be swollen by acetic acid, since the acetic acid is the selective solvent for P2VP block. Final experiment of this chapter has shown thermal annealing treatment did not induce structure with regular in the thin films. This is due to the fact that PS-*b*-P2VP does not have high enough mobility to attain the regular morphology by thermal annealing treatment.

Chapter 4 has discussed about two important strategies for aligning ferritin protein onto a striped line pattern polystyrene-*block*-poly(2-vinylpyridine) (PS-*b*-P2VP) template which are known by controlling pH value of ferritin protein and ferritin protein affinity onto PS-*b*-P2VP surface. The striped line pattern of PS-*b*-P2VP template was produced by a treatment with good solvent vapor for both blocks. Then, the template was etched by UV-irradiation in order to expose the surface of P2VP. Finally, the ferritin protein in acidic condition at pH3 was spin-coated onto the template. This experiment showed that the electrostatic interactions not caused by only on appropriate pH condition but also depends on remaining THF solvent on the P2VP surface that contains oxygen atom and obtained electronegative. These factors are important for ferritin adsorption onto this thin film.

Chapter 5 has mentioned about quantum dots (QDs). Cadmium sulphide (CdS) quantum dots are toxic and hydrophobic, making it impossible to be applied into biomaterials. A template is needed to make CdS QDs nontoxic and hydrophilic. Besides, the optical properties of these QDs are also needed to be protected. To achieve this purpose, the template for CdS QDs has been designed by capping CdS QDs with apo-ferritin shells before aligning them onto cylindrical perpendicular PS-*b*-P2VP template, with the aim of locating CdS QDs appropriately in sequence. Using that method, a host-guest system can be developed. This encapsulated CdS QDs inside ferritin core is presented as the smallest particles among the others due to the absorption UV spectrum and rendered to increase CdS QDs band gap energy. By applying polyethilenemine (PEI), the photoluminescence spectrum was enhanced. It also prevented photo-bleaching even after 12 days especially for encapsulated CdS QDs inside ferritin core. Moreover, the self-assembly of CdS QDs on PS-*b*-P2VP block copolymer has been introduced by ex situ approach to form hybrid CdS-PS-*b*-P2VP. Furthermore, swelling effect occurred when CdS-apo QDs were arrayed onto the PS-*b*-P2VP template.

Chapter 6 has mentioned about how to develop safe capsule for QDs that can be utilized as bio-labelling. In this study, I managed to synthesize Cadmium Sulphide (CdS) QDs with a mean size of 8 nm by capping it with thioglycolic acid - which has hydrogen bonding - to make QDs soluble in aqueous solutions. Polyethilenimine has functioned to render the QDs to be water soluble and enhances photo-oxidation even in aqueous solution. It also acted as a ligand to modify CdS QDs to prevent surface trap that can increase CdS QDs' quantum yield. Furthermore, non-toxicity and improved stability of the QDs in polymer sphere are needed. Therefore, the ideal bio-labelling QDs should be dense and equal in size and shape to achieve constant photoluminescence peak. Hence, the CdS QDs have been capsulated with poly(2-vinylpyridine) (P2VP) homopolymers and apo-ferritin in order to compare which one is the best capsule for QDs with the desired properties for applications in bio-labelling. This CdS QDs encapsulation process has resulted in CdS QDs with small particle size compared to CdS QDs without capsule. Therefore, the developed QDs with high band gap energy have the possibility of being employed as bio-labelling due to the water solubility and non-toxicity properties.

List of Publications

1. "Influence of Temperature and Type of Solvents on the Microdomain Orientation of PS-*b*-P2VP Ultrathin Films by Solvent Annealing"

   Siti Aisyah B. Shamsudin, Go Sakaguchi, Mikihito Takenaka, Hirokazu Hasegawa

   Macromolecular Symposia **2013**, *327*, 72–79

   (Chapter 2)

2. "Controlling Ordered Structures of PS-*b*-P2VP Block Copolymer Thin Film by Tuning Solvent's Annealing Time"

   Siti Aisyah B. Shamsudin, Mikihito Takenaka, Hirokazu Hasegawa

   To be submitted to *Polymer*

   (Chapter 3)

3. "Alignment of Ferritin Protein Molecules on Diblock Copolymer Patterns by Using Self-Assembly"

   Siti Aisyah B. Shamsudin, Go Sakaguchi, Mikihito Takenaka, Hirokazu Hasegawa

   To be submitted to *Biomacromolecules*

   (Chapter 4)

4. "Aligning CdS Quantum Dots in Apo-ferritin Protein and PS-*b*-P2VP Organic Templates"

   Siti Aisyah B. Shamsudin, Hirokazu Hasegawa, Mikihito Takenaka, Kenji Saijo

   Journal of Advanced Material Research (in press)

   (Chapter 5)

5. "Introducing the Safe Capsule for CdS Quantum Dots as Bio-labelling Device"

   S. A. Shamsudin, M. Takenaka, H. Hasegawa

   Journal of the Japan Society of Powder and Powder Metallurgy (Submitted)

   (Chapter 6)

Other Publications

1. "Optical Properties Effect of Cadmium Sulfide Quantum Dots towards Conjugation Process"

   S. A. Shamsudin, N. F. Omar, S. Radiman

   5th Kuala Lumpur International Conference on Biomedical Engineering 2011, *IFMBE Proceedings* **2011**, *35*, 92-96

2. "Synthesis CdS Nanocrystals in Various pH Values"

   S. Aisyah Shamsudin, Shahidan Radiman, M. S. Ghamsari, Khoo Kok Siong

   Nanoscience and Nanotechnology: International Conference on Nanoscience and Nanotechnology 2008, *AIP Conference Proceedings* **2008**, *1136*, 292-296

Acknowledgements

I am grateful to the one and only God with the permission and the gift; I was able to complete this thesis for the requirements of Doctoral Degree of Polymer Chemistry, Graduate School of Engineering. I would like to extend my warmest appreciation to my advisors and co-advisors Prof. Dr. Hirokazu Hasegawa, Prof. Dr. Kazunari Akiyoshi, Assoc. Prof. Dr. Mikihito Takenaka and Dr. Kenji Saijo for their encouragement, guidance, support, patience and understanding during the research and writing of this dissertation. Not least are the lecturers who are involved directly or indirectly to advice, discuss ideas, and provide encouragement. May God bless for all.

A warm appreciation to my research group and for those took a part in many helpful technical, experimental and discussions especially regarding the entitled research. I wish all of them success in their careers. I am particularly grateful for the assistance given by Mr. Go Sakaguchi who taught me how to start the experiment, since I was not familiar with this laboratory apparatus and instruments before. I would like to thank to Mrs. Oda Naoko for the excellent hospitality that have helped me on managing my life in Japan. I would like to thank them for their contributions and times.

I would like to express my sincere gratitude to Japan Government in funding the Monbukagakusho Scholarship (文部科学省奨学金) which enabled me to undergo a PhD program at the Kyoto University.

Finally, specials thank to my mother and father, Rodziyah Binti Ismail and Shamsudin Bin Salleh, and my fellow friends for their love and inspiration. Thanks for believing in me when I did not believe in myself. This would not have been possible if it were not for the love of my savior ALLAH SWT and His messenger Muhammad PBUH.

"*Who is trying to, he will succeed*"

May 2013 Siti Aisyah Binti Shamsudin